SUPPRESSION OF ROTATING STALL BY THROTTLE RINGS CONTROL IN VANELESS DIFFUSERS OF CENTRIFUGAL COMPRESSORS

A THESIS IN MECHATRONICS
ENGINEERING

Presented to the faculty of the American University of Sharjah
School of Engineering
in partial fulfillment of
the requirements of the degree of

MASTER OF SCIENCE

by
DHAFAR S. MOHAMMED
B.S. 1993
M.Sc. 1997

Sharjah, UAE
April 2006

We approve the thesis of Dhafar S. Mohammed

Date of signature

Dr. Saad A. Ahmed Chair of Committee	
Dr. Ameen el-Sinawi Graduate Committee	
Dr. Mamoun Abdel-Hafez Graduate Committe	
Dr. Mohammed Ameen Al-Jarrah Program Director	
Dr. Yousef Al-Assaf Interim Dean of Engineering	
Judith Killen Director, Graduate Studies and Research	

SUPPRESSION OF ROTATING STALL BY THROTTLE RINGS CONTROL IN VANESLESS DIFFUSERS OF CENTRIFUGAL COMPRESSORS

Dhafar S. Mohammed, Candidate for the Master of Science Degree

American University of Sharjah

ABSTRACT

Centrifugal compressor systems are widely used in many industrial applications. However, the operation of such systems is limited at low-mass flow rates by fluid flow instabilities. These instabilities lead the compressor to rotating stall or surge.

Compression systems of gas turbines can exhibit several types of instabilities: impeller flow instabilities, surge and finally flow instabilities in the diffuser known as rotating stall which this investigation is restricted to. These instabilities limit the flow range in which the compressor can operate. Surge and rotating stall also restrict the performance and efficiency of the compressor.

Experimental techniques are used for investigating a model of radial vaneless diffuser at stall as well as stall-free operating conditions. The speed of the impeller was kept constant while the mass flow rate was reduced gradually to scan the steady and unsteady operating conditions of the compressor. Generally speaking, for stall-free conditions only, the flow rate through the compressor was kept constant at its optimum design value while studying the flowfield for each of the three-impeller speeds tested ranging from 1000 to 2000 RPM. For each speed, the flow rate through the compressor was gradually decreased until flow instability is initiated at the diffuser. The flow rate was further reduced to study the characteristics of rotating stall. These measurements were also repeated for diffuser diameter ratios, D_o / D_i, of 1.5, 1.75, and 2.0 with diffuser width ratio, b / D_i, of 0.055 to determine the effects of diffuser diameter ratios on rotating stall characteristics. At stall-free operating conditions were also reported. Furthermore, the frequency of the stall cells, as well as its strength, was found to increase as the impeller speed increases, irrespective of the number of stall cells. For a fixed diffuser width, the frequency of the stall cells increases as the diffuser diameter ratio was decreased. At a constant impeller speed and lower flowrates than the critical flowrate, the rotating stall pattern with one stall cell was dominant over the pattern with two stall cells. In addition, the instability in the diffuser was successfully delayed to a lower flow coefficient when throttle rings were attached to either / or both of the diffuser walls in order to reduce the diffuser exit flow area. Finally, the results showed that an increase of the blockage ratio improves the stability of the system.

This work involves new technologies and offers opportunities to develop techniques that can handle the analysis of unsteady flow signals and pattern recognition techniques. This

work might play a major role in air-conditioning industries as well as small gas turbines using centrifugal compressors.

Key words: stall, vaneless diffuser, centrifugal compressors, and unsteady flow.

CONTENTS

ABSTRACT iii

LIST OF ILLUSTRATIONS ix

LIST OF TABLES xv

ACKNOWLEDGMENTS xvi

CHAPTER 1

INTRODUCTION, BACKGROUND & SIGNIFICANCE ..... - 1 -

1.1 Stability of Compression Systems ..... - 2 -

1.2 Rotating Stall ..... - 6 -

1.3 Literature Review ..... - 7 -

CHAPTER 2

RESEARCH OBJECTIVES ..... - 34 -

2.1 Contradictory Results & the Importance of Current Research ..... - 34 -

2.2 The Focus of Current Work ..... - 35 -

CHAPTER 3

EXPERIMENTAL FACILTIY ..... - 36 -

3.1 Test Facility ..... - 36 -

3.2 Instrumentation ..... - 39 -

3.2.1 Dynamic Pressure Sensors ..... - 39 -

3.2.2 Pressure Fluid Manometer ..... - 43 -

3.2.2.1 Multi-tube H_2O mm Manometer ..... - 43 -

3.2.2.2 Precision Single Limb Airflow Manometer ..... - 45 -

3.3 Measurement Techniques ..... - 46 -

3.4 Test Conditions ..... - 48 -

CHAPTER 4

STEADY & UNSTEADY FLOW RESULTS & DISCUISSIONS ..... - 49 -

4.1 Steady Flow ..... - 49 -

4.1.1 Static Pressure Measurements on Diffuser Shroud ..... - 49 -

4.2 Unsteady Flow ..... - 54 -

4.2.1 Static Pressure Measurements on Diffuser Shroud ..... - 54 -

4.3 Steady & Unsteady Flow ..... - 59 -

CHAPTER 5

ROTATING STALL CHARACTERISTICS ..... - 70 -

5.1 Effects of Impeller Speed ..... - 70 -

5.1.1 Diameter Ratio Do / Di = 1.5 ..... - 71 -

5.1.1.1 N = 1000 RPM ..... - 72 -

5.1.1.2 N = 1500 RPM ..... - 82 -

5.1.1.3 N = 2000 RPM ..... - 86 -

5.1.2 Diameter Ratio D_o / D_i = 1.75 ..... - 91 -

5.1.2.1 N = 1000 RPM ..... - 92 -

5.1.2.2 N = 1500 RPM ..... - 99 -

5.1.2.3 N = 2000 RPM ..... - 103 -

5.1.3 Diameter Ratio D_o / D_i = 2.0 ..... - 108 -

5.1.3.1 N = 1000 RPM ..... - 109 -

5.1.3.2 N = 1500 RPM ..... - 116 -

5.1.3.3 N = 2000 RPM ..... - 120 -

CHAPTER 6

ROTATING STALL RESULTS ..... - 125 -

6.1 Effect of Impeller Angular Speed on the Frequency of Pressure Fluctuations ..... - 125 -

6.2 Effect of Impeller Angular Speed on the Strength of Rotating Stall Cells ..... - 127 -

6.3 Effect of Diffuser Diameter Ratio on the Frequency of Pressure Fluctuations ..... - 130 -

6.4 Effect of Diffuser Diameter Ratio on the Strength of Rotating Stall Cells ..... - 134 -

CHAPTER 7

CONTROL OF ROTATING STALL ..... - 137 -

7.1 Effects of Blockage Ratio on the Performance of the Compressor ..... - 139 -

7.1.1 25% Blockage Ratio ..... - 139 -

7.1.2 50% Blockage Ratio ..... - 140 -

7.1.3 75% Blockage Ratio ..... - 141 -

7.2 Effects of Blockage Ratio on the Diffuser Flow Characteristics ..... - 143 -

7.2.1 Effects of Blockage Ratio on Diffuser Stability ..... - 143 -

7.2.2 Effects of Blockage Ratio on the Strength of Rotating Stall Cells ..... - 147 -

7.2.3 Effects of Blockage Ratio on the Frequency of Pressure Fluctuations ..... - 148 -

CHAPTER 8

CONCULSIONS & RECOMMENDATIONS ..... - 151 -

8.1 Conclusions ..... - 151 -

8.2 Recommendations ..... - 153 -

REFERENCES ..... - 155 -

NOMENCLATURE ..... - 164 -

APPENDIX ..... - 165 -

A. MATLAB Program ..... - 166 -

B. Statistical Signal Processing ..... - 170 -

C. Uncertainty Analysis ..... - 177 -

LIST OF ILLUSTRATIONS

Figure page

Figure 1.1: Operational Stability, both Compressor and Throttle Characteristics - 5 -

Figure 1.2: Effects of Rotor RPM on Compressor Performance and Stability - 5 -

Figure 3.1: Assembled Experimental Test Rig - 37 -

Figure 3.2: A Schematic of Experiment Test Rig - 38 -

Figure 3.3a-b: A Schematic of the Dynamic Pressure Transducer & its Installation - 40 -

Figure 3.4: Factory–Supplied Calibration Curves for the Dynamic Pressure Transducer - 41 -

Figure 3.5: A Schematic of the Line-Powered Signal Conditioner - 42 -

Figure 3.6: Dynamic Pressure Transducer Locations on the Shroud Wall - 43 -

Figure 3.7: P3202 Multitube Manometer - 44 -

Figure 3.8: Precision Single Limb Airflow Manometer Type 4 - 46 -

Figure 4.1: Pressure Coefficient Distribution (λ) on the Shroud Wall, b / D_i = 0.055 & D_o / D_i = 1.5 & N = 1000, 1500, 2000 RPM - 51 -

Figure 4.2: Pressure Coefficient Distribution (λ) on the Shroud Wall, b / Di = 0.055 & Do / Di = 1.75 & N = 1000, 1500, 2000 RPM - 52 -

Figure 4.3: Pressure Coefficient Distribution (λ) on the Shroud Wall, b / D_i = 0.055 & D_o / D_i = 2.0 & N = 1000, 1500, 2000 RPM - 53 -

Figure 4.4: Pressure Coefficient Distribution (λ) on the Shroud Wall, b / D_i = 0.055 & D_o / D_i = 1.5 & N = 1000, 1500, 2000 RPM - 55 -

Figure 4.5: Pressure Coefficient Distribution (λ) on the Shroud Wall, b / D_i = 0.055 & D_o / D_i = 1.75 & N = 1000, 1500, 2000 RPM - 56 -

Figure 4.6: Pressure Coefficient Distribution (λ) on the Shroud Wall, b / D_i = 0.055 & D_o / D_i = 2.0 & N = 1000, 1500, 2000 RPM - 57 -

Figure 4.7: Pressure Coefficient Distribution (λ) on the Shroud Wall, b / D_i = 0.055 & D_o / D_i = 1.50, 1.75 & 2.0, & N = 2000 RPM - 58 -

Figure 4.8: Pressure Coefficient Distribution (λ) on the Shroud Wall, b / D_i = 0.055 & D_o / D_i = 1.75 & N = 1000, 1500 & 2000 RPM - 58 -

Figure 4.9: Pressure Distribution on the Shroud Wall, b / D_i = 0.055 & D_o / D_i = 1.5 & N = 1000 RPM - 60 -

Figure 4.10: Pressure Distribution on the Shroud Wall, b / D_i = 0.055 & D_o / D_i = 1.5 & N = 1500 RPM - 60 -

Figure 4.11: Pressure Distribution on the Shroud Wall, b / D_i = 0.055 & D_o / D_i = 1.5 & N = 2000 RPM - 61 -

Figure 4.12: Pressure Distribution on the Shroud Wall, b / D_i = 0.055 & D_o / D_i = 1.75 & N = 1000 RPM - 61 -

Figure 4.13: Pressure Distribution on the Shroud Wall, b / D_i = 0.055 & D_o / D_i = 1.75 & N = 1500 RPM - 62 -

Figure 4.14: Pressure Distribution on the Shroud Wall, b / D_i = 0.055 & D_o / D_i = 1.75 & N = 2000 RPM - 62 -

Figure 4.15: Pressure Distribution on the Shroud Wall, b / D_i = 0.055 & D_o / D_i = 2.0 & N = 1000 RPM - 63 -

Figure 4.16: Pressure Distribution on the Shroud Wall, b / D_i = 0.055 & D_o / D_i = 2.0 & N = 1500 RPM - 63 -

Figure 4.17: Pressure Distribution on the Shroud Wall, b / D_i = 0.055 & D_o / D_i = 2.0 & N = 2000 RPM - 64 -

Figure 4.18: Pressure Distribution on the Shroud Wall, b / D_i = 0.055 & D_o / D_i = 1.50, 1.75, & 2.0, & N = 2000 RPM - 64 -

Figure 4.19: Pressure Distribution on the Shroud Wall, b / D_i = 0.055 & D_o / D_i = 1.75 & N = 1000, 15000, & 2000 RPM - 65 -

Figure 4.20: Pressure Distribution on Shroud Wall with Volumetric Flow Rate, b / D_i = 0.055 & D_o / D_i = 1.5 & N = 1000 RPM - 65 -

Figure 4.21: Pressure Distribution on Shroud Wall with Volumetric Flow Rate, b / D_i = 0.055 & D_o / D_i = 1.5 & N = 1500 RPM - 66 -

Figure 4.22: Pressure Distribution on Shroud Wall with Volumetric Flow Rate, b / D_i = 0.055 & D_o / D_i = 1.5 & N = 2000 RPM - 66 -

Figure 4.23: Pressure Distribution on Shroud Wall with Volumetric Flow Rate, b / D_i = 0.055 & D_o / D_i = 1.75 & N = 1000 RPM - 67 -

Figure 4.24: Pressure Distribution on Shroud Wall with Volumetric Flow Rate, $b / D_i = 0.055$ & $D_o / D_i = 1.75$ & N = 1500 RPM - 67 -

Figure 4.25: Pressure Distribution on Shroud Wall with Volumetric Flow Rate, $b / D_i = 0.055$ & $D_o / D_i = 1.75$ & N = 2000 RPM - 68 -

Figure 4.26: Pressure Distribution on Shroud Wall with Volumetric Flow Rate, $b / D_i = 0.055$ & $D_o / D_i = 2.0$ & N = 1000 RPM - 68 -

Figure 4.27: Pressure Distribution on Shroud Wall with Volumetric Flow Rate, $b / D_i = 0.055$ & $D_o / D_i = 2.0$ & N = 1500 RPM - 69 -

Figure 4.28: Pressure Distribution on Shroud Wall with Volumetric Flow Rate, $b / D_i = 0.055$ & $D_o / D_i = 2.0$ & N = 2000 RPM - 69 -

Figure 5.1: Effect of N on System Characteristic Curves, $b / D_i = 0.055$, $D_o / D_i = 1.5$ - 71 -

Figures 5.2a-c: Pressure Traces at Different ϕ's, DR 1.5, N = 1000 RPM - 74 -

Figures 5.2d-f: Pressure Traces at Different ϕ's, DR 1.5, N = 1000 RPM - 75 -

Figures 5.3a-c: Spectra of Pressure Fluctuations (CSD) at Different ϕ's, DR 1.5 & N = 1000 RPM - 78 -

Figures 5.3d-f: Spectra of Pressure Fluctuations (CSD) at Different ϕ's, DR 1.5 & N = 1000 RPM - 79 -

Figures 5.4a-c: Spectra of Pressure Fluctuations (PSD) at Different ϕ's, DR 1.5 & N = 1000 RPM - 80 -

Figures 5.4d-f: Spectra of Pressure Fluctuation (PSD) at Different ϕ's, DR 1.5 & N = 1000 RPM - 81 -

Figures 5.5a-d: Pressure Traces at Different ϕ's, DR 1.5, N = 1500 RPM - 83 -

Figures 5.6a-d: Spectra of Pressure Fluctuation (CSD) at Different ϕ's, DR 1.5 & N = 1500 RPM - 84 -

Figures 5.7a-d: Spectra of Pressure Fluctuation (PSD) at Different ϕ's, DR 1.5 & N = 1500 RPM - 85 -

Figures 5.8a-d: Pressure Traces at Different ϕ's, DR 1.5, N = 2000 RPM - 88 -

Figures 5.9a-d: Spectra of Pressure Fluctuation (CSD) at Different ϕ's, DR 1.5 & N = 2000 RPM - 89 -

Figures 5.10a-d: Spectra of Pressure Fluctuation (PSD) at Different ϕ's, DR 1.5 & N = 2000 RPM - 90 -

Figure 5.11: Effect of N on System Characteristic Curves, b / D_i = 0.055, D_o / D_i = 1.75 - 91 -

Figures 5.12a-c: Pressure Traces at Different ϕ's, DR 1.75, N = 1000 RPM - 93 -

Figures 5.12d-f: Pressure Traces at Different ϕ's, DR 1.75, N = 1000 RPM - 94 -

Figures 5.13a-c: Spectra of Pressure Fluctuations (CSD) at Different ϕ's, DR 1.75 & N = 1000 RPM - 95 -

Figures 5.13-f: Spectra of Pressure Fluctuations (CSD) at Different ϕ's, DR 1.75 & N = 1000 RPM - 96 -

Figures 5.14a-c: Spectra of Pressure Fluctuations (PSD) at Different ϕ's, DR 1.75 & N = 1000 RPM - 97 -

Figures 5.14d-f: Spectra of Pressure Fluctuation (PSD) at Different ϕ's, DR 1.75 & N = 1000 RPM - 98 -

Figures 5.15a-d: Pressure Traces at Different ϕ's, DR 1.75, N = 1500 RPM - 100 -

Figures 5.16a-d: Spectra of Pressure Fluctuations (CSD) at Differentϕ's, DR 1.75 &N=1500 RPM - 101 -

Figures 5.17a-d: Spectra of Pressure Fluctuations (PSD) at Differentϕ's, DR 1.75 & N=1500 RPM - 102 -

Figures 5.18a-d: Pressure Traces at Different ϕ's, DR 1.75, N = 2000 RPM - 105 -

Figures 5.19a-d: Spectra of Pressure Fluctuation (CSD) at Different ϕ's, DR 1.75 & N = 2000 RPM - 106 -

Figures 5.20a-d: Spectra of Pressure Fluctuation (PSD) at Different ϕ's, DR 1.75 & N = 2000 RPM - 107 -

Figure 5.21: Effect of N on System Characteristic Curves, b / D_i = 0.055, D_o / D_i = 2.0 - 108 -

Figures 5.22a-c: Pressure Traces at Different ϕ's, DR 2.0, N = 1000 RPM - 110 -

Figures 5.22d-f: Pressure Traces at Different ϕ's, DR 2.0, N = 1000 RPM - 111 -

Figures 5.23a-c: Spectra of Pressure Fluctuations (CSD) at Different ϕ's, DR 2.0 & N = 1000 RPM - 112 -

Figures 5.23d-f: Spectra of Pressure Fluctuations (CSD) at Different ϕ's, DR 2.0 & N = 1000 RPM - 113 -

Figures 5.24a-c: Spectra of Pressure Fluctuations (PSD) at Different ϕ's, DR 2.0 & N = 1000 RPM - 114 -

Figures 5.24d-f: Spectra of Pressure Fluctuation (PSD) at Different ϕ's, DR 2.0 & N = 1000 RPM - 115 -

Figures 5.25a-d: Pressure Traces at Different ϕ's, DR 2.0, N = 1500 RPM - 117 -

Figures 5.26a-d: Spectra of Pressure Fluctuations (CSD) at Differentϕ's, DR 2.0 &N=1500 RPM - 118 -

Figures 5.27a-d: Spectra of Pressure Fluctuations (PSD) at Differentϕ's, DR 2.0 & N=1500 RPM - 119 -

Figures 5.28a-d: Pressure Traces at Different ϕ's, DR 2.0, N = 2000 RPM - 121 -

Figures 5.29a-d: Spectra of Pressure Fluctuation (CSD) at Different ϕ's, DR 2.0 & N = 2000 RPM - 122 -

Figures 5.30a-d: Spectra of Pressure Fluctuation (PSD) at Different ϕ's, DR 2.0 & N = 2000 RPM - 123 -

Figure 6.1: Effects of Impeller Angular Speed on the Frequency of Pressure Fluctuations, $b / D_i = 0.055$ - 126 -

Figure 6.2: Effects of Impeller Angular Speed on Non-Dimensional Frequency of Pressure Fluctuations, $b / D_i = 0.055$ - 126 -

Figure 6.3: Effects of Impeller Speed on the Strength of Rotating Stall Cells, $b / D_i = 0.055$ - 128 -

Figure 6.4a-b: Effects of Diffuser Diameter Ratio on the Frequency of Pressure Fluctuations, $b / D_i = 0.055$ - 132 -

Figure 6.5a-b: Effects of Diffuser Diameter Ratio on the Non-Dimensional Speed of the Stall Cells, $b / D_i = 0.055$ - 133 -

Figure 6.6a-b: Effects of Diffuser Diameter Ratio on the Strength of Rotating Stall Cells, $b / D_i = 0.055$ - 135 -

Figure 7.1: Modes of Diffuser Exit Blockage Used Throttle Rings - 138 -

Figure 7.2: Effects of Throttle Ring Attached on Hub, Shroud, and Simultaneous Walls on Compressor Characteristics with $D_o / D_i = 1.5$, N = 2000 RPM & $b / D_i = 0.055$ - 142 -

Figure 7.3: Effects of Throttle Ring Attached on Hub, Shroud, and Simultaneous Walls on Compressor Characteristics with $D_o / D_i = 1.75$, N = 2000 RPM & $b / D_i = 0.055$ - 142 -

Figure 7.4: Effects of Throttle Ring Attached on Hub, Shroud, and Simultaneous Walls on Compressor Characteristics with $D_o / D_i = 2.0$, N = 2000 RPM & $b / D_i = 0.055$ - 143 -

Figure 7.5: Effects of Throttle Ring Attached on Hub & Shroud Walls on Velocity Profile with $D_o / D_i = 1.5$, N = 2000 RPM & $b / D_i = 0.055$ - 145 -

Figure 7.6: Effects of Throttle Ring Attached on Hub & Shroud Walls on Velocity Profile with $D_o / D_i = 1.75$, N = 2000 RPM & $b / D_i = 0.055$ - 145 -

Figure 7.7: Effects of Throttle Ring Attached on Hub & Shroud Walls on Velocity Profile with $D_o / D_i = 2.0$, N = 2000 RPM & $b / D_i = 0.055$ - 146 -

Figure 7.8: Effects of Throttle Ring Attached on Hub Wall on Compressor Characteristics with N = 2000 RPM & $b / D_i = 0.055$ - 146 -

Figure 7.9: Effects of Throttle Ring Attached on Hub Wall on Compressor Characteristics with N = 2000 RPM & $b / D_i = 0.055$ - 147 -

Figure 7.10: Effects of Throttle Rings Attached to Hub Wall on the Strength of Rotating Stall at N = 2000 RPM & b / Di = 0.055 - 148 -

Figure 7.11: Effects of Throttle Rings Attached to Hub Wall on Frequency of Rotating Stall at N = 2000 RPM & b / Di = 0.055 - 149 -

Figure 7.12: Effects of Throttle Rings Attached to Hub Wall, Shroud Wall, & their Combinations on Frequency of Pressure Fluctuations at $D_o / D_i = 1.75$, N = 2000 RPM & b / Di = 0.055 - 150 -

Figure B.1: The Periodogram - 172 -

Figure B.2: Averaged Periodogram (no overlap) - 172 -

Figure B.3: Averaged Periodogram (128 sample overlap) - 173 -

Figure B.4: Averaged Periodogram (128 sample overlap, Hanning window) - 174 -

Figure B.5: Plot from psd without an output - 175 -

Figure B.6: Coherence Function - 176 -

LIST OF TABLES

Table	page
Table 1.1: Summery of Investigations on Rotating Stall (2006 - 1980)	- 31 -
Table 3.1: Test Matrix	- 48 -
Table 5.1: Summery of Stall Characteristics, $b / D_i = 0.055$	- 124 -
Table 6.1: Comparison of Stall characteristic Results	- 129 -
Table 6.2: Effect of Diffuser Diameter Ratios on Stall Characteristics, $b / D_i = 0.055$	- 136 -

ACKNOWLEDGMENTS

The author would like to thank Professor Saad Ahmed for his guidance, constructive criticism, and encouragement in this research, the committee members, and all other faculty at AUS-SOE for making available the facility, labs and equipments used in this research.

Finally, I also would like to give my sincere and especial thanks and gratitude to my wife whose patient and love enabled me to accomplish this achievement.

CHAPTER 1

INTRODUCTION, BACKGROUND & SIGNIFICANCE

Compressors are used in a wide variety of applications. These includes turbojet engines used in aerospace propulsion, power generation using industrial gas turbines, turbo-charging of internal combustion engines, pressurization of gas and fluids in the process industry, transport of fluids in pipelines and so on.

There are four general types of compressors: reciprocating, rotary, centrifugal and axial. Some authors use the term radial compressor when referring to a centrifugal compressor. Reciprocating and rotary compressors work by the principle of reducing the volume of the gas, and will not be considered further in this project. Centrifugal and axial compressors, also known as turbo-compressors or continuous flow compressors, work by the principle of accelerating the fluid to a high velocity and then converting this kinetic energy into potential energy, manifested by an increase in pressure, by decelerating the gas in diverging channels. This energy will be lost and the efficiency of the compressor will be reduced if there is no suitable device at the exit of the impeller to conserve it. As a result, different types of collectors have been used over the years to ensure that the compressor operates at a reasonably high efficiency. In axial compressors the deceleration takes place in the stator blade passages, and in centrifugal compressor it takes place in the diffuser. One obvious difference between these two types of compressors is, in axial compressors, the flow leaves the compressor in the axial direction, whereas, in centrifugal compressors, the flow leaves the compressor in a direction perpendicular to the axis of the rotating shaft.

Among the several devices used at the exit of the impeller of a centrifugal compression system are vaned diffusers, vaneless diffusers, and scrolls. The scroll or volute is sometimes used in conjunction with either of the diffusers when there is the need for additional pressure recovery more than what could be obtained in the diffuser. The basic function of the diffusers and scroll is to increase the static pressure of the fluid at the expense of reduced velocity.

The type of diffuser to be used in a centrifugal compression system depends on the type of application because the two main types of diffusers differ in operational characteristics. For example, the vaned diffuser generally gives higher maximum attainable compressor efficiency when compared to the vaneless diffuser, if the same impeller is used. However, the stable operating range of the compressor is usually larger in compressors with vaneless diffusers than in those with vaned diffusers. In addition, the vaneless diffuser has a very simple geometry and is easier to make when compared to a vaned diffuser.

1.1 Stability of Compression Systems

The nature of the oscillations that characterizes the operation of a centrifugal compression system at low flow rates have been investigated extensively due to the importance of such flow oscillations in the overall performance of the compressor. Under the applications of compressed gas at very high pressure or similar circumstances, operating the compressor below certain flow rate may result in flow instability. This instability is often associated with a drop in the compressor overall efficiency and sometimes results in self-induced vibrations which makes the operation of the compressor unsafe.

Compression systems of gas turbines can exhibit several types of instabilities: combustion instabilities, aero-elastic instabilities such as flutter and finally aerodynamic flow instabilities, which this investigation is restricted to. Two types of aerodynamic flow instabilities can be encountered in compressors. These are known as surge and rotating stall. The instabilities limit the flow range in which the compressor can operate. Surge and rotating stall also restrict the performance (pressure rise) and efficiency of the compressor. According to De Jager (1995) this may lead to heating of the blades and to an increase in the exit temperature of the compressor.

In particular, the stability in a compressor is the ability of a compressor to recover from disturbances that alter the compressor operation about an operational equilibrium point. Disturbances may be considered as transient or deliberate changes to the operating point. In the case of transient disturbances, the system is stable if it returns to its original operating point. If the disturbances drive the compressor away from the original point, the system is unstable. The steady state match between a compressor and its drive turbine or jet nozzle, which is perturbed by a transient change of mass-flow, is a good example of this case. When there are deliberate changes to the operating point, the performance is considered stable if a new operational equilibrium point can be achieved, e.g., shifting the operating point by changing the compressor shaft speed. If steady state operation at a new operating point is not possible, the system is unstable.

Stability in compressors may be studied from two different perspectives. The first is called operational stability, which deals with the matching of compressor performance with a downstream flow device such as a turbine or throttle. The second is aerodynamic stability, which deals with deteriorations in the operation due to flow separation, stall or surge.

The operational stability of a compression system depends on the characteristic of both the compressor and the downstream flow device. Mathematically, if the slope of compressor performance map is less than the slope of characteristic map of the throttle (points P1 and P2 shown in Figure 1.1a) the system is stable. Otherwise, as shown in Figure 1.1b for point P3, the system is not stable. Compressors, by design, usually operate near point P1 on the performance map shown in Figure 1.1. Operations at lower mass flow ratios (near point P2) can trigger instabilities as discussed later.

The stable range of operation of axial and centrifugal compressors is limited at both very high and very low mass flow rates, as shown in Figure 1.2. If the mass flow rate is too high, shocks will form and the flow through the compressor will be choked (sonic condition). On the other hand, as the mass flow rate through the compressor decreases, flow instabilities will occur. These instabilities include rotating stall and surge. If they are allowed to persist or grow, catastrophic damage to the compressor and the engine will occur. Surge, in particular, is to be avoided at all costs.

In looking at a map of the characteristic performance of a compressor, Figure 1.2, a dashed line known as the surge or stall line, can be seen. Rotating stall and surge usually occur at low flow rates, but may still occur on the right side of the surge line if the flow becomes unstable as a result of the instability. Therefore, a second line parallel to the surge line is usually introduced as a surge avoidance line. Another reason for introducing the surge avoidance line is that the compressor characteristic, and consequently the surge line, may be poorly known. Operating at the surge avoidance line provides a safety margin for the compressor operation and prevents the compressor from operating in a region where stall or surge may occur. The closer the operating point is to

the surge line, the greater the pressure ratio achieved by the compressor, but the greater the risk of stall or surge.

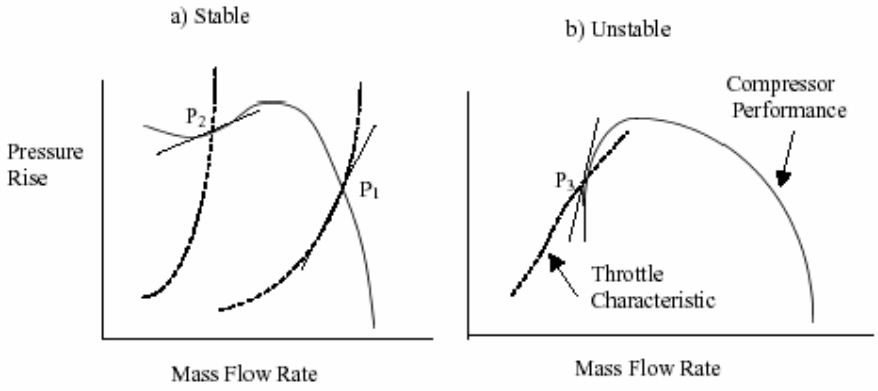

Figure 1.1: Operational Stability, Both the Compressor and Throttle Characteristics

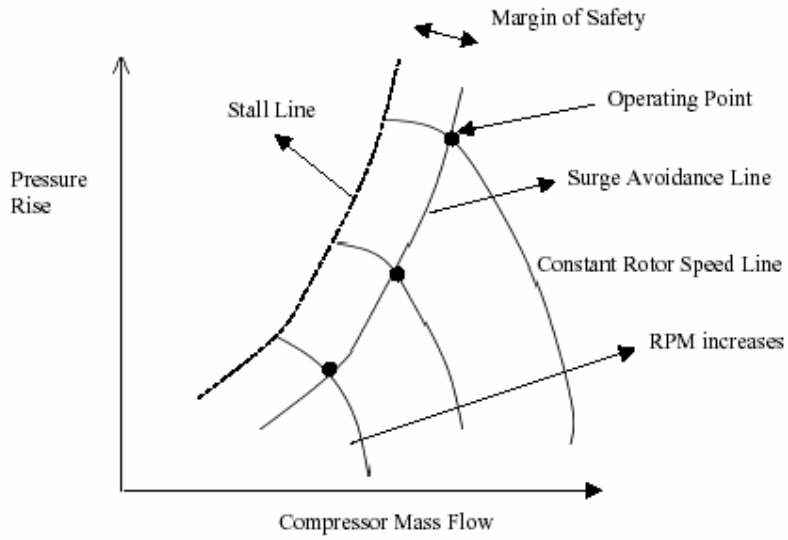

Figure 1.2: Effects of Rotor RPM on Compressor Performance and Stability

1.2 Rotating Stall

It is well known that one or more areas of the opposite flow (which rotate in the direction of the rotor rotation) appear in the annular channel of the compressor during the gradual flow regulation through the compressor. This phenomenon is called the rotating stall and the regions of the opposite flow are called the stalled regions. In many cases the transient to the rotating stall can lead to some undesirable consequences. An evident decrease of the pressure and of the flow is possible beyond the compressor, as well as the rapid decrease of the efficiency. The life time of the compressor blades is shortened which is caused by the tensions during the compressor operation in the region of the rotating stall. In regard to the above mentioned special attention has been paid to the rotating stall. The analyses show that two different types of the stall are presented in the propagation speed and in the number of the stalled regions.

Rotating stall can occur in both axial and centrifugal compressors. Although rotating stall is known to occur in centrifugal compressors there exists little theory on the subject.

Rotating stall has general characteristics of self-induced circumferential flow distortions, which may rotate around the component in which it occurs. When it occurs in the impeller, it is generally believed to have been caused by flow separation over the blades at large positive angles. This is treated in detail by Wang and Krstic (1997a), Sepulchre and Kokotovic (1996) and Protz and Paduano (1997). One of the characteristics of pure rotating stall is that the average flow is steady with respect to time, but the flow has a circumferentially non-uniform mass deficit. During rotating stall, the cyclical variation of the pressures on the blades can cause them to fatigue and eventually

break. The flow temperature may also increase due to uneven distribution of shaft work, reducing blade life.

Rotating stall is inherently a 2-D unsteady local phenomenon in which the flow is no longer uniform in the azimuthal direction. It often takes only a few seconds for rotating stall to build up, and the compressor can operate under rotating stall for several minutes before damage develops. Rotating stall can occur in both compressible and incompressible flow and it is not known for certain why all blades do not stall at the same time, Niazi (2000).

1.3 Literature Review

Researchers who have investigated flow instability in the impeller include Eckardt (1975, 1976), Krain (1981), Moore et al. (1984), D. Fred Marshall and James M. Sorokes (1996), S. Ljevar et al. (2006). On the other hand, William K. Ritter et al. (1946), Guy R. Bradshaw and Fugene B. Laskin (1948), Whitfield et al. (1976), Senoo and Kinoshita (1977, 1978), Ligrani et al. (1983), Abdelhamid and Bertrand (1980), Van Den Braembussche et al. (1980), Van Den Braembussche (1982), Abdelhamid (1980, 1983a and b, 1986), Frigne and Van Den Braembussche (1984a and b), Kinoshita and Senoo (1985), Ohashi and Shoji (1987), Mounts and Brasz (1992), Inoue (1983), Abraham Engeda (1994), Hunziker R and Gyarmathy G (2004), Watanabe et al. (1994), Saad A. Ahmed and Kamorudeen B. Abidogun (2000), Harri Pitk¨anen et al. (2000), Junichi Kurokawa et al. (2000), Ahmed, S. (2002a and b), Jean-Luc Di Liberti (2003), Giovanni Ferrara et al. (2003a, b, c, d, and e), Jeong-Seek Kang and Shin-Hyoung Kang (2003), Y. Levy and J. Pismenny (2003), C. Georgakis et al. (2003), Chaoqun Nie (2003), Gary J. Skoch (2003, 2004), Z. S. Spakovszky (2004), and Oleg Dubitsky and David Japikse

(2005) have studied and characterized flow instabilities associated with vane / vaneless diffusers. These studies were experimental and/or theoretical. A detailed discussion of some of the theoretical and experimental studies on radial vaneless diffusers of centrifugal compressors and blowers are presented in the following paragraphs.

Several analytical methods have been reported in the open literature for investigating rotating stall characteristics in vaneless diffusers. For example, William K. Ritter et al. (1946) designed an experimental radial-discharge impeller. By comparison with conventional impellers, a long radius of axial-plane curvature, a large axial depth, and a small inlet-blade root diameter. The impeller had conventional inlet-bucket bending and inlet and discharge diameters similar to an existing commercial impeller. The experimental impeller was tested as part of an investigation to improve the flow capacity of radial impellers. The performance effect of impeller passage area was investigated by tests of a series of three impeller front-shroud profiles.

Their conclusion was that the volume flow capacity of a conventional-type radial-discharge impeller may be greatly increased by utilizing a rear shroud profile of large radius of curvature and a large impeller axial depth to give a gradual change in direction through the impeller passage.

After a while, a lot of experimental works had been done on the vaneless diffuser initiating by Guy R. Bradshaw and Fugene B. Laskin (1948) used and studied different vaneless-diffuser diameters of 34, 27, 24, and 20 inches by successively cutting down a 34-inch vaneless diffuser and running it in a variable-component rig with a commercial mixed-flow impeller to determine the variations in both compressor and diffuser efficiency with diffuser diameter. Total-pressure surveys were made at several radii throughout the diffuser and these together with the standard measurements, provided

information concerning the magnitude and the location of the important losses in efficiency through the diffuser.

Substantial variations in over-all compressor performance were produced by change in diffuser diameter; over-all compressor efficiency increased with increasing diffuser diameter. In all the diffuser, losses in efficiency were limited to the entrance and exit regions, losses in the interior of the diffusers being negligible. Diffuser-exit losses increased from 3 to 15 points as diffuser diameter decreased, the losses being approximately inversely proportional to the square of the diffuser diameter. Finally, they reached to the conclusion that the mean entrance and exit losses varied only slightly with load coefficient and tip speeds.

Then to develop mathematical models for the flow in centrifugal compressors, Dean and Senoo (1960) proposed a theory based upon a simplified model for flow discharged from a centrifugal compressor or pump into a diffuser.

Jansen (1964a) performed an extensive analytical and experimental study of the flow in radial diffusers in the absence of unsteady flow. The results suggest that the formation of a boundary layer on the diffuser walls was the main cause of a loss in diffuser efficiency in the absence of wakes from the impeller or other unsteady flow phenomena.

Jansen (1964b) developed an analytical model for flow in a diffuser based upon superposition of a steady and an unsteady flow. The steady flow solution was assumed to be independent of the axial coordinate. In applications, the investigation indicates that steady flow may become unstable if separation occurs on either of the diffuser walls. In addition, with a given radius ratio, the flow can be made stable by decreasing the inlet

flow angle. The overall effect of decreasing either/or both of the diffuser width and the radius ratio was adjudged to be beneficial.

Johnston and Dean (1966) developed two simple analyses to predict losses in centrifugal compressor vaneless diffusers. These analyses were one-dimensional, axi-symmetric friction loss and sudden expansion mixing to account for losses in the diffuser caused by wakes of separated impeller blades. It was shown that these theories might be substituted for the more complex theory of Dean and Senoo.

Rodgers and Mnew (1975) developed an approximate analytical model for free rotating vaneless diffuser for application to high-pressure ratio single-stage centrifugal compressors. Diffuser performance was determined under braked and free rotating conditions at entry Mach numbers up to unity. A close examination of Mach number at the inlet and exit of the diffuser rotor indicate, according to the authors, that the flow was not a representative of the flow at the discharge of an actual centrifugal compressor impeller. Variations of measured static pressure recoveries, total pressure loss coefficients, air angles and Mach numbers were presented and may be valuable conditions for checkout of computer codes.

Senoo et al. (1977) proposed an analytical method to evaluate the flow behavior in vaneless diffusers assuming that the flow is not symmetric between the diffuser walls. Momentum integral equations, together with some special relations for the main flow or for the maximum velocity flow, were used in this analysis.

Van Den Braembussche et al. (1980) employed the Euler's equations to analyze an inviscid flow in the vaneless diffuser. These authors discussed the correlation of the data for rotating instabilities in vaneless diffusers and attempted to apply the

contradictory analytical methods of Jansen and Senoo in the correlations. According to these authors, most experimental results agree with one of the correlations (Jansen's or Senoo's). However, no conclusions can be drawn from this comparison. This almost suggests the existence of two distinct types of rotating stall in vaneless diffusers. In order to predict a better correlation in view of the recognized viscous effects, the authors formulated a new method based on the novel concept that the inviscid flow allows oscillations but the boundary layers are the destabilizing influence. The Euler equations were used. It was concluded that rotating stall in radial, vaneless diffusers is mainly potential core instability, triggered by viscous effects.

In another dimension, Kinoshita and Senoo (1985) compared their experimental results with the predictions of Senoo et al. (1977) for three very small specific speeds centrifugal compressors. The impellers were specially designed to be stall-free at very small flow rates so that the cause of rotating stall could be attributed to the vaneless diffusers. Their experimental results demonstrated that the blowers did not stall until the flow coefficient was reduced to very small values, which, according to the authors, had never been reported in the literature.

Jansen (1964b) demonstrated that the only condition for rotating stall to occur in the vaneless diffuser of a centrifugal blower is for the flow to reverse on any of the diffuser walls. As a result of this idea, Senoo and Kinoshita (1977) employed the momentum integral analysis of Senoo et al. (1977) to examine the conditions for reverse flow to occur on any of the diffuser walls. The authors presented the results of radial variations of the critical inlet flow angle (measured with respect to the tangential direction), the pressure recovery coefficient, and the boundary layer thickness with fixed diffuser width and inlet radius, and a constant Reynolds number (1.43×10^6). When no

flow distortions were instituted at the diffuser inlet, no reverse flow occurred. Small distortion of the radial component of velocity showed a significant effect on the critical flow angle. The results for distortion of the circumferential component of velocity were not specifically stated in this paper; however it appears that no reverse flow occurs. Furthermore, flow cannot reverse for locations where the boundary layer fills the diffuser.

Inoue and Cumpsty (1978) examined, theoretically, the behavior of distorted flow discharged from a centrifugal impeller within a vaneless diffuser by assuming small disturbances to a main flow. The inlet static pressure distribution was found in the calculation and allowance was made for circumferential non-uniformity in the relative flow angle. For a coordinate system fixed to the impeller, the relative radial and circumferential velocity components of the steady mean flow were related to the volume flow rate and the circulation around the impeller in an inertial coordinate system. The sum of the mean flow and an unsteady or perturbed flow was substituted into conservation of mass and momentum for a two-dimensional, incompressible, inviscid fluid and the equations were linearized. Superposition was employed to obtain an analytical solution with and without rotation. The boundary conditions employed were: no circumferential variation in static pressure at the diffuser outlet, circumferential component of the perturbation velocity was prescribed by a Fourier series (only for the rotational case) and the radial component of fluctuating velocity was prescribed as a Fourier series for both rotational and irrotational flows.

Results for irrotational disturbances showed that distortion of radial velocity and total pressure attenuates for ratio of radius to impeller exit radius of 1.2 while static pressure distortions disappeared for radius ratios greater than 3. Increasing the wave number (or the number of blades) produces more rapid decay of distortion. Diffuser outlet

radius produced little effect on magnitude of total pressure perturbations for outlet radius/impeller radius. For rotational flow, however, the radial velocity and static pressure fluctuation attenuates rapidly but the tangential velocity and total pressure fluctuations grow close to the impeller and attenuate much more slowly. With increasing flow rate, the amplitude of the distortion in radial velocity decreases. In general, it was concluded that the rotational fluctuations decay more slowly than the irrotational ones. It was also found that the phase angle between the radial and tangential velocity fluctuations at the diffuser inlet has a significant influence on the disturbances and amplification of the radial velocity fluctuations was actually found in the inlet region. For 20 or more impeller blades, it was discovered that the circumferential variation in relative flow angle was smaller and the results of this investigation were similar to the results of Dean and Senoo but showed a significant disagreement for impeller blades less than 20.

Abdelhamid (1980) used the linearized equations of motion for unsteady flows to analyze the self-excited flow oscillations that occur in radial diffusers of centrifugal compressors. Solutions of the differential equations were made to satisfy boundary conditions at diffuser inlet and exit which, in typical conversion systems, represent the coupling between the diffuser and upstream and downstream components. The results indicate that the rotational speed of the stall pattern was dependent on the diffuser radius ratio and the coupling conditions between the impeller and the diffuser. It was shown that the dependence of the onset of the flow oscillations on the diffuser radius ratio was strong if the conditions at diffuser inlet are such that low speed rotating stall patterns are generated in the diffuser. The author predicts that the onset of high speed rotating stall patterns was more affected by the coupling conditions between the impeller and the diffuser than by the diffuser radius ratio. The flow in the vaneless diffuser was assumed to be two-dimensional, incompressible and inviscid. Superposition of a steady mean flow

and an unsteady perturbation flow was employed in the equations for conservation of mass and momentum and the equations were linearized. The mean flow was assumed to be axi-symmetric and the perturbation quantities were assumed to be harmonic functions of time and circumferential angle. The flow from the diffuser was assumed to discharge into a large reservoir with constant pressure. The unsteady diffuser inlet conditions were obtained from a linearized one-dimensional analysis applied to the impeller passage. An indirect method of solution was employed whereby the diffuser inlet conditions for neutral stability were computed for given number of stall cells, inlet flow angle for the diffuser, and outer diffuser radius.

Frigne and Van Den Braembussche (1985) proposed a theoretical model for rotating stall in the vaneless diffuser of a centrifugal compressor. It consists of a time-evaluative calculation of the strong interaction between the inviscid flow core and the unsteady boundary layers along the walls. Depending on the diffuser geometry and the diffuser inlet flow angle, it was shown that a transient fluctuation of the outlet static pressure will generate a rotating flow pattern, if the periodicity of this perturbation corresponds to the experimentally observed number of cells. Their theoretical model employs an iterative, boundary layer approach. The Euler's equations for the inviscid core were manipulated into the form of the vorticity transport equation with the definition of vorticity applied to compute the velocity field.

Y. Levy and J. Pismenny (2003) analyzed various aspects of numbers and speed of stall cells using an original interpretation method based on the pressure distribution in the circumference of a specific transverse cross-section at a specific time as the number of stall cells and their rotational speed are distinctive features of the rotating stall phenomenon and play an important role in the prediction and analysis of the pressure

fields during rotating stall. This characteristic is similar to that of the pressure variation with time at a certain location on the compressor circumference. It is shown that whereas the numbers of stall cells in different transverse cross-sections of a multistage compressor may vary, the pressure field rotational speeds and accordingly the rotation speeds of all stall cells seem to be the same.

In conclusion, the frequency of pressure oscillation and the frequency of cell rotation are different parameters and may have identical or different values. The characteristic of pressure variations in the circumference of a specific transverse cross-section at a specific time appears to be similar to the characteristic of pressure variation with time at a certain location on the compressor circumference of the same cross-section.

Z. S. Spakovszky (2004) reported for the first time the rotating stall waves that travel against the direction of rotor rotation and introduced a new, low-order analytical approach to model centrifugal compressor stability. The model is capable of dealing with unsteady radially swirling flows and the dynamic effects of impeller-diffuser component interaction as it occurs in centrifugal compression systems. It is experimentally demonstrated that this injection scheme is robust to impeller tip-clearance effects and that a reduced number of injectors can be applied for similar gains in surge-margin. In addition, guidelines are given for the design of centrifugal compressors with enhanced stability.

In summary, his work reports a new phenomenon related to rotating stall in centrifugal compressors. The model findings together with definite measurements explain the mechanism for first-ever observed backward traveling rotating stall in centrifugal compressors. The results firmly establish the connection between the experimentally

observed dynamic phenomena in the centrifugal compressor and first principles based coupling criterion.

Oleg Dubitsky and David Japikse (2005) developed a new vaneless diffuser model. Upon thorough examination of the change in average total pressure, the average static pressure and the average flow angle through a vaneless diffuser. Consequently, a new model was built. It was learned that it was necessary to use a two-zone model of the flow entering the vaneless diffuser and to carefully model the two-zone degradation as the flow passes through the vaneless diffuser. The new model is presented with detailed testing. The impact upon future design is outlined, and the expectation is established that various future designs will require the integrity of the new model.

They concluded that the periodic model affords much improved modeling of both total pressure and flow angle along the diffuser radius. While the older models are approximately correct near the end of very long vaneless diffusers, the new model is necessary to understand the inlet and developing flow. It is necessary and appropriate to use the new periodic model only with two-zone impeller modeling. Improved impeller and diffuser models are resulted from their work.

Further, researches are done on the inspection of rotary stall by using predictable models. Abraham Engeda (1994) worked on rotating stall and flow induced vibration for centrifugal compressors by predicting of the inception of rotating stall for a specific geometry and operation, let alone to directly correlate a stall with a blade vibration, as rotating stall is mainly caused dangerous compressor and blade vibrations. Results examined the basic knowledge in both rotating stall and blade vibration, in order to explore whether a knowledge-stage has been reached to enable a direct correlation.

Computational methods, numerical techniques, like computational fluid dynamic are used to get very accurate simulations and description of the flowfield in the centrifugal compressor. D. Fred Marshall and James M. Sorokes (1996) provided detailed description of the flow field, and other source of the excitation. This included the use of computational fluid dynamic (CFD) analytical results to describe the flow where applicable.

Their assessment was that the forces acting within centrifugal compressor can cause a variety of responses in the rotor system. A general discussion of compressor rotor-dynamic behavior was presented including discussions on free and forced vibrations. Distinctions were made between significant subsynchronous vibration characteristics, such as rotor instability, and aerodynamically forced vibration of various types. Ways to distinguish between these various causes using vibration data were also provided.

Furthermore, various aerodynamic phenomena that contributed to increased radial vibrations were discussed including impeller stall, diffuser stall, and interaction "stall". A general description of the flow physics was provided as were the commonly held identification criteria for each., Finally, various frequency spectra and waveform plots were offered to illustrate how the various phenomena may appear in vibration or pressure pulsation data: (i.e. on a spectrum analyzer or oscilloscope).

Harri Pitk¨anen et al. (2000) performed and practiced the time-dependent flow in a radial compressor with a vaneless diffuser and a volute is simulated. A quasi-steady approach, where the impeller is rotating and the rest is stationary, and a time-accurate simulation are performed. In the latter case a sliding-mesh technique is utilized and second-order fully implicit time integration is applied. Dual time-stepping is performed

inside a physical time step. In both cases the Baldwin-Lomax turbulence model is used. Results obtained from the simulations are compared with the available experimental data.

Recently, S. Ljevar et al. (2006) reported a numerical study on the vaneless diffuser core flow instability in centrifugal compressors. Their analysis is performed for the purpose of better understanding of the rotating stall flow mechanism in radial vaneless diffusers. A commercial code with the standard incompressible viscous flow solver is applied to model the vaneless diffuser core flow in the plane parallel to the diffuser walls. At the diffuser inlet, rotating jet-wake velocity pattern is prescribed and at the diffuser outlet constant static pressure is assumed. Under these circumstances, two-dimensional rotating flow instability similar to rotating stall is found to exist. Performed parameter analysis reveals that this instability is strongly influenced by the diffuser geometry and the inlet and outlet flow conditions.

As a conclusion, their analysis does not explain the flow mechanism of rotating stall, but it suggests a few of the physical phenomena that might contribute to the rotating stall mechanism in the wide vaneless diffuser. Current model points towards the possibility that the core flow instability might be one of the flow mechanisms responsible for the rotating stall in wide vaneless diffusers.

Other theoretical works on flow instability in vaneless diffusers of centrifugal compressors include those of Moore and Moore (1980), Cumpsty and Greitzer (1982), Frigne and Van Den Braembussche (1985), and Moore (1989). These works were based on the flow pattern in the blade-to-blade plane. Although these theories have been developed for particular cases that restricted their applicability, the results from these theoretical efforts enabled rotating stall main characteristics to be calculated.

In summary, the analytical methods employed for the study of the flowfield characteristics in the vaneless diffusers are momentum integral equations of the boundary layer (Jansen (1964b), Schumann (1985), Dou and Cheng (1986)), stability of the inviscid axi-symmetric flow in the diffuser or the interaction of the inviscid core with the boundary layer for predicting rotating stall (Jansen (1964b), Abdelhamid (1980), Frigne and Van Den Braembussche (1985), Moore (1991)), and predicting the flow losses and the performance of the diffusers (Johnston and Dean (1966), Bammert et al. (1978, 1980), Dou (1989)).

Experimental works on vane / vaneless diffusers are generally of two types, steady and unsteady flow investigations. Eckardt (1975) and Krain (1981) have studied steady flow at the impeller exit while the steady flow measurements made by Senoo and Ishida (1975) were carried out in the diffuser. For these and other similar works on steady flow measurements in the diffuser, the onset of rotating stall and its resulting effect on compressor performance were not investigated as expected.

Many investigators have reported unsteady flow characteristics in the diffuser. They include Senoo and Kinoshita (1977 and 1978), Whitfield et al. (1976), Van Den Braembussche et al. (1980), Van Den Braembussche (1982), Ligrani et al. (1983), Arnulfi et al. (1996), Ishida et al. (1995), and Abdelhamid (1980). Pressure transducers and hot-wire anemometers were mainly the measurement tools employed in these studies. In addition, different analyzing tools have been used. For instance, Abdelhamid (1983a) used spectrum analyzers that enabled him to extract all possible perturbations, at a fixed flow rate, propagating at different frequencies and their direction of rotation relative to the impeller rotation. On the other hand, Otugen et al. (1988) determined the stall characteristics from the physical examination of the time-series signal output of the

transducers photographed from the oscilloscope display. As such, relative dominance of the propagating frequencies was not reported. The findings of Senoo and Kinoshita (1978) and Abdelhamid and Bertrand (1980) indicated that pressure fluctuations were sinusoidal at the onset of instability in the diffuser. In addition, these results showed that lines of equal phase were radial. Frigne and Van Den Braembussche (1984a) observed that the amplitude and rotational speed of the pressure pattern increased when the mass flow rate was decreased. Saad A. Ahmed (2002) investigated detailed measurements of the unsteady periodic-flow characteristics were taken in a radial vaneless diffuser. G. Ferrara et al. (2003a) conducted a series of experimental researches and tests on the rotating stall in centrifugal vaneless radial diffuser. Test results are shown in terms of critical diffuser inlet flow angles, flow coefficients at stall inception and stage working ranges. The main task of the presented work is to increase the knowledge and the amount of available data to characterize rotating stall phenomena. Chaoqun Nie (2003) focused on implementing active control and intelligent casing treatment, and expanding operational ranges of compressors to improve their operational stability. C. Georgakis et al. (2003) illustrated that multi-sensor fast response probes are widely used on several applications concerning unsteady flow measurements. G. Ferrara et al. (2003c and d) reported the comparison of the tests results in terms of impeller influence on diffuser stability. G. Ferrara et al. (2003d) applied successfully low solidity vane diffuser on centrifugal compressor especially for high pressure applications. In-depth discussions of some of the experimental measurements in radial vaneless diffusers are provided in the following paragraphs.

Abdelhamid and Bertrand (1980) conducted experiments to determine the characteristics of oscillating flows in a centrifugal compression system with vaneless diffusers. The system was operated without a diffuser and with eight different diffuser

configurations to determine the effects of diffuser diameter and width ratios on the unsteady behavior of the system. Mean and fluctuating velocity and static pressure measurements were carried out in the time and frequency domains. The system without a diffuser was found to be stable at all operating conditions. The installation of any of the eight diffusers resulted in the generation of self-excited oscillations at some operating conditions. The main thrust was to determine the effects of diffuser geometry on the generation of self-excited oscillations in the system. For each geometrical configuration and speed of the system, the mass flow rate was gradually reduced (thereby increasing the flow angle of attack on the blades) and the system performance was observed. After the onset of oscillations, the waveform frequency and lobe number of the fluctuating pressure and velocity were measured for every mass flow rate. In all cases studied, the slope of the curve of system pressure coefficient as a function of the flow coefficient was negative when the oscillations were first detected. Data by other investigators indicated the occurrence of oscillations when the pressure coefficient-flow coefficient curve has positive slope. The critical flow coefficients (upper bound for detection of oscillations) were dependent on diffuser diameter and width ratios. With width ratios less than 0.038, the critical flow coefficient decreases with diffuser diameter ratio. Also, for constant diffuser diameter ratio, the critical flow coefficient increased with decrease in width ratio with greater sensitivity as the diameter ratio decreases. The rotational speeds of the oscillation patterns had a strong dependence on the diffuser diameter ratio and weak dependence on the width ratio. The distortion patterns rotated in the same direction as the impeller but at a fraction of the speed. The fraction became smaller as the diffuser diameter increased. Patterns possessing a larger number of lobes rotated more slowly. Since several characteristics of the distortion patterns differed from the characteristics observed by other investigators, it was proposed that more than one set of flow conditions

could produce the distorted patterns. An alternate suggestion might be that patterns have different characteristics for different flow conditions.

The distinction between impeller and diffuser rotating stall; the triggering mechanism of diffuser rotating stall and resulting flow patterns; and stability criteria for diffuser rotating stall and prediction of relative rotational speeds were experimentally investigated by Van Den Braembussche (1982). The author compared the unsteady flow patterns observed at rotor inlet and inside the vaneless diffuser and concluded that a distinction should be made between impeller rotating stall and diffuser rotating stall. The unsteady flow theory of Jansen was shown to provide a valuable prediction of the diffuser rotating stall, if combined with an improved boundary layer calculation method. The first series of tests examined flow in an axial compressor without pre-rotation. Only one type of stall was found and judged to originate in the rotor. The oscillations gradually increased in amplitude and extended downstream. One stall cell rotated at high relative velocity. With pre-rotation, however, the impeller characteristic map shifts 6o toward higher flow angles and a 6o increase in critical flow angle for impeller stall was obtained. With a further 1o increase in the flow angle, impeller stall vanished but the diffuser stall remained unchanged. Another slight increase (0.5^{o}) in the flow angle produced instability only in the diffuser with two stall cells (instead of the previous one cell) at a lower frequency. The first series of tests with a centrifugal compressor showed no discontinuity in the performance curves at the onset of rotating stall. In the second series of tests (again with a centrifugal compressor), rotating stall occurred at a flow coefficient of 0.0088. For this test series, oscilloscope traces from hot film and hot wire instrumentation were employed to define the characteristics of stall and surge in the compressor. The conclusion was that the linearized analysis of Jansen (1964b) and Abdelhamid (1980) are valuable for predicting rotating stall.

Abdelhamid (1983b) conducted an experiment to evaluate the effectiveness of axi-symmetric diffuser exit throttle in delaying the occurrence of self-excited flow oscillation in vaneless diffusers. This technique involved installing sharp-edged rings at the diffuser exit in order to change the exit flow area. Tests were carried out with the rings attached to one or both of the diffuser walls. Steady and unsteady flow measurements were used to determine the flowfield in the diffuser at the onset of flow oscillations. The results presented showed that the occurrence of flow oscillations was continuously delayed as the diffuser exit flow area was reduced. In addition, the use of the throttle rings at the exit of the diffuser resulted in the overall improvement of diffuser performance at low flow rates.

Frigne and Van Den Braembussche (1984a) described the results of an experimental investigation of the sub-synchronous rotating flow patterns in a centrifugal compressor with vaneless diffuser. Several compressor configurations were examined by means of hot wire anemometry.

Ahmed, S. A. (2002) investigated detailed measurements of the unsteady periodic-flow characteristics were taken in a radial vaneless diffuser. The measurements were made using hot-wire miniature probes and several static- and dynamic-pressure transducers. The rig was found to be stable at all operating conditions without the vaneless diffuser. The mass-flow rate through the diffuser was gradually reduced until full-fledged flow instability in the diffuser occurred. This enabled the onset and propagation of rotating stall to be fully described. The results agreed with earlier tested data on the condition of instability. In addition, the results showed that there is a recirculation region on the diffuser shroud wall with and without stall; however, it grown in size to fill the entire diffuser after instability has set in. Furthermore, the data indicated

that the maximum number of stall cells found is limited to two for the current diffuser test conditions.

G. Ferrara et al. (2003a) conducted a series of experimental researches and tests on the rotating stall in centrifugal vaneless radial diffuser. Test results are shown in terms of critical diffuser inlet flow angles, flow coefficients at stall inception and stage working ranges. The main task of the presented work is to increase the knowledge and the amount of available data to characterize rotating stall phenomena, in particular for very narrow stages. Research on the rotating stall in centrifugal compressors, focusing on a final stage configuration with the volute presence of high-pressure centrifugal compressors is assessed. Extensive experimental research focused on free vortex diffuser rotating stall characterization is reviewed as well.

In conclusion, their study clearly illustrated how the presence of the volute at the discharge of the diffuser could have a significant impact on the free vortex diffuser stability, in particular when the length of the diffuser itself is reduced.

Chaoqun Nie (2003) focused on the aerodynamic mechanism, identifications, and advanced capturing methods of stall inception, making use of active control and intelligent casing treatment, and expanding operational ranges of compressors to improve their operational stability. The aim of his experimental research is imperative to study the interconnection between radial loading distribution of rotor and patterns of stall inception. Whereas, the main experimental results are:

1) With two sets of different pre-whirl order of inlet guide vanes (IGV), the incidences along blade height are modified, which provide different radial loading distribution.

2) It is discovered that spiky stall inception corresponds to high loading distribution near the tip of rotor blade. However modal stall inception is related to low loading distributed near the tip.

3) The different loading conditions near the hub of the rotor do not apparently change the pattern of stall inception.

4) It is also found that adjusting the stagger angles of IGVs can change the steady characteristics and stall inception pattern.

C. Georgakis et al. (2003) illustrated that multi-sensor fast response probes are widely used on several applications concerning unsteady flow measurements. Also using the single sensor probes are sometimes preferred in the survey of the unsteady flows in the turbomachinery applications. This in turn can be of benefit due to the limited space often found in compressors. They examined the behavior of a fast response probe in detail.

G. Ferrara et al. (2003d) applied successfully low solidity vane diffuser on centrifugal compressor especially for high pressure applications. In addition to a series of tests on five different low solidity vane diffusers, the configurations have been methodically changed in order to achieve a design of experiments analysis: the influence of the blade leading and trailing edge radius, maintaining the same solidity and null deflection, was investigated as well. The aim of their work was to present and discuss the influence of these parameters on stall inception and on working range.

In particular, the following pertinent conclusions may be drawn from their work: The high natural frequency of the sensors, in comparison with the blade passing frequency, was indispensable in allowing the unsteady measurements to be taken at high

rotor speeds. The fast response probe was found to be largely sensitive to pressure fluctuations that, after correction with temperature, result in an absolute pressure with temperature, result in an absolute pressure reading. The curve fitting algorithms showed consistency with the actual measurements, whilst the data reduction method followed by the 'least squares' approach proved to be satisfactory.

Once the stall phenomenon is understood, the natural question that follows is how to suppress it whenever it occurs. In other word, how could rotate stall occurrence be delayed to a much lower flow coefficient than normal? There is scarcity of work in this area. Several techniques have been used to delay the occurrence of flow oscillations in centrifugal compression systems. Lawless and Fleeter (1991 and 1993) proposed a model for an active control of rotating stall in low-speed centrifugal compression systems. This model was based on the assumption that rotating stall in a centrifugal compressor can be modeled as a weak disturbance that grows in a region of preferential application on the compressor map. The proposed control scheme involves the introduction of a weak inlet distortion that was meant to damp out the stall condition at its onset before reaching significant amplitude. Since, according to the authors, there have been no experimental studies of active control of rotating stall in centrifugal compressors, an experimental study was embarked upon by them (see Lawless and Fleeter (1999)) aimed at investigating and validating the centrifugal compressor rotating stall modeling and the conclusions drawn from their model under reference. The experimental control technique involved the use of a phase-controlled inlet distortion generated by an array of 12 air injection ports located in the compressor inlet end wall. The active control of one-cell rotating stall was successfully demonstrated. Their experimental results showed that the control technique used in suppressing rotating stall succeeded in improving the stall margin only slightly. On a general analysis, however, the control technique demonstrated

an ability to restore system stability to the compressor when exhibiting a developed stall condition.

In another dimension, Abdelhamid (1986) investigated the effects of using small exit vanes on the characteristics of an otherwise vaneless diffuser. The steady and unsteady characteristics of the diffuser were evaluated as the angle of the vanes was varied at several diffuser inlet conditions. The results showed that the influence of the exit vanes on the diffuser flowfield increased as the diffuser inlet flow angle was decreased. Appropriate setting of the angle of the diffuser exit vanes enabled the elimination of self-excited flow oscillations in the diffuser.

Investigations are continued developing up. Thus, Hunziker R and Gyarmathy G (1994) tested a centrifugal compressor with three different diffusers with circular-arc vanes. The vane inlet angle was varied from 15 to 30 deg. Detailed static wall pressure measurements showed that the pressure field in the diffuser inlet is very sensitive to flow rate. The stability limit regularly occurred at the flow rate giving the maximum pressure rise for the overall stage. Mild surge arises as a dynamic instability of the compression system. The analysis of the pressure rise characteristic of each individual subcomponent (impeller, diffuser inlet, diffuser channel, etc) reveals their contribution to the overall pressure rise. Results showed that the diffuser channels played an inherently destabilizing role while the impeller and the diffuser inlet are typically stabilizing. And the stability limit was mainly determined by a change in the characteristic of the diffuser inlet. Further, the stability limit was found to be independent of the development of inducer-tip recirculation.

Kamorudeen B. Abidogun and Ahmed, S. A. (2000) conducted an experimental investigation of flow characteristics in a radial vaneless diffuser of a centrifugal blower:

Their results showed that the flow exiting the impeller is strongly skewed as revealed by the triple velocity product correlations. The non-uniformity in the radial as well as tangential velocity profiles disappeared as pressure builds up, with radial distance, in the diffuse. Reynolds stresses profiles showed that turbulent mixing, which also diminishes with diffuser radial distance, is more in the vicinity of the shroud as compared to the hub.

Jeong-Seek Kang and Shin-Hyoung Kang (2003) presented an experimental and analytical investigation of a rotating stall inception in a vaneless diffuser of a centrifugal compressor. Eight fast-response pressure transducers are equally spaced around the circumference at the inlet and exit of a parallel vaneless diffuser. Instantaneous pressure data is measured near the stall inception point and characteristics of a rotating stall, a stall-initiating mechanism, a stall precursor and its warning schemes are discussed.

Finally the outcome of these warning schemes is useful because their warning time is long enough to be applied in active control of a compressor stall.

G. Ferrara et al. (2003c) reported the comparison of the tests results in terms of impeller influence on diffuser stability. The impeller influence was analyzed in terms of both:

• Working range

The impeller with the greatest diffuser outlet width/radius value allows the use of a larger diffuser in order to get the same working range value. This is a great advantage in terms of pressure losses in the diffuser and so, of overall performance. In addition, the useful effects in terms of diffuser stability are greater for diffusers with greater diffusion ratios.

• Performance

In terms of efficiency at design point, the impeller influence does not seem to play a key role, since for both the impellers, and the trends are quite similar with respect to diffuser width.

Gary J. Skoch (2004) resulted from a series of experiments to investigate whether centrifugal compressor stability could be improved by injecting air through the diffuser hub surface. The research was conducted in a 4:1 pressure ratio centrifugal compressor configured with a vane-island diffuser. Injector nozzles were located just upstream of the leading edge of the diffuser vanes. Several injection flow rates were tested using both an external air supply and recirculation from the diffuser exit. The results also suggested that a different application of hub-side techniques may produce a range improvement in centrifugal compressors.

Further, the benefits to centrifugal compressor stability provided by injecting air adjacent to the diffuser vanes through the hub surface of the diffuser were evaluated. Diffuser data from the nozzle configurations without injection were compared to data obtained in earlier experiments where control-tubes inserted through the shroud surface were found to improve stability. A comparison of the change in diffuser performance between the various hub nozzle orientations and different immersions of the control tubes found that both had a similar effect.

Due to the great number of geometries tested it is possible to analyze their influence on stall behavior. As previously said, four test parameters influence on stall, which they are:

1. Peripheral Mach Number (Mu) 2. Diffuser Width (D)

3. Diffusion Ratio (DR) 4. Pinch Shape (P)

And thus, G. Ferrara et al. (2003b) experienced three impellers characterized by different blade-outlet-width-to-impeller- radius-ratios. The basic configuration comprises a 1:1 geometrical scale stage with a return channel upstream, a 2D impeller with a vaneless diffuser and a volute with a constant cross sectional area downstream. Several diffuser types with different widths, pinch shapes and diffusion ratios were tested.

In their investigation, a wide-ranging study on the centrifugal compressor rotating stall, focused on a last stage configuration of high pressure centrifugal compressors including a volute, has been presented.

Giovanni Ferrara et al. (2004) stated a wide-ranging study on the influence of diffuser geometry on high pressure last stage centrifugal compressors. Their study was to characterize the geometry modifications in terms of stall behavior and stage performance. The use of dynamic pressure sensors, their position, and the applied analysis methodology, provided much information on stall inception and evolution.

As can be easily deduced from the discussions so far, experimental and theoretical investigations of rotating stall characteristics in the vaneless diffuser of a centrifugal compressor or blower has attracted the attention of many researchers over the last four decades. Each of these investigators concentrated on one factor or the other that a summary of some of the important features discussed in the literature is essential. Table 1.1 shows a summary of some of the investigators and the important features examined. The table also indicates whether the investigation was experimental and/or theoretical with a brief mention of the instrumentation used and summary of the findings.

Table 1.1: Summery of Investigations on Rotating Stall (2006 - 1980)

Author (s)	Investigation	Instrumentation & major factors investigated
S. Ljevar et al. (2006)	Theoretical	A commercial code with the standard incompressible viscous flow solver used; rotating stall flow mechanism in radial vaneless diffusers investigated; two-dimensional rotating flow instability similar to rotating stall found.
Oleg Dubitsky and David Japikse (2005)	Theoretical & Experimental	New vaneless diffuser model used; both total pressure and flow angle along the diffuser radius investigated; periodic model affords much improved modeling of both total pressure and flow angle along the diffuser radius reported.
Gary J. Skoch (2004)	Experimental	Injecting air through the diffuser hub surface used; compressor flow range investigated; different application of hub-side techniques may produce a range improvement in centrifugal compressors found.
Z. S. Spakovszky (2004)	Theoretical & Experimental	New low-order analytical approach to model centrifugal compressor stability used; backward traveling rotating stall investigated; the connection between the experimentally observed dynamic phenomena and first principles based coupling criterion established.
Giovanni Ferrara et al. (2004)	Experimental	Diffuser geometry on high pressure last stage centrifugal compressors used; stall behavior and stage performance investigated; a lot information on stall inception and evolution provided.
G. Ferrara et al. (2003d)	Experimental	Five different low solidity vaned diffusers used; stall inception and working range investigated
G. Ferrara et al. (2003c)	Experimental	Impeller with the greatest diffuser outlet used; working range and performance investigated; diffuser stability is greater for diffusers with greater diffusion ratios observed.

(Table Continues)

Author (s)	Investigation	Instrumentation & major factors investigated
Jeong-Seek Kang and Shin-Hyoung Kang (2003)	Theoretical & Experimental	Eight fast-response pressure transducers used; rotating stall inception in a vaneless diffuser of a centrifugal compressor investigated; one-cell, two-cell and three-cell found.
Gary J. Skoch (2003)	Experimental	Both the compressor discharge and an external source used; stable flow range, parametric variations of injection angle, injection flow rate, number of injectors, injector spacing, and injection vs. bleed investigated; Surge margin improved.
Y. Levy and J. Pismenny (2003)	Experimental	An original interpretation method based on the pressure distribution in the circumference of a specific transverse cross-section used; rotating stall phenomenon investigated; the frequency of pressure oscillation and the frequency of cell rotation are different parameters and may have identical or different values concluded.
C. Georgakis et al. (2003)	Experimental	Multi-sensor fast response probes used; behavior of a fast response probe investigated; the high natural frequency of the sensors was indispensable in allowing the unsteady measurements to be taken at high rotor speeds concluded.
Chaoqun Nie (2003)	Experimental	Active control and intelligent treatment used; operational stability investigated; the interconnection between radial loading distribution of rotor and patterns of stall inception studied.
G. Ferrara et al. (2003a)	Experimental	Critical diffuser inlet flow angles, flow coefficients at stall inception and stage working ranges investigated; increase the knowledge and the amount of available data to characterize rotating stall phenomena presented.

(Table Continues)

Author (s)	Investigation	Instrumentation & major factors investigated
Saad A. Ahmed (2002)	Experimental	Hot-wire miniature probes and several static- and dynamic-pressure transducers used; two rotating stall found; rotating stall investigated.
Kamorudeen B. Abidogun and Saad A. Ahmed (2000)	Experimental	Vaneless centrifugal compressor used; flow characteristics in a radial vaneless diffuser of a centrifugal blower investigated; flow exiting the impeller is strongly skewed as revealed by the triple velocity product correlations resulted.
Harri Pitk¨anen et al. (2000)	Theoretical & Experimental	Computational fluid dynamic with time-dependent flow in a radial compressor with a vaneless diffuser used; quasi-steady simulation of the whole compressor is almost as accurate as the time-accurate calculation concluded.
Junichi Kurokawa et al. (2000)	Theoretical	A passive method of utilizing radial shallow grooves used; significant decrease in tangential velocity and a remarkable increase in radial velocity summarized.
Lawless and Fleeter (1999)	Experimental	Microphones and hot-film sensors used; found up to three stall cells.
Arnulfi et al. (1996)	Experimental	Single and X-wires used; found one stall cell; blower stages (two and four stages tested), and impeller speed investigated.
Tsujimoto et al. (1996)	Theoretical	Two-dimensional inviscid and incompressible flow analysis used; diffuser radius ratio investigated.
Abdelhamid and Bertrand (1980)	Experimental	Single hot-wire and pressure sensors used; found up to four stall cells; diffuser radius and width ratios investigated.

CHAPTER 2

RESEARCH OBJECTIVES

2.1 Contradictory Results & the Importance of Current Research

From the available results in the literature so far, there is not enough information that guarantees a clear and conclusive understanding of rotating stall in vaneless diffusers. In addition, there are apparent contradictions of the flowfield characteristics in the open literature due to the complexity of the flow in the vaneless diffuser (Van Den Braembussche (1984, 1985), Greitzer (1981), Japikse (1984), Japikse and Baines (1994), Pampreen (1993), and Cumpsty (1989)). In particular, reported propagating frequencies and their periodicities, as available in the open literature to date, differ from one investigator to the other. For example, Abdelhamid and Bertrand (1980) found up to four rotating stall cells in their study with their number increasing while decreasing flow coefficient. On the other hand, Jansen (1964b) and Watanabe et al. (1994) reported only a maximum of two stall cells. The periodic pattern with single stall cell was found to be dominant at lower flow coefficient when compared to the one with two stall cells.

It is clear from the above review that the phenomenon of rotating stall in vaneless diffuser is not well understood. The onset of stall and the mechanism that triggers stall are not clear. The area of contention includes:

- There is no agreement on whether the existence of zones of separated boundary layers on the diffuser walls are a necessary condition for stall to occur?

- Would one zone of separation be enough for strong fluctuations to occur or more than one zone is required?

- It is not well-understood how and under what conditions would these zones start to appear?

2.2 The Focus of Current Work

The answers to the questions in the preceding sub-section, which are vital for a proper understanding and description of the inception and propagation of rotating stall in vaneless diffusers, require more experimental investigations for a conclusive and concise description to be made. Therefore, the current effort is aimed at answering/clarifying some of these questions. To achieve this objective, a detailed experimental investigation of the vaneless diffuser flowfield was undertaken. This includes a comprehensive measurement of diffuser flow characteristics before and after rotating stall inception. A number of parameters were varied to see what effect they have either on the flowfield characteristics in the diffuser or the overall performance of the compressor. The variables include the impeller speed, the diffuser width, mass flow rate through the compressor, and the diffuser width blockage ratio. The detailed analysis of the flowfield in the diffuser presented in this dissertation ensures a clearer qualitative and quantitative description of rotating stall characteristics from its point of inception to its full development. In particular, the number of rotating stall cells associated with centrifugal compressors / blowers and their speed of rotation, for which there has been no agreement in the literature, were clarified.

CHAPTER 3

EXPERIMENTAL FACILTIY

3.1 Test Facility

The experimental test rig of a centrifugal compressor, a schematic of it is shown in Figures 3.1 and 3.2, initially was designed and built in house at KFUPM then it is shifted and re-assembled again at AUS. It consists of a well-designed air intake for minimum losses and near uniform inlet velocity distribution, impeller housing, an actual impeller, and a vaneless diffuser. The centrifugal impeller was used to deliver the flow into the vaneless diffuser. A moving, streamlined, axisymmetric plug mounted at the air intake was used to control the mass flow rate through the impeller. The setup was also equipped with a variable speed motor to allow for speed control.

The impeller, provided by Saudi Arabian Airlines, has 28 blades with no splitter plates at its inlet. The blades are aligned in the radial direction. The diameter of the pipe at the impeller inlet is 185 mm, while the impeller has a diameter of 228 mm at its outlet. The diffuser has parallel walls with an adjustable maximum channel height of 12.6 mm, which is the same as the impeller tip-height. Diffuser outlet to inlet diameter ratios, D_o / D_i; 1.5, 1.75, and 2.0 were investigated. The diffuser inlet diameter is 229 mm. The impeller is driven by a variable speed, 2.36 hp FIMEC electric motor with a maximum speed, N, of 2350 RPM (2 KW, 5.1 A, 380 V, Shaft Type P, Standard Bottom Fixing, and IEC 34-1). The speed of the motor was varied from 1000 RPM to 2000 RPM with an interval of 500 RPM (three speeds in all). This is done to determine the effect of impeller speed on the flow characteristics in the diffuser. The range of speed variation produced Reynolds number, based on the impeller tip speed and outlet diameter, ranging from

1.8 x 10^5 to 3.2 x 10^5. A digital inverter FOXM (it is efficient and flexible control of motor speed. In this way, the asynchronous can be used in a wider range of applications, with a more regular rotation and significant reduction of noise compared to the older inverters) was used. The speed of the motor was measured using process time-indicator (Microprocessor tachometer (Compact Model CT7) with an accuracy of +1 digit, resolution of 1 digit per reading, optical range of 25-1000 mm, and rpm of 3-99999).

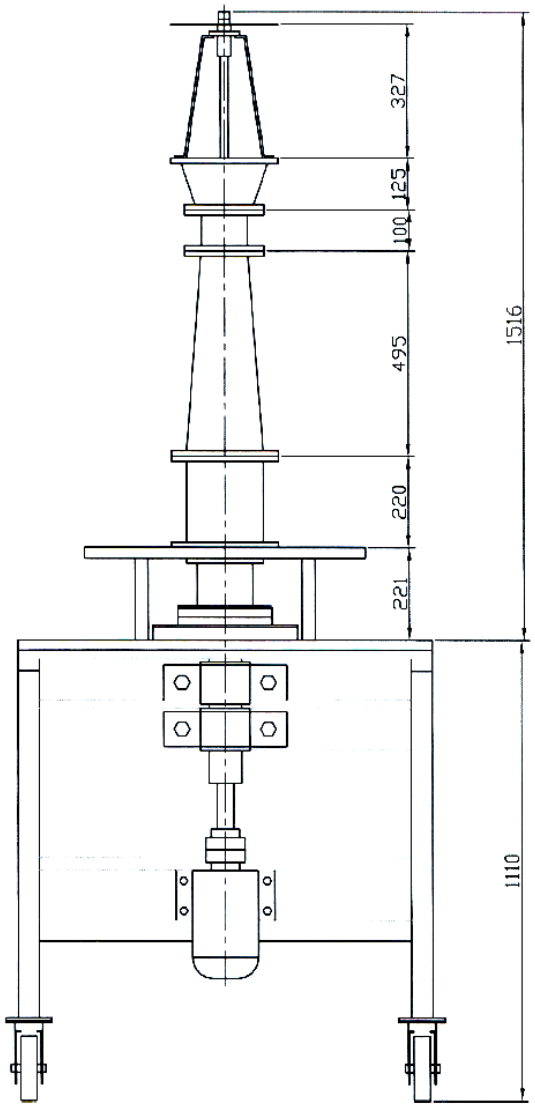

Figure 3.1: Assembled Experimental Test Rig

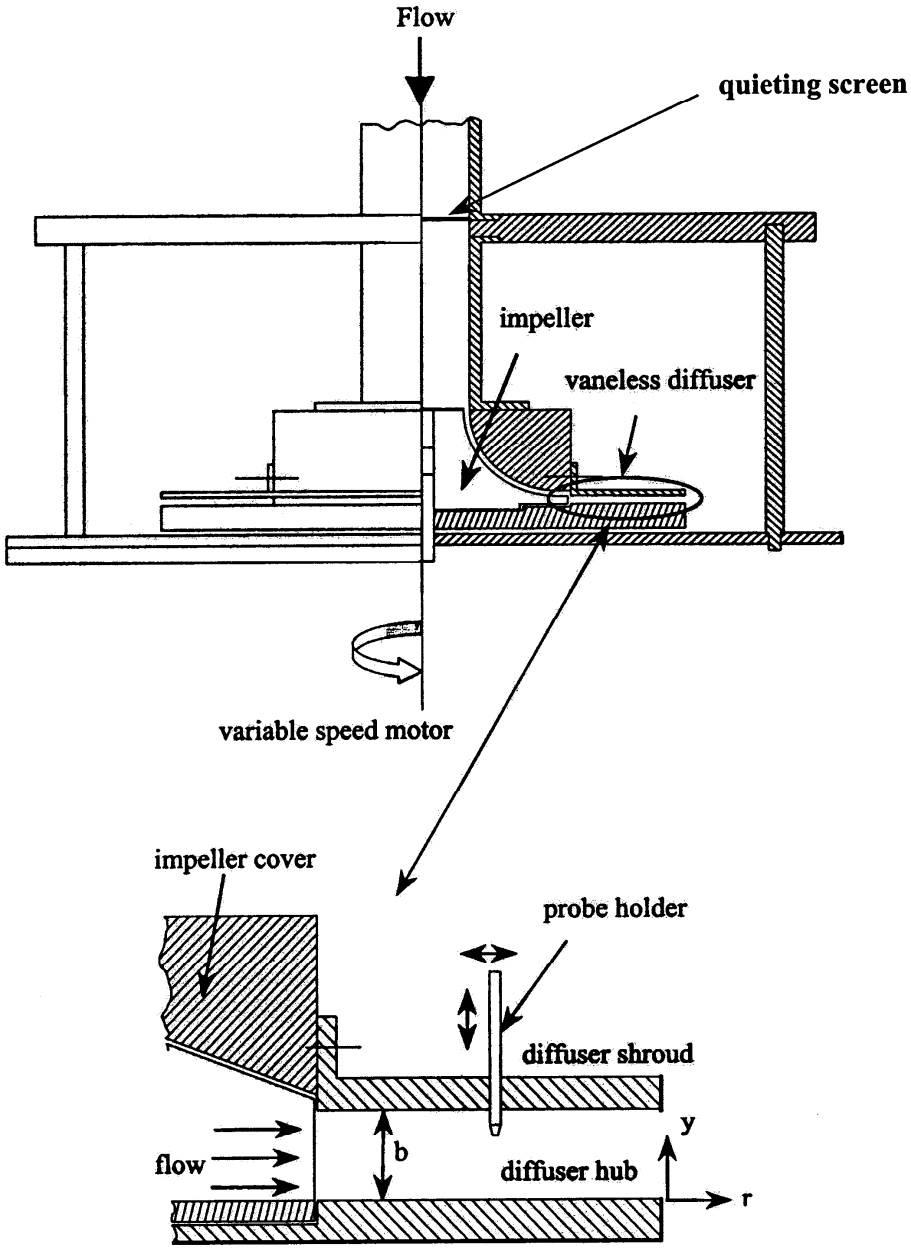

Figure 3.2: A Schematic of Experiment Test Rig

3.2 Instrumentation

3.2.1 Dynamic Pressure Sensors

The unsteady flow characteristics were measured using two dynamic PCB Piezotronics pressure transducers Model 112A22. The natural frequency of the pressure sensors is 300 kHz. They were designed for low pressure, high-resolution applications which make them suitable for the current study. The transducers were flush mounted on the diffuser shroud wall in order to determine the stall cells characteristics. The sensing element, which has a diameter of 5.6 mm, was made of quartz and completely sealed with epoxy. Dynamic pressure can be measured from 0.005 to 690 kPa. All the two transducers were calibrated at the factory. Model 112A22 pressure sensor and the type of mounting on the diffuser shroud wall are shown in Fig. 3.3 while the calibration curves supplied by the factory are shown in Fig. 3.4. These transducers were used in conjunction with PCB line-powered signal conditioner Model 482A21, which is a single-channel, line-operated signal conditioner. It provides constant current excitation to the built-in transducer amplifier and decouples the signals from the DC bias voltage. This unit also contains provision for fault-monitoring the channel, as well as provision for externally varying the constant current output over 2 to 20 mA range. Externally powered by PCB Model 488A04 Universal Power Supply, Model 482A21 signal conditioner has, on its rear panel, one jack for transducer signal Input and another for signal Output connection. The signal information is decoupled from the sensor bias level by a coupling capacitor and brought out to the OUTPUT jack. The bias monitor consists of a color-coded front panel meter that permanently monitors the sensor bias level. Figure 3.5 shows a schematic of Model 482A21 line-powered signal conditioner. The dynamic pressure transducer locations are shown in Fig. 3.6.

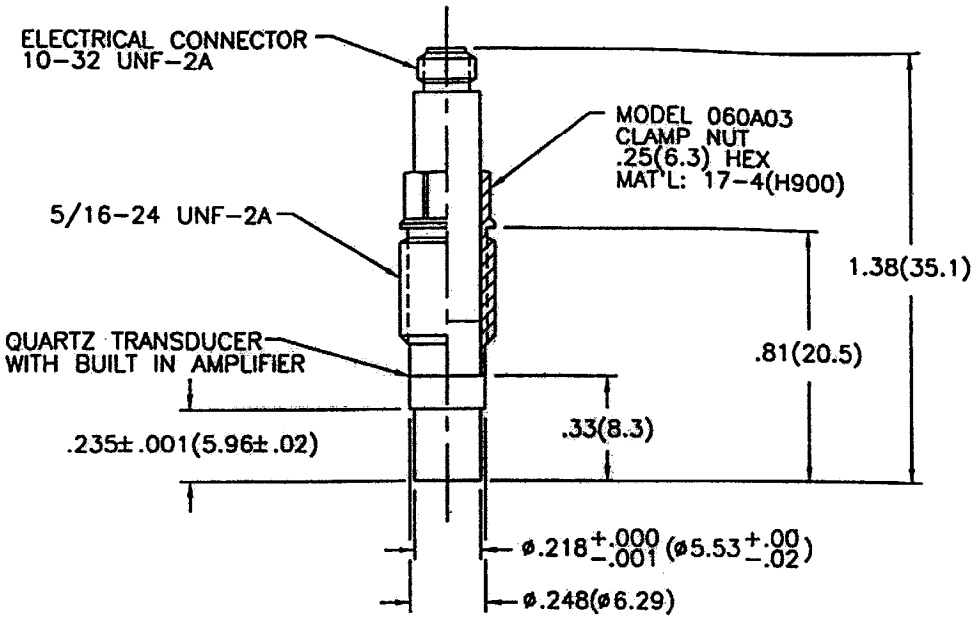

(a) PCB Dynamic Pressure Sensor Model 112A22 (Courtesy of PCB, Inc.)

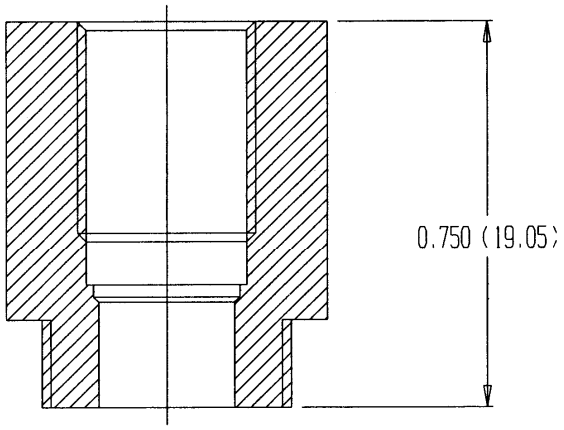

(b) Flush Installation Adaptor
(Dimensions in inches & mm equivalent in parenthesis)

Figure 3.3a-b: A Schematic of the Dynamic Pressure Transducer & its Installation

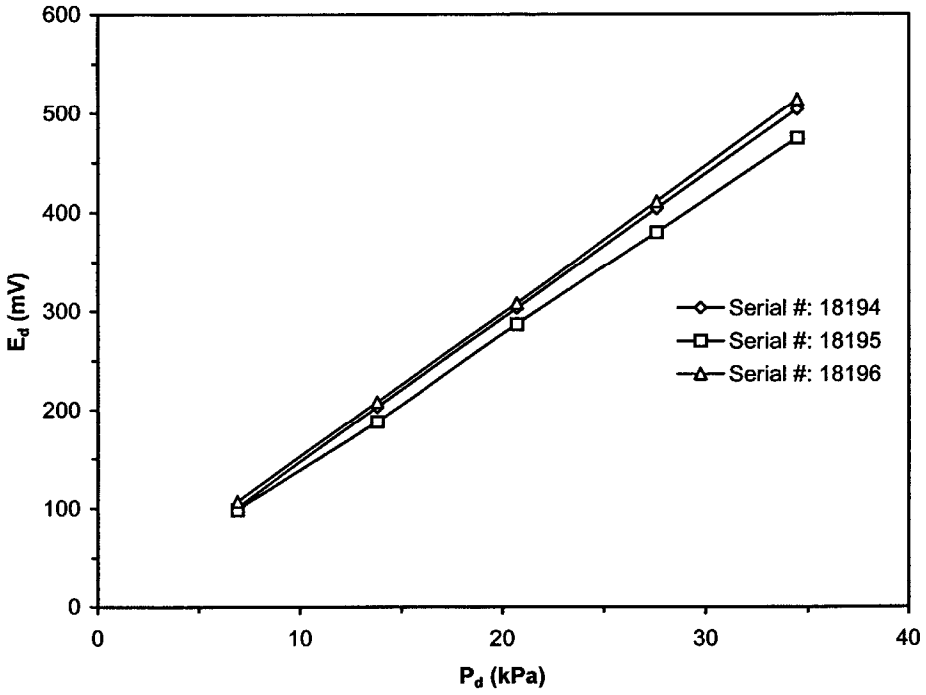

Figure 3.4: Factory–Supplied Calibration Curves for the Dynamic Pressure Transducer

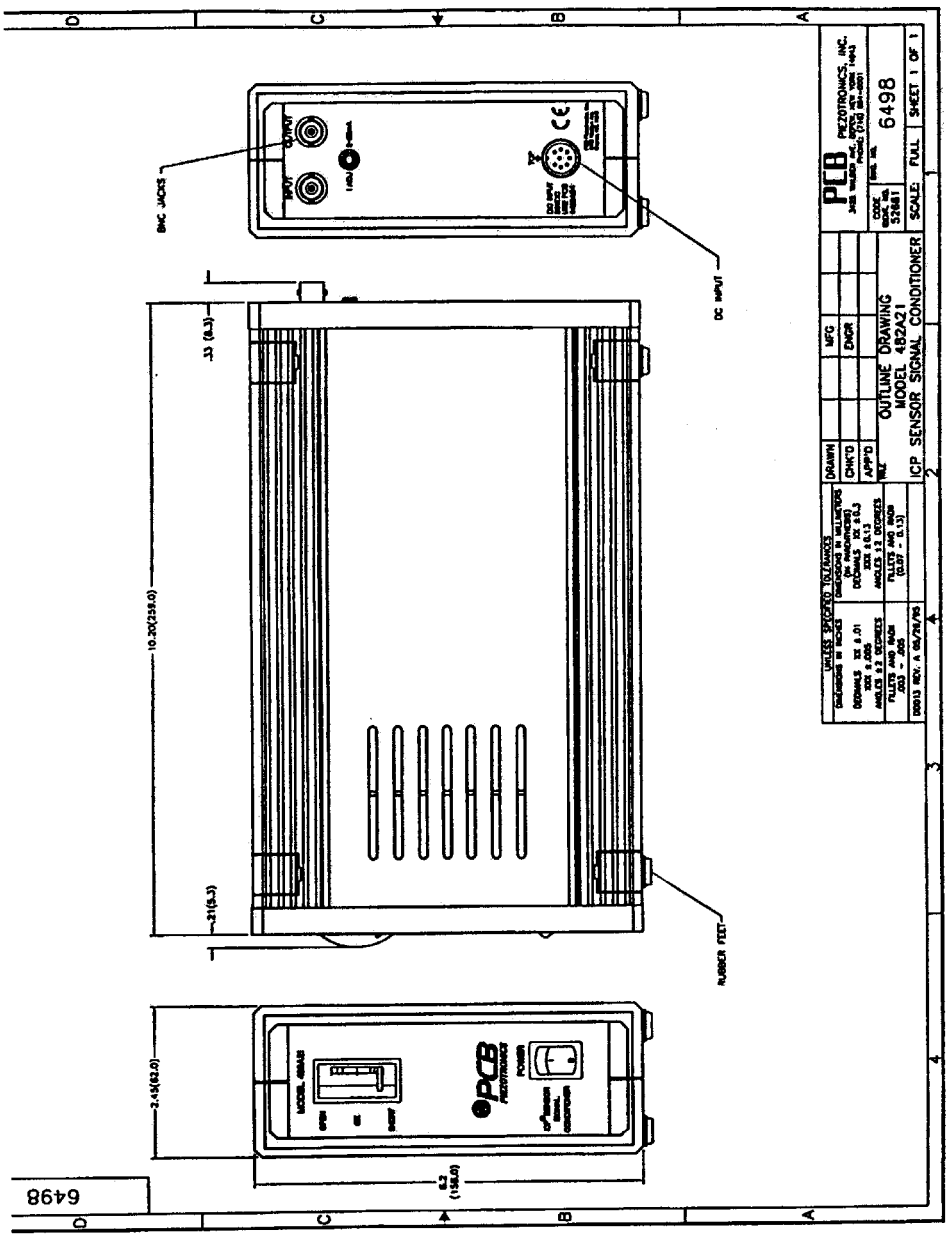

Figure 3.5: A Schematic of the Line-Powered Signal Conditioner

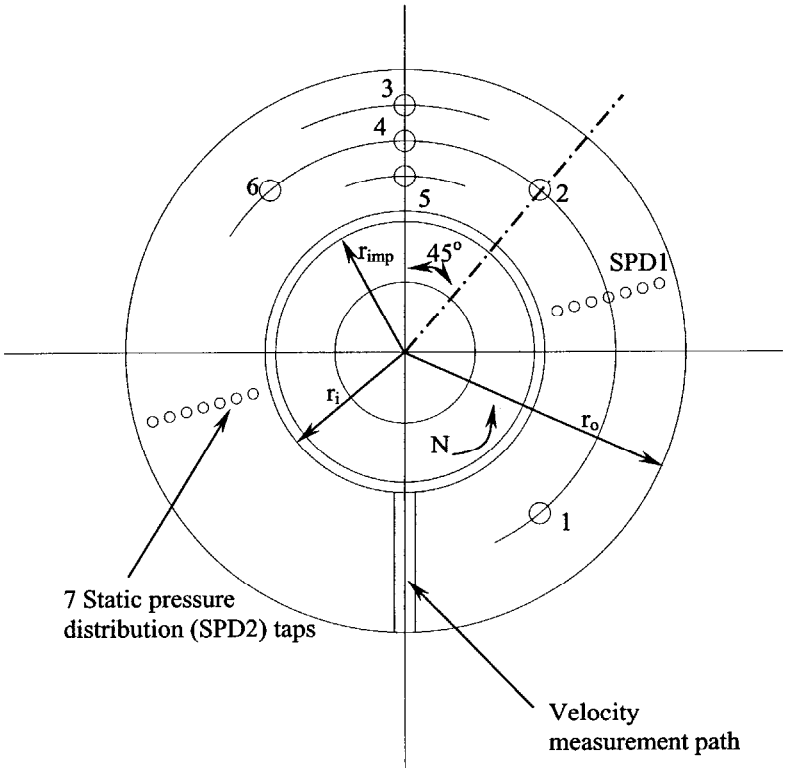

(Labels 1, 2, 3, 4, 5 & 6 are Dynamic Pressure Transducer Locations)

Figure 3.6: Dynamic Pressure Transducer Locations on the Shroud Wall

3.2.2 Pressure Fluid Manometer

3.2.2.1 Multi-tube H_2O mm Manometer

- Introduction

In certain experiments, it is useful to have a visual appreciation of the pressure pattern existing along the flow path under consideration. Providing the flow path has a sufficient number of pressure tapping points, Cussons P3202 Multitube Manometer (see Fig. 3.7) can be used to give this overall pressure picture as well as giving

simultaneous measurements of up to fourteen pressures referenced to atmospheric pressure, or other datum pressure.

- Description

The manometer, which uses blended paraffins of Specific Gravity 0.784 as the working fluid, consists of fourteen vertical tubes connected to a common manifold and from there to a large reservoir which can be raised or lowered for adjustment of the zero reading. A tapping point on the reservoir allows datum pressures other than atmospheric to be employed. The instrument is directly scaled with a range extending from -230 mm to +110 mm H20.

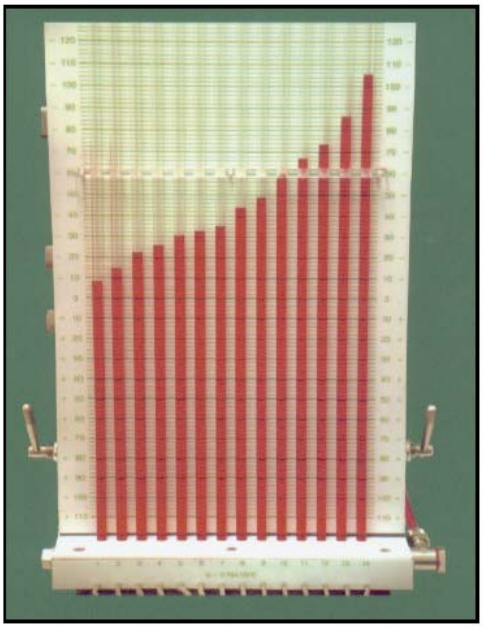

Figure 3.7: P3202 Multitube Manometer

3.2.2.2 Precision Single Limb Airflow Manometer

- Test Sets

Employing the same fundamental principles as the industrial manometers, Airflow's range of precision portable manometers are complete test sets. They incorporate one or two adjustable-range single limb manometers providing a wide choice of ranges from 0-125 Pa to 0-5000 Pa. Each manometer has a reservoir tank with a built-in metal bellows system which allows fine settings of the fluid level without changing the calibration. Once set up the instrument panel is accurately leveled with a three point rapid leveling system using a precision compound built-in spirit level. The close fitting of the scale to the glass tube minimizes parallax and the choice of manometer fluid ensures a crisp meniscus for accurate reading. Each portable instrument is individually calibrated and comes complete with pitot static tube, connecting flexible tube, spare fluid and a manometer balancing valve which isolates the pressure signal to allow zero checking without disconnecting the pressure lines as shown in Fig. 3.8.

1. Measure positive, negative or differential (velocity) pressure
2. Adjustable manometer limbs give good resolution, sensitivity and wide range
3. Free flowing fluid with positive meniscus
4. Low relative density fluid gives expanded scale
5. Not susceptible to parallax error
6. Barometer included with Type

Figure 3.8: Precision Single Limb Airflow Manometer Type 4

3.3 Measurement Techniques

The overall performance of the compressor was evaluated by measuring the difference between the static pressure at the impeller inlet and the static pressure at the diffuser outlet. This was done by the use of both multitube airflow manometer (pressure fluid measurement) made by Cussons Technology, (Model P3202 Multi-Tube), and single limb precision manometer made by Airflow Development LTD UK, (Model Type 4 Single Limb Manometer) The output from these pressure manometers were multiplied by factors to covert them into Pascal Unit.

The unsteady flow characteristics were analyzed using two dynamic pressure transducers (PCB Piezotronics pressure transducer Model 112A22) that were flush mounted on the diffuser shroud wall. These transducers were used in conjunction with PCB line-powered signal conditioner Model 482A21 as described earlier. The output

signals from the pressure transducers were appropriately conditioned and digitized using PICO 212/50 (High accuracy and resolution data acquisition with 10 bit resolution, 22 channels, 0 to 2.5 V input ranges, 10KS/s sampling rate, and ±1% accuracy). The digitized data were exported into MATLAB software for both time-domain and frequency-domain analysis. The SPECTRUM function in MATLAB, which provides the power spectral densities (PSDs) and cross-spectral density (CSD) of the signals, was employed to extract any frequency in the digitized data. Parametric studies were performed by digitizing and analyzing known sine-wave signals from a function generator. This enabled an optimization of the several parameters required in the SPECTRUM function. A detailed discussion of how this parameter affects the output from the SPECTRUM functions is provided in Appendix B.

To monitor the onset of any perturbation in the flow, the signals from the pressure transducers were connected to a TEKTRONIX oscilloscope Model TDS-3032. With an appropriate angular and radial positioning of the transducers on the diffuser shroud, the frequency of any rotating stall and its periodicity, as well as its speed of rotation and spatial distribution, could be determined. For instance, the physical angular distance between locations 2 and 4 in Fig. 2.8 is $\theta_f = 45^o$. If the phase angle between the two signals from the pressure transducers placed at locations 2 and 4 is θ_p, then the number of rotating stall cells, n, with a frequency of propagating stall cell of f_p and their speed, Ns (rev/s), are determined from the following relations:

$$n = \theta p / \theta_f \qquad \ldots. (3.1)$$

$$Ns = fp / n \qquad \ldots. (3.2)$$

There are six radial locations in the diffuser. At each of the six measurement locations, instantaneous velocity data were recorded at twelve points in the axial direction spacing 1 mm apart. This type of probe allowed the determination of the direction of the radial velocity component and to find out whether it is inward (reverse flow) or outward.

3.4 Test Conditions

The properties of the air at the compressor inlet pipe are considered to be equal to those of the room conditions since the inlet flow pipe is open to the surrounding atmosphere. Therefore, the temperature of the air was considered to be the measured room temperature of 25^{o}C while its pressure is atmospheric. All other required properties of the air at the compressor inlet pipe were estimated at these conditions. Since the diffuser is open to the atmosphere, the properties of the air at the diffuser exit are also assumed atmospheric. The variation of the density of air through the compressor was assumed to be insignificant as the compressor speed was low when compared to a real compressor. The test matrix is shown in Table 3.1.

Table 3.1: Test Matrix

Parameters	Description
Re, ρ, μ	Effect were neglected
Impeller Angular Speed (N)	Values: 1000, 1500, and 2000 rpm
Diffuser Width Ratio (b / D_i)	Value: 0.055
Diffuser Diameter Ratio (D_o / D_i)	Values: 1.5, 1.75, and 2.0

CHAPTER 4

STEADY & UNSTEADY FLOW RESULTS & DISCUISSIONS

In this chapter, first the flowfield characteristics at stall-free conditions are reported. This type of measurements is necessary as a baseline testing in order to fully understand the effect of stall on the flowfield characteristics in the diffuser. In other words, knowing the flowfield patterns before any type of flow instability sets in will, without doubt, enable one to compare results and fully appreciate how flow instabilities would affect the flowfield features.

Secondly, the flowfield characteristics of the diffuser flow after the inception of rotating stall are presented in this chapter. The data are presented in a format similar to the results of steady flow. A comparison between the steady and unsteady flow results is made to illustrate the effect of stall on the flowfield characteristics.

4.1 Steady Flow

4.1.1 Static Pressure Measurements on Diffuser Shroud

Figures 4.1, 2, & 3 show the pressure coefficient distribution (λ) on the shroud wall at one radial path (see Fig. 3.6). The pressure coefficient measured for three different diameter ratios (Do / Di); 1.50, 1.75, & 2.0 and different speed; 1000, 1500, & 2000 RPM as well. These figures indicate that the pressure on the shroud wall, Ps, increases with radial distance due to the diffusion process (Ps increases when λ decreases).

Furthermore, Ps increases with increase in the impeller speed, although this trend is not directly visible from the figure. Note that the pressure Ps was made non-

dimensional (λ) by dividing over a value in the order of the square of the representative velocity, V^2_{imp}. Note that λ is defined relative to the diffuser exit pressure, which is translated into the decrease of λ with radial distance as shown in the plots of Figs. 4.1, 2, & 3.

Finally, a comparison of the pressure coefficient (λ) is done among different diameter ratios. It is concluded that the pressure distribution coefficient (λ) decreases more with bigger diameter ratio use. In other words (Ps) increases more with large diameter ration use.

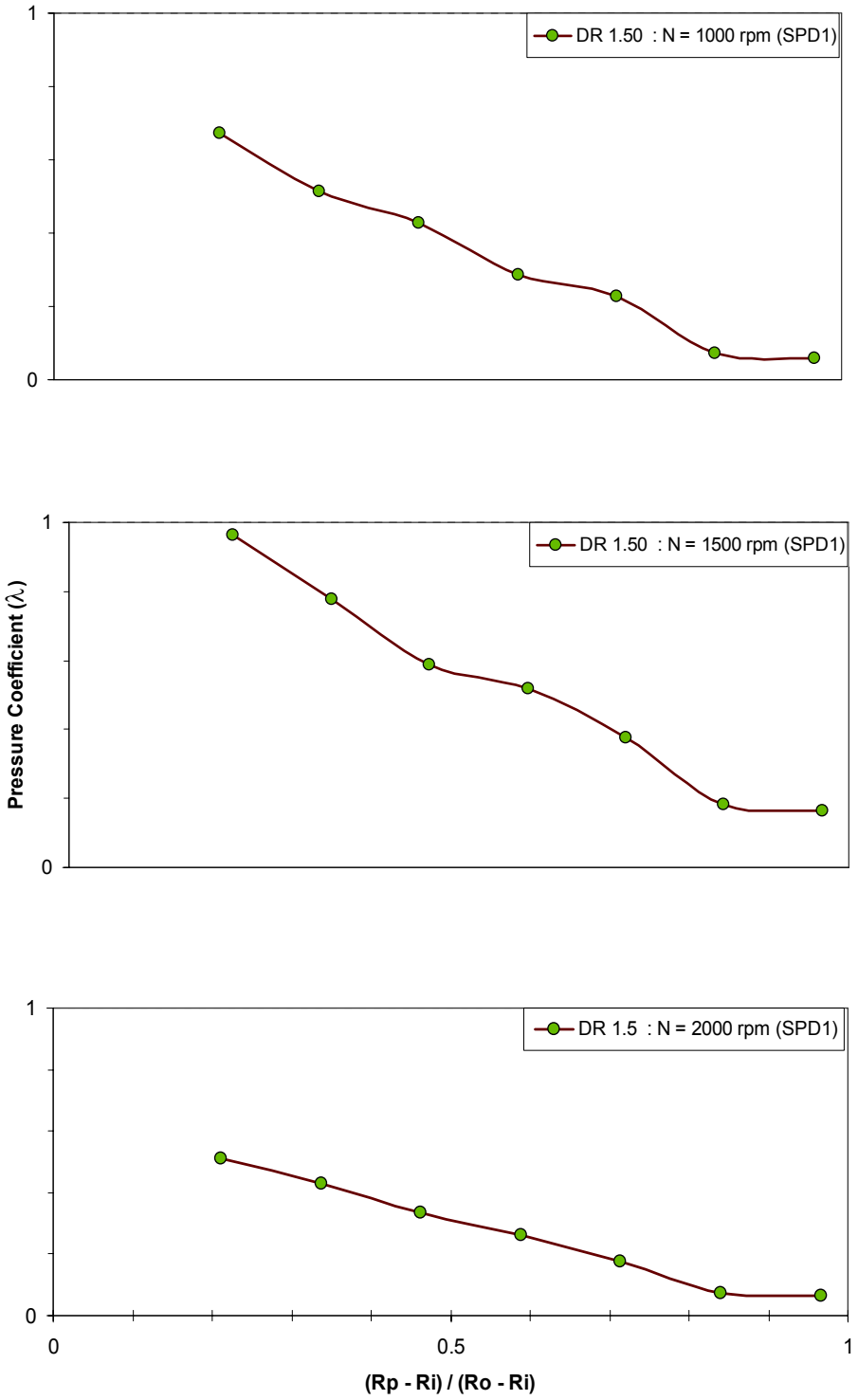

Figure 4.1: Pressure Coefficient Distribution (λ) on the Shroud Wall, $b / D_i = 0.055$ & $D_o / D_i = 1.5$ & N = 1000, 1500, 2000 RPM

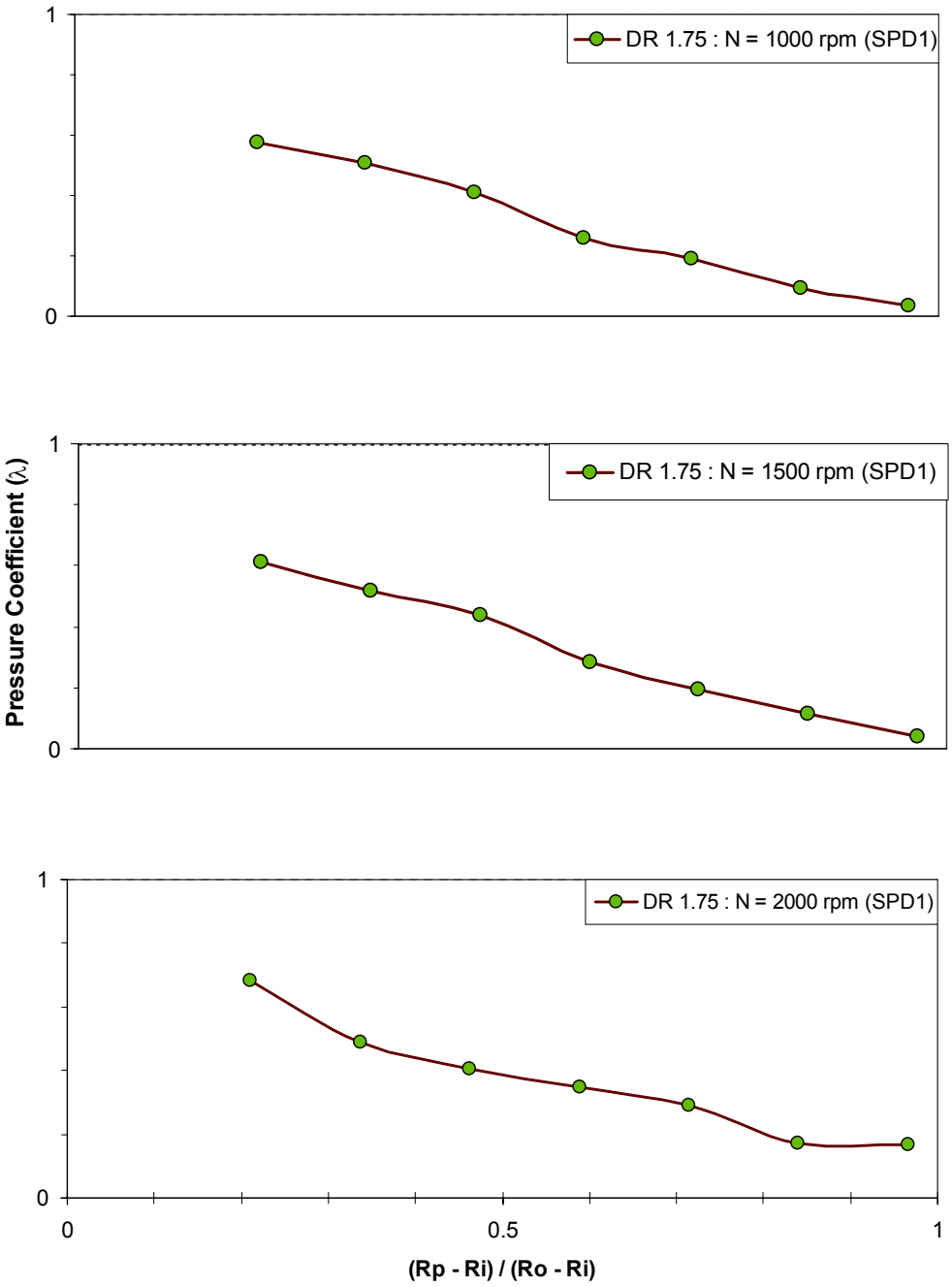

Figure 4.2: Pressure Coefficient Distribution (λ) on the Shroud Wall, $b / D_i = 0.055$ & $D_o / D_i = 1.75$ & N = 1000, 1500, 2000 RPM

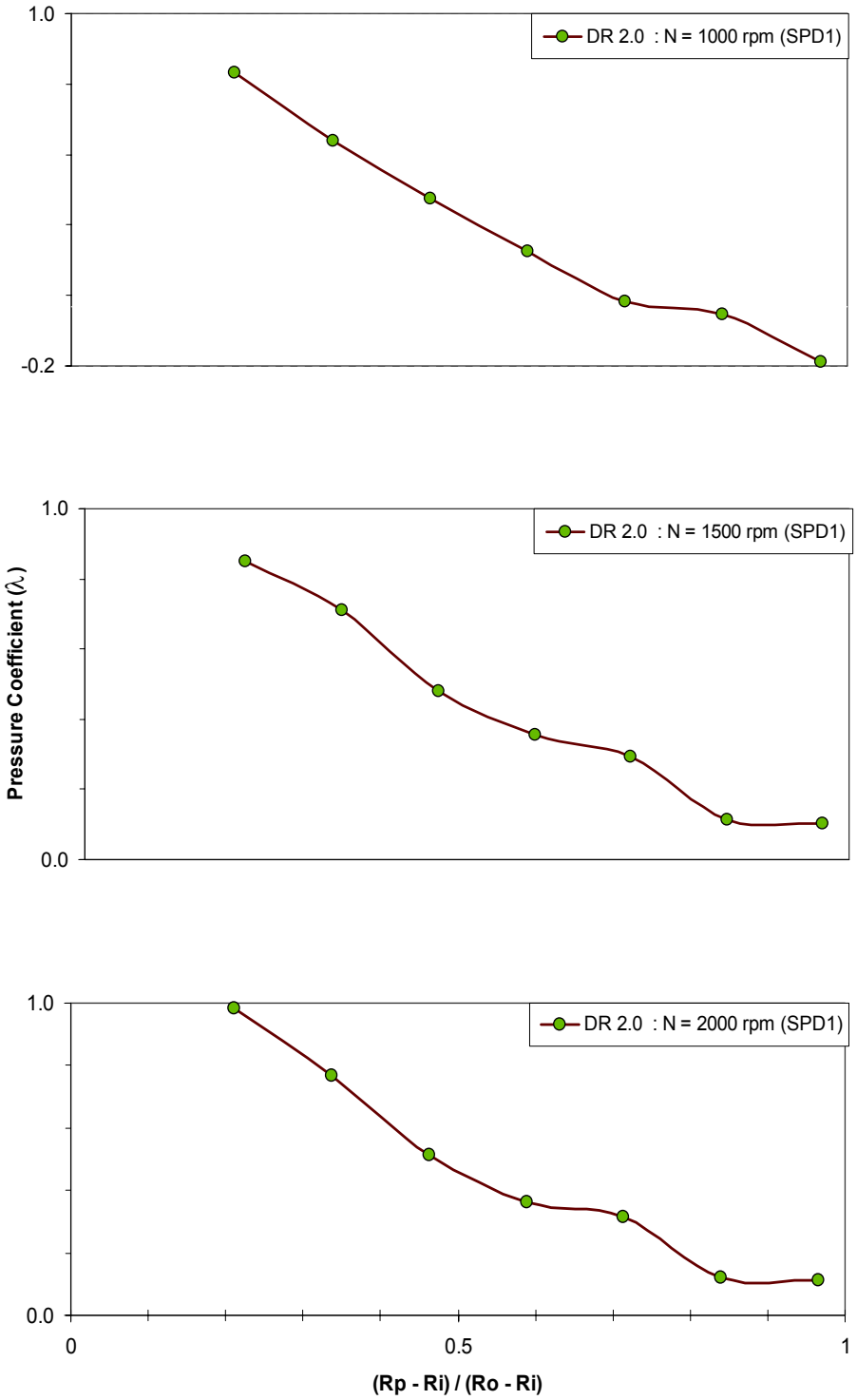

Figure 4.3: Pressure Coefficient Distribution (λ) on the Shroud Wall, $b / D_i = 0.055$ & $D_o / D_i = 2.0$ & N = 1000, 1500, 2000 RPM

4.2 Unsteady Flow

4.2.1 Static Pressure Measurements on Diffuser Shroud

The pressure coefficient distribution on the diffuser shroud wall was measured using the seven pressure taps, SPD1, shown in Fig. 3.6. To demonstrate the effect of rotating stall on the axi-symmetricity of the diffuser flow, the static pressure coefficient distributions measured for three diameter ratios (D_o / D_i);1.50, 1.75 & 2.0 for three different speeds; 1000, 1500 and 2000 RPM as shown in Figs. 4.4, 5, & 6. The static pressure on the diffuser shroud increases with radial distance. It is important to reiterate here that a decrease in λ translate to an increase in the static pressure because of the definition of λ as given in the nomenclature. This expectation was confirmed, as shall be shown later, by the nearly sinusoidal nature of the signal output from dynamic pressure transducers at much lower flow coefficient after rotating stall inception. Furthermore, this figure also confirmed that the pressure distribution on the shroud wall is lower at lower mass flow rate (flow coefficient) when compared to its value at higher mass flow rate as presented previously in this chapter.

Also, a comparison done for the pressure distribution coefficient (λ) with respect to different diameter rations is illustrated in this chapter. And the same conclusion found as in steady flow, where λ decreases with increase in diameter ratio (see Figs. 7 & 8).

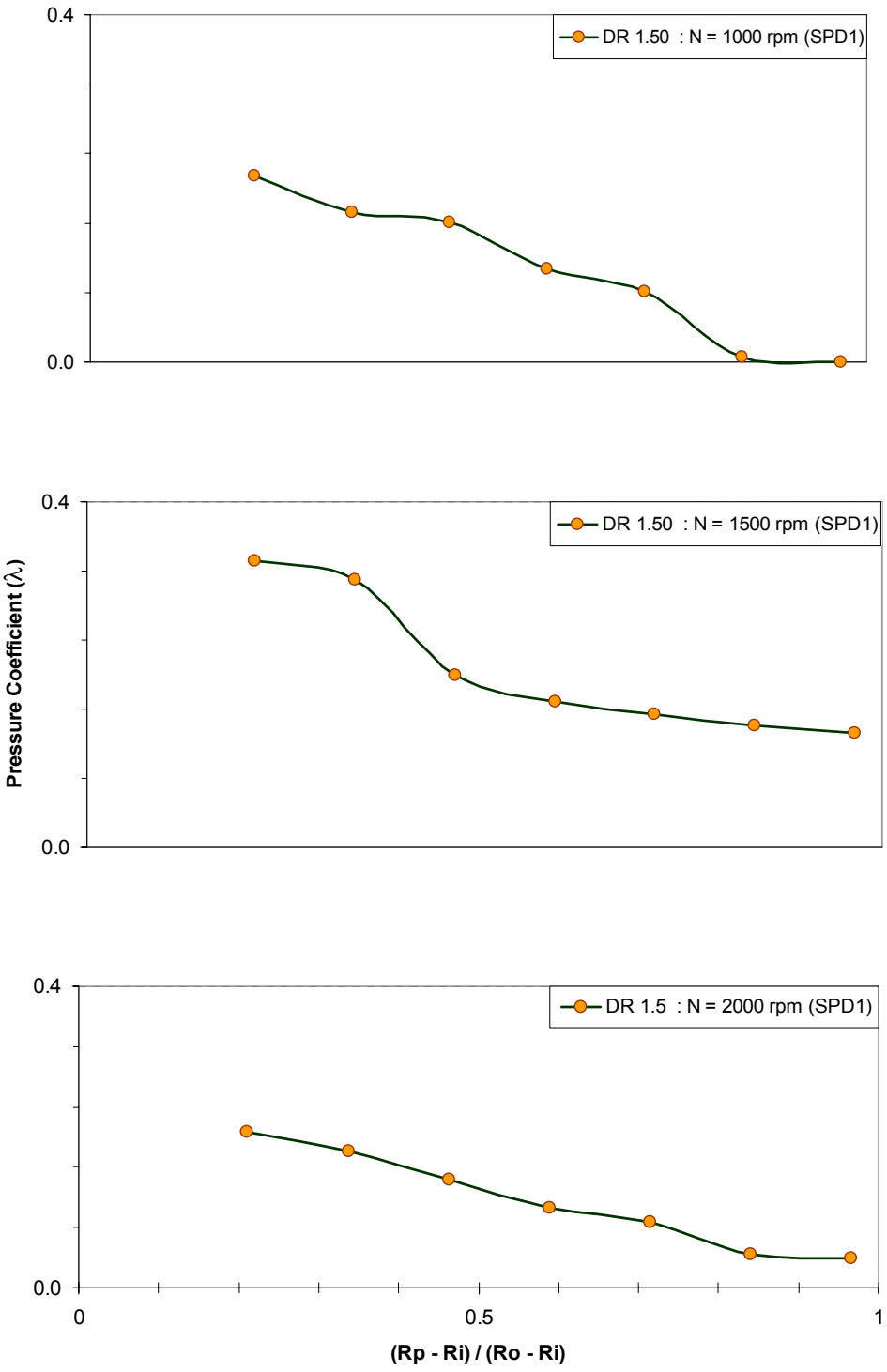

Figure 4.4: Pressure Coefficient Distribution (λ) on the Shroud Wall, b / D_i = 0.055 & D_o / D_i = 1.5 & N = 1000, 1500, 2000 RPM

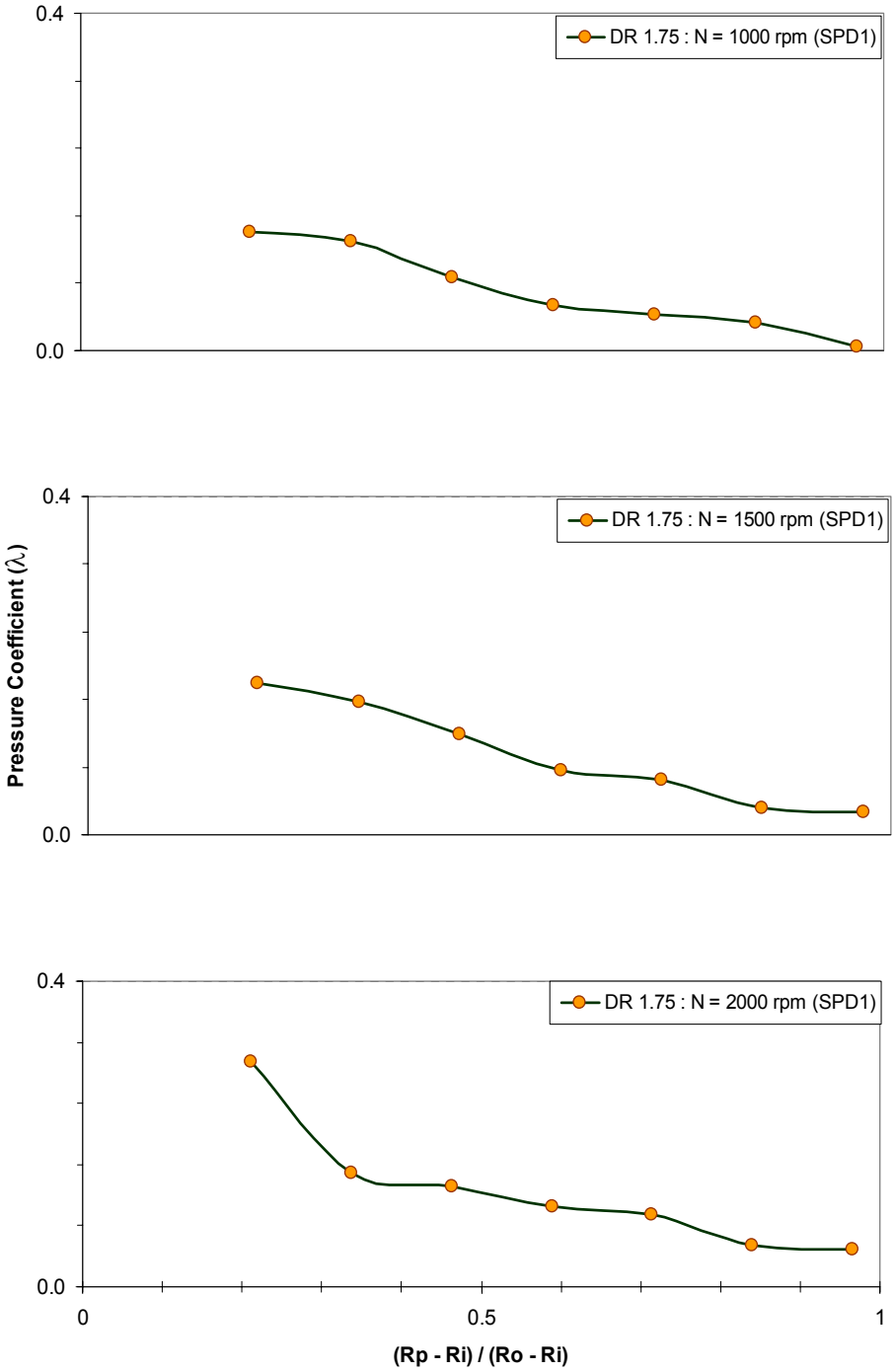

Figure 4.5: Pressure Coefficient Distribution (λ) on the Shroud Wall, $b / D_i = 0.055$ & $D_o / D_i = 1.75$ & N = 1000, 1500, 2000 RPM

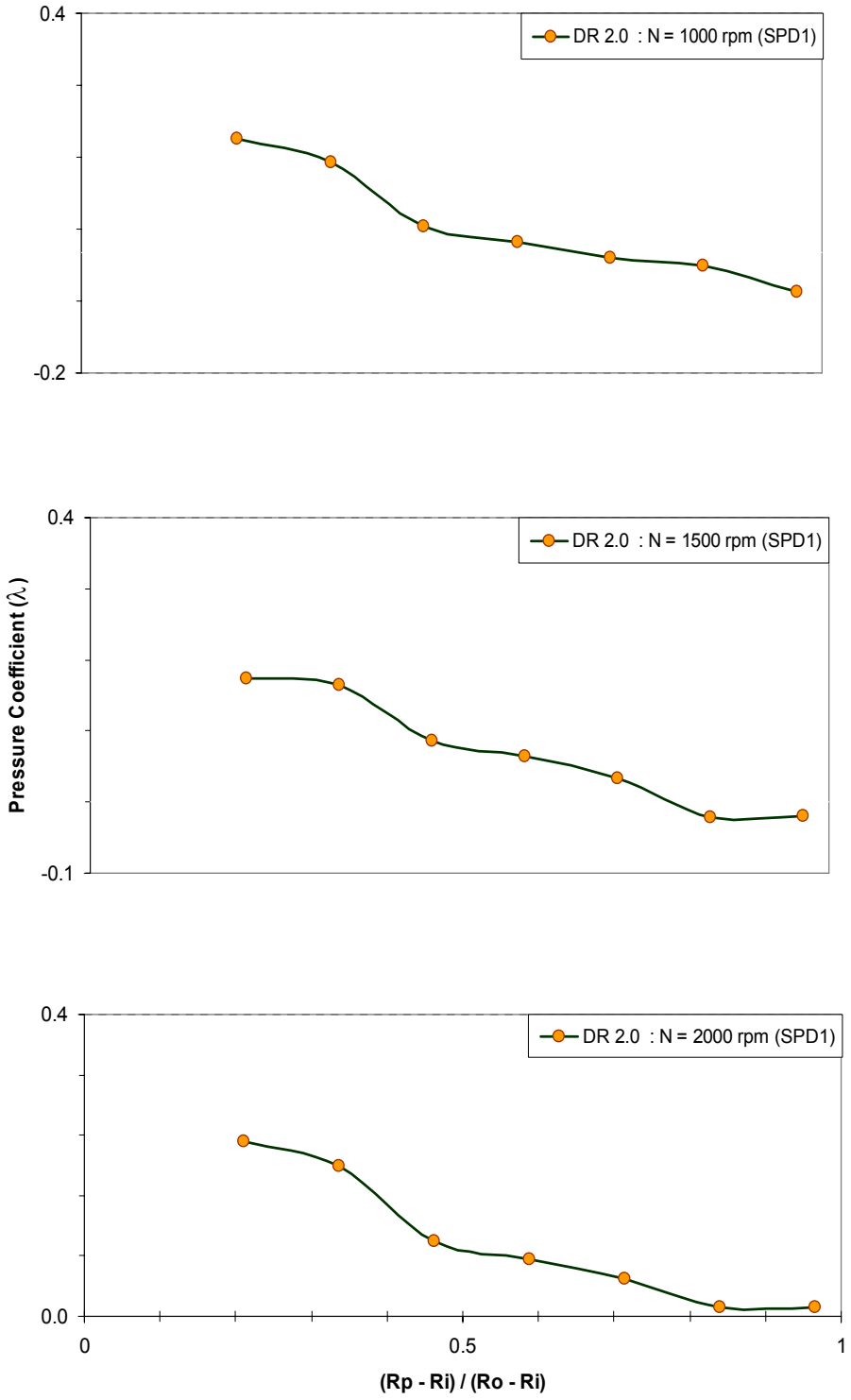

Figure 4.6: Pressure Coefficient Distribution (λ) on the Shroud Wall, b / D_i = 0.055 & D_o / D_i = 2.0 & N = 1000, 1500, 2000 RPM

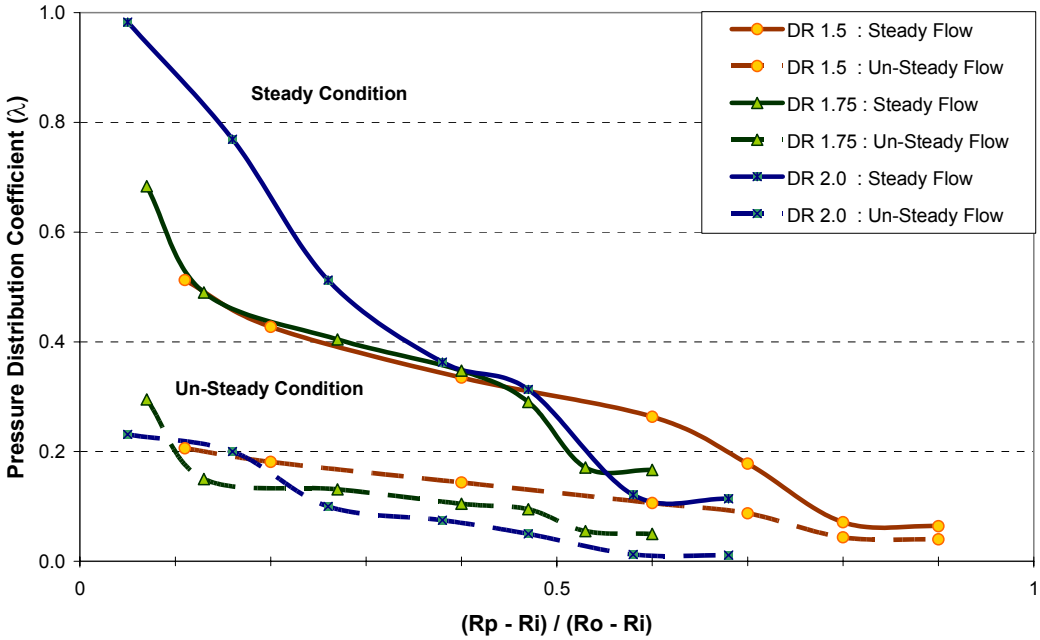

Figure 4.7: Pressure Coefficient Distribution (λ) on the Shroud Wall, b / D_i = 0.055 & D_o / D_i = 1.50, 1.75 & 2.0, & N = 2000 RPM

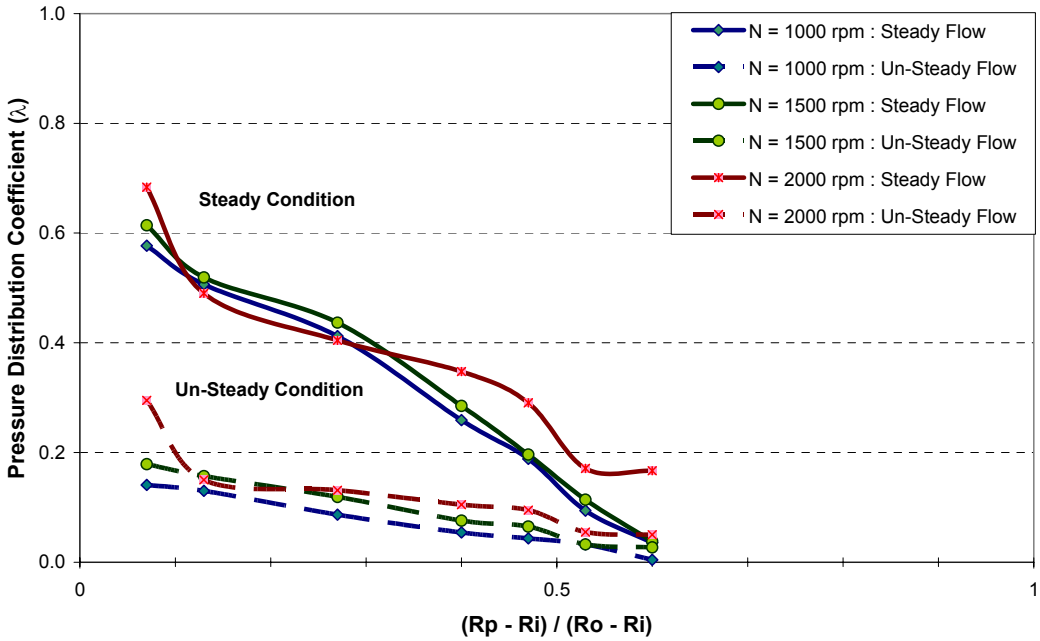

Figure 4.8: Pressure Coefficient Distribution (λ) on the Shroud Wall, b / D_i = 0.055 & D_o / D_i = 1.75 & N = 1000, 1500 & 2000 RPM

4.3 Steady & Unsteady Flow

Figures 4.9 – to – 4.17 show the pressure distribution on the shroud wall at one radial path (see Fig. 2.6). These figures indicate that the pressure on the shroud wall, Ps, increases with radial distance due to the diffusion process (Ps increases when λ decreases).

In addition, a comparison between pressure distribution on shroud wall for different diameter ratios shows (see Fig. 4.8) that the pressure decreases with increase of diameter ratio (Comparison done on $D_o / D_i = 1.50, 1.75, \& 2.0$).

The same above conclusion can be applied on the effect of the impeller speed on the pressure distributed on shroud wall (see Fig. 4.9). Therefore, the pressure decreases with increase of impeller speed (Pressure drop at N = 2000 RPM is higher than at N = 1000 RPM).

Furthermore, Figs. 4.20-28 clarify that volume flow rate decreases with increase in static pressure throughout the diffuser, this trend is obviously from the figures. Note that pressure is defined relative to the diffuser inlet / exit locations, which is translated into the decrease of pressure with radial distance.

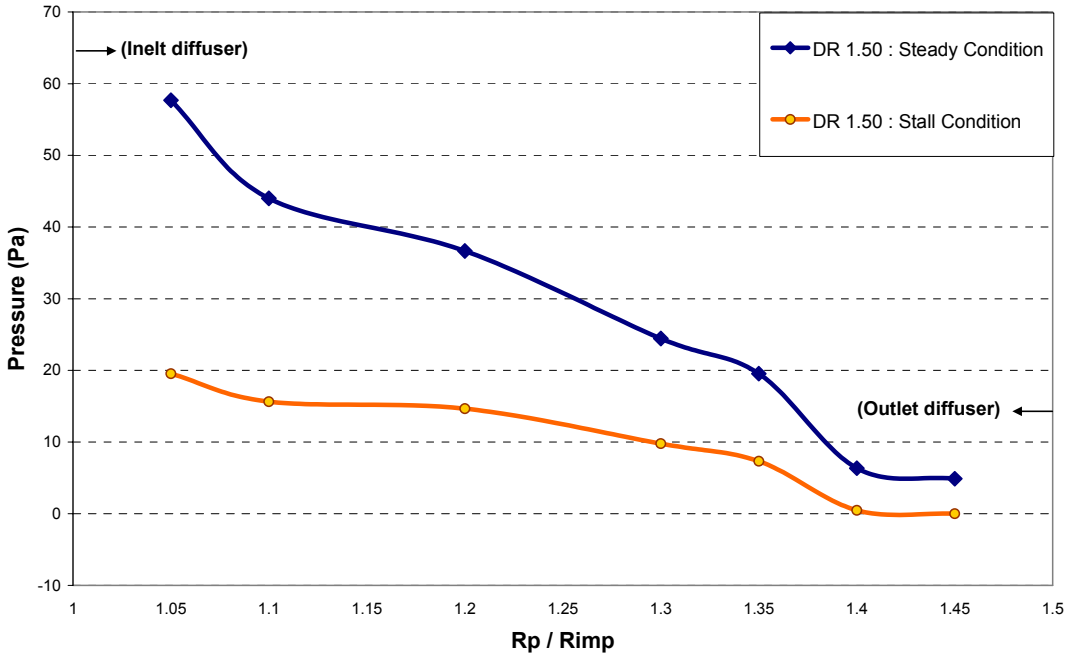

Figure 4.9: Pressure Distribution on the Shroud Wall, $b / D_i = 0.055$ & $D_o / D_i = 1.5$ & N = 1000 RPM

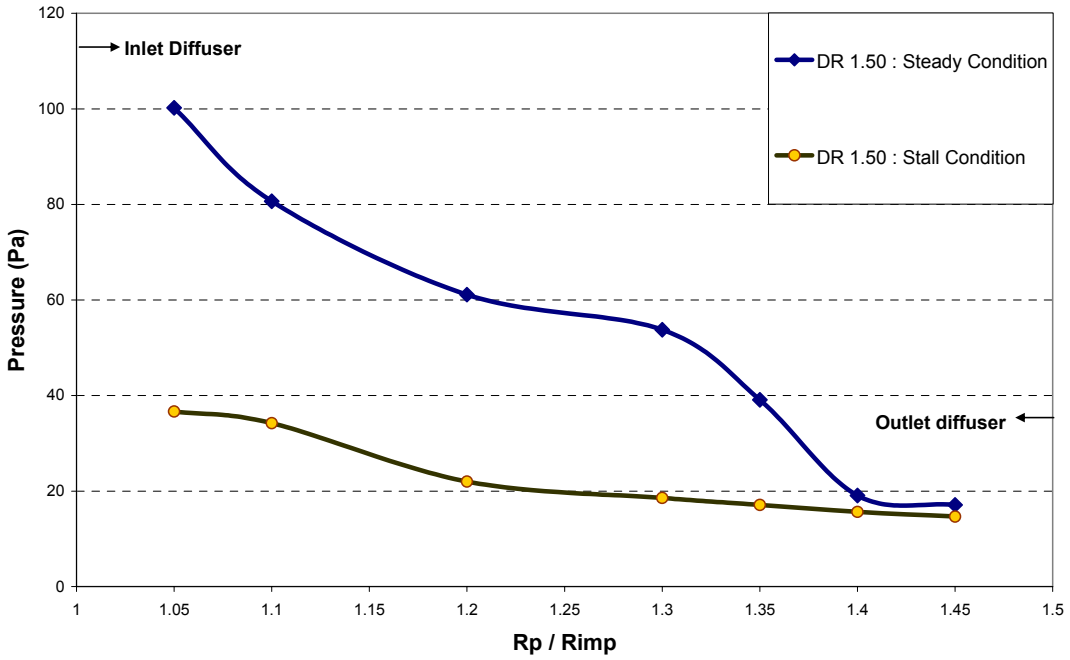

Figure 4.10: Pressure Distribution on the Shroud Wall, $b / D_i = 0.055$ & $D_o / D_i = 1.5$ & N = 1500 RPM

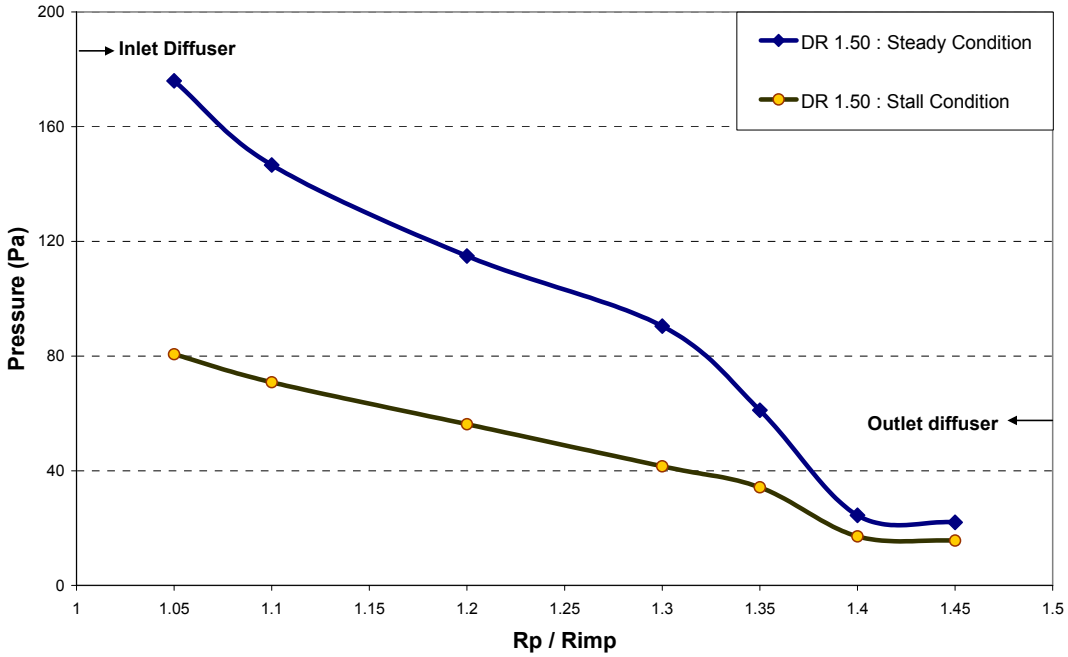

Figure 4.11: Pressure Distribution on the Shroud Wall, b / D_i = 0.055 & D_o / D_i = 1.5 & N = 2000 RPM

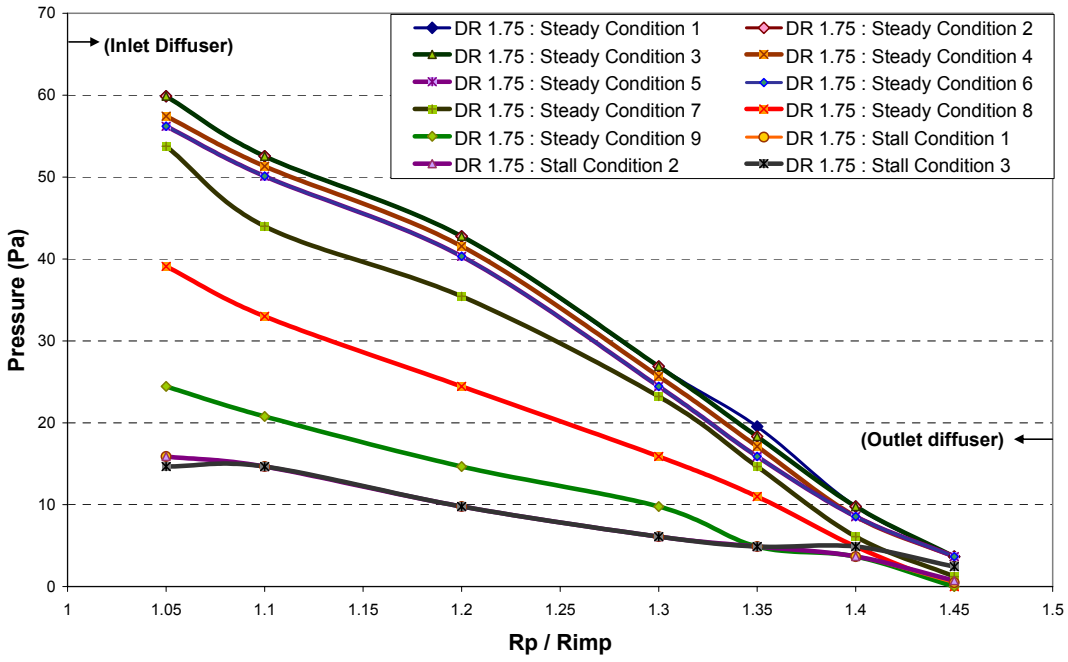

Figure 4.12: Pressure Distribution on the Shroud Wall, b / D_i = 0.055 & D_o / D_i = 1.75 & N = 1000 RPM

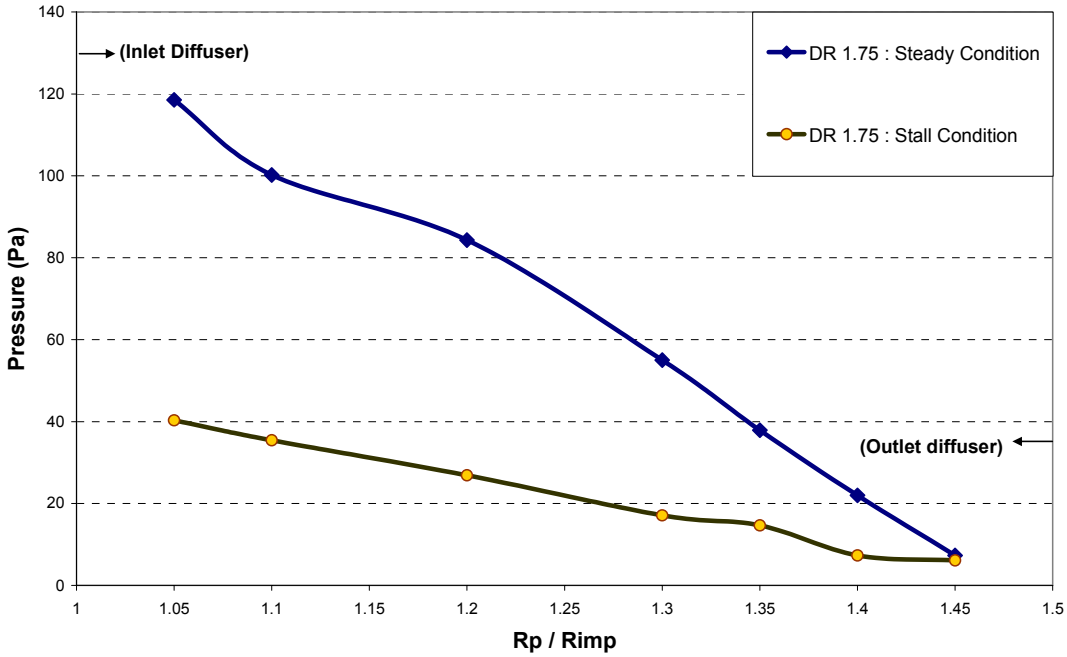

Figure 4.13: Pressure Distribution on the Shroud Wall, b / D_i = 0.055 & D_o / D_i = 1.75 & N = 1500 RPM

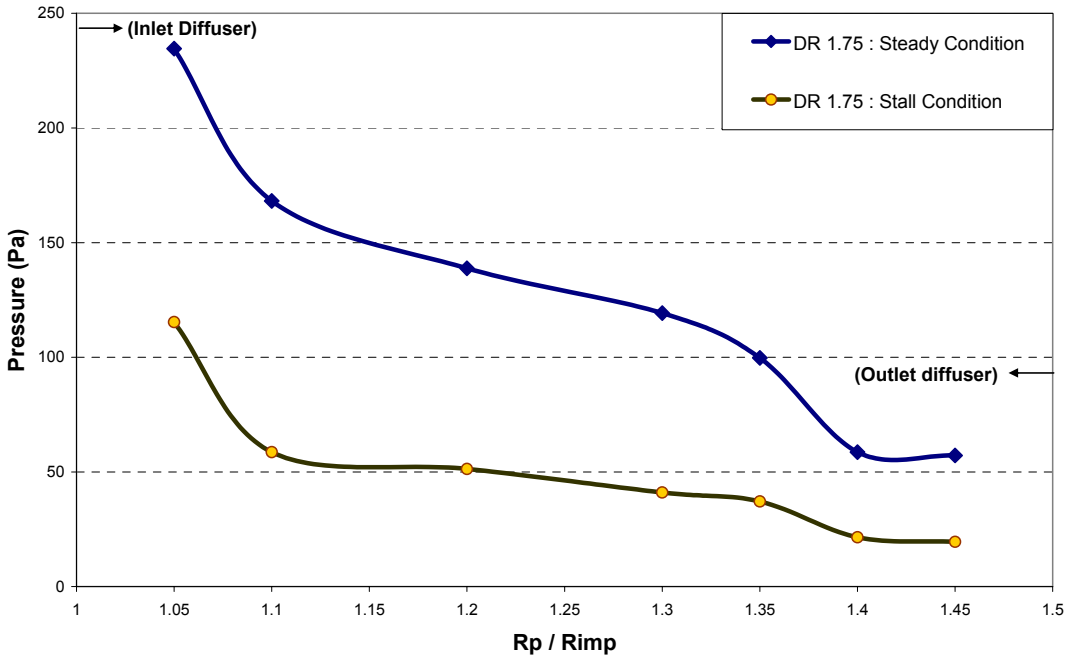

Figure 4.14: Pressure Distribution on the Shroud Wall, b / D_i = 0.055 & D_o / D_i = 1.75 & N = 2000 RPM

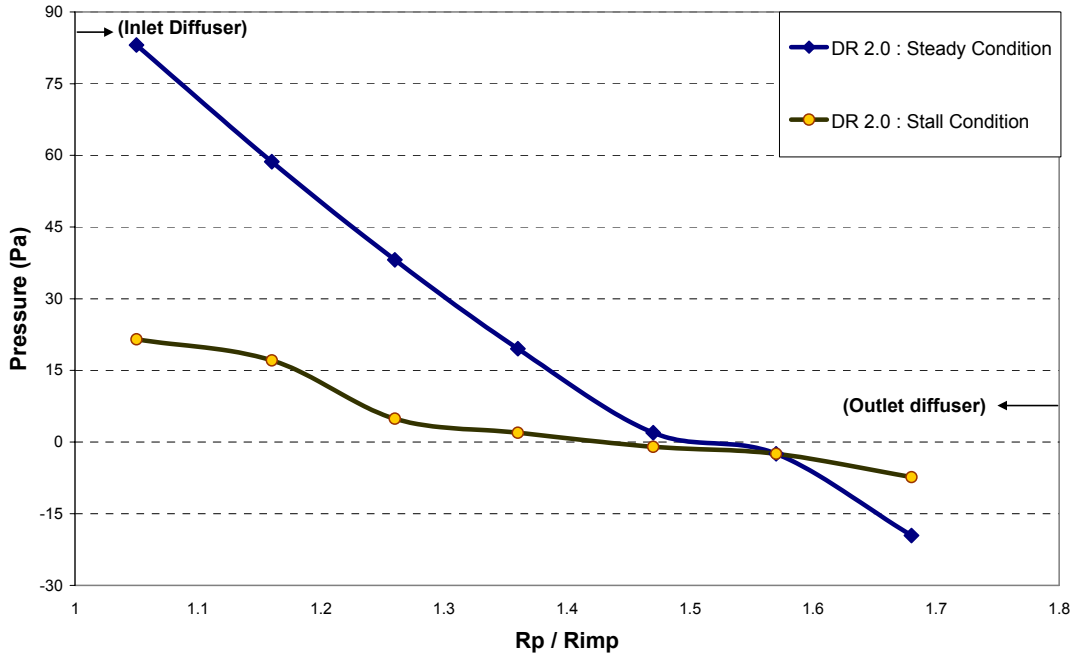

Figure 4.15: Pressure Distribution on the Shroud Wall, b / D_i = 0.055 & D_o / D_i = 2.0 & N = 1000 RPM

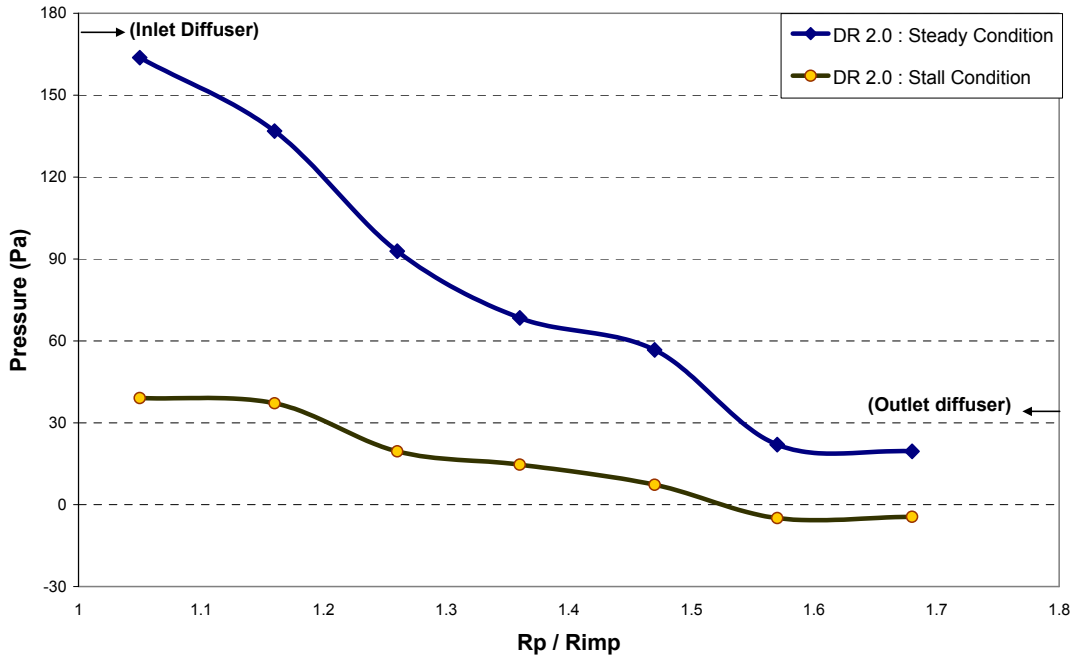

Figure 4.16: Pressure Distribution on the Shroud Wall, b / D_i = 0.055 & D_o / D_i = 2.0 & N = 1500 RPM

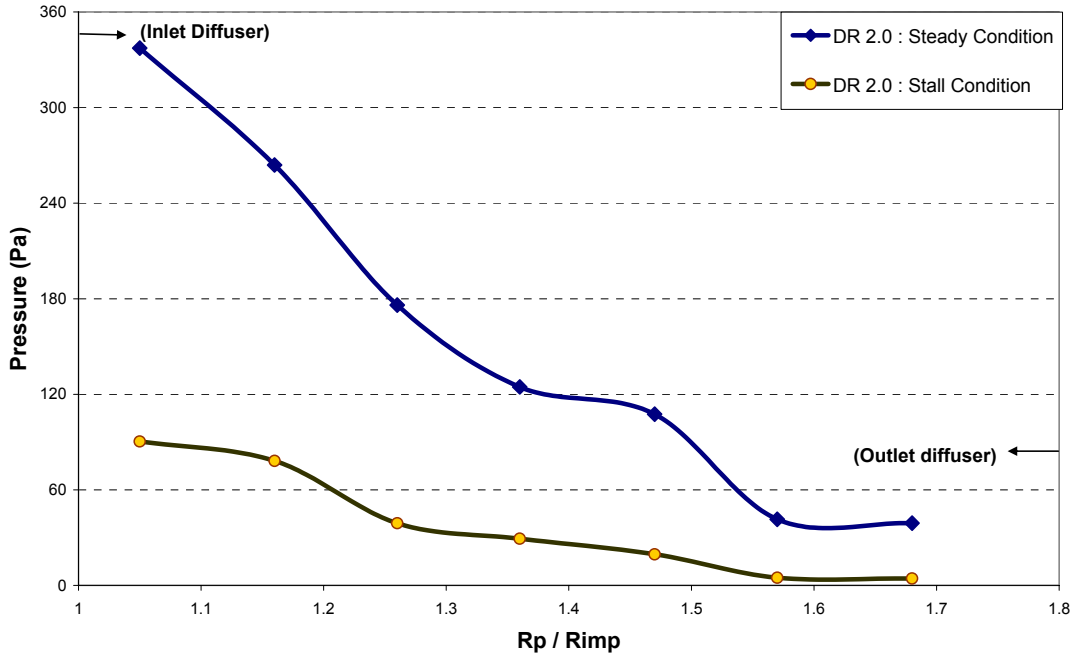

Figure 4.17: Pressure Distribution on the Shroud Wall, b / D_i = 0.055 & D_o / D_i = 2.0 & N = 2000 RPM

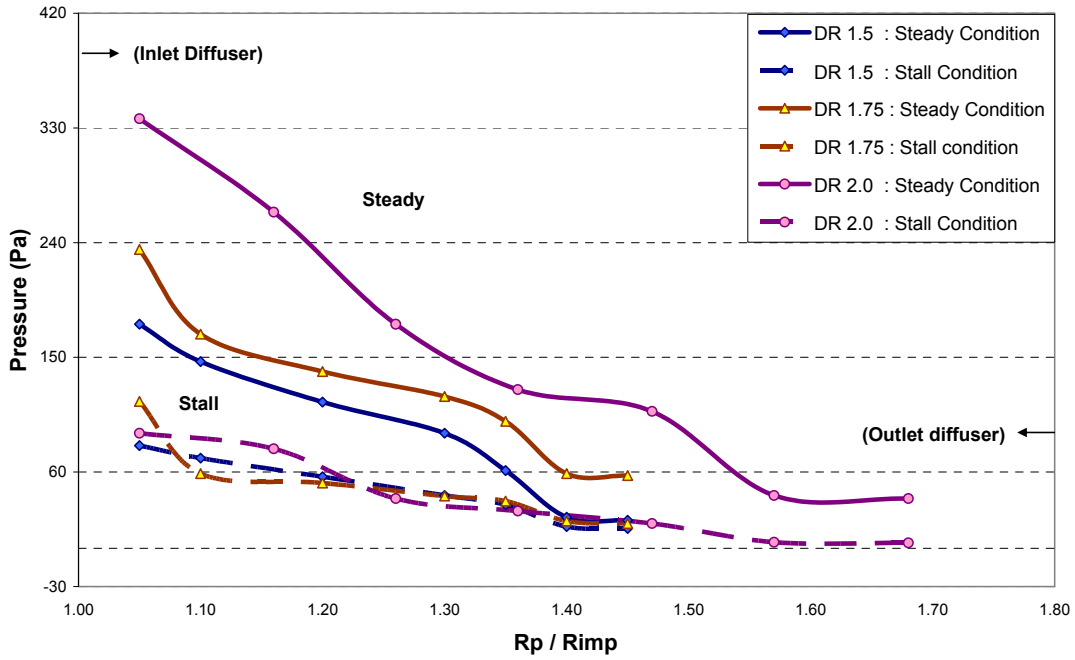

Figure 4.18: Pressure Distribution on the Shroud Wall, b / D_i = 0.055 & D_o / D_i = 1.50, 1.75, & 2.0, & N = 2000 RPM

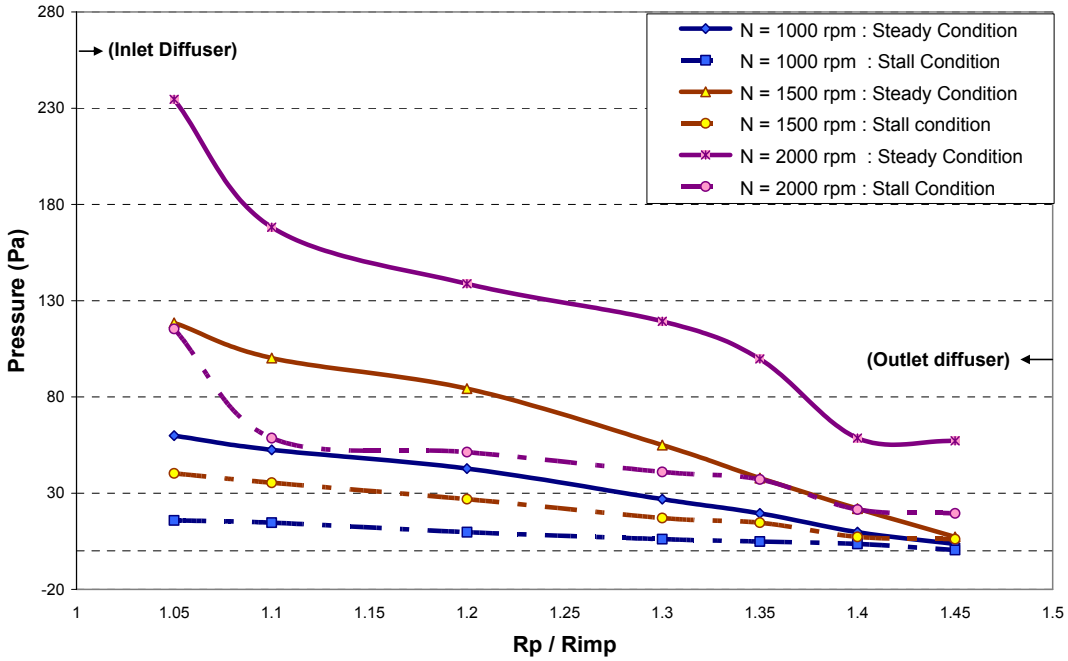

Figure 4.19: Pressure Distribution on the Shroud Wall, b / D_i = 0.055 & D_o / D_i = 1.75 & N = 1000, 15000, & 2000 RPM

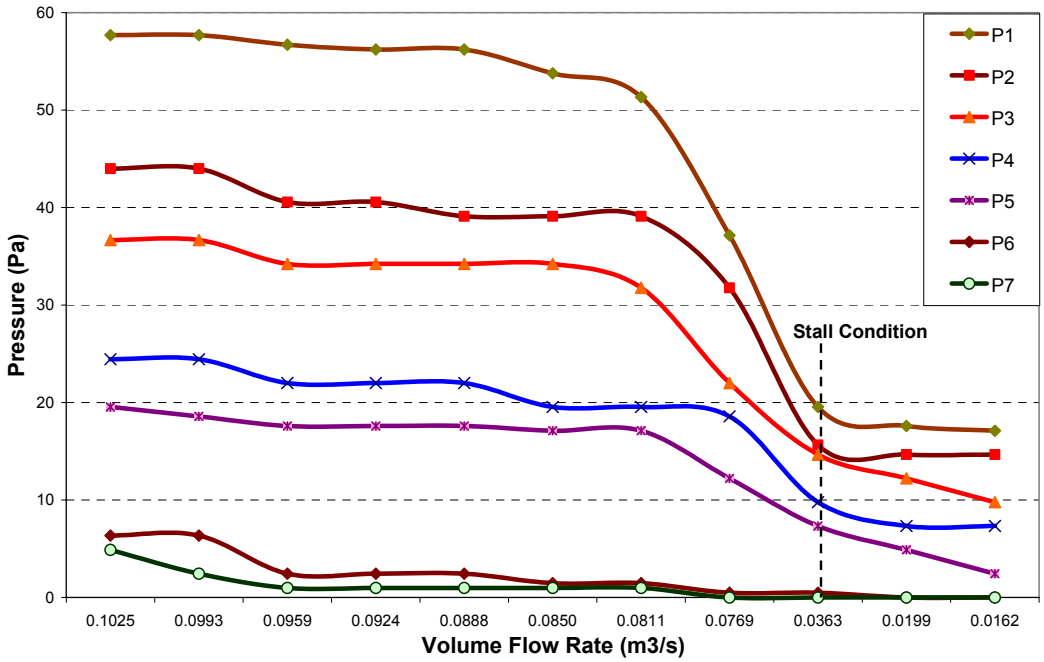

Figure 4.20: Pressure Distribution on Shroud Wall with Volumetric Flow Rate, b / D_i = 0.055 & D_o / D_i = 1.5 & N = 1000 RPM

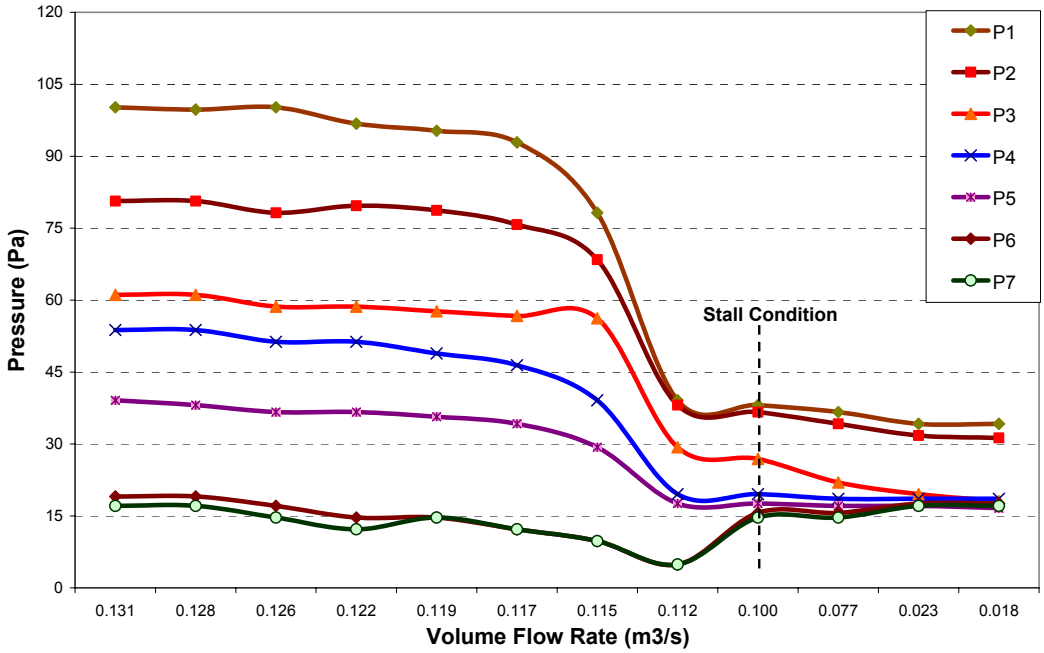

Figure 4.21: Pressure Distribution on Shroud Wall with Volumetric Flow Rate, $b / D_i = 0.055$ & $D_o / D_i = 1.5$ & N = 1500 RPM

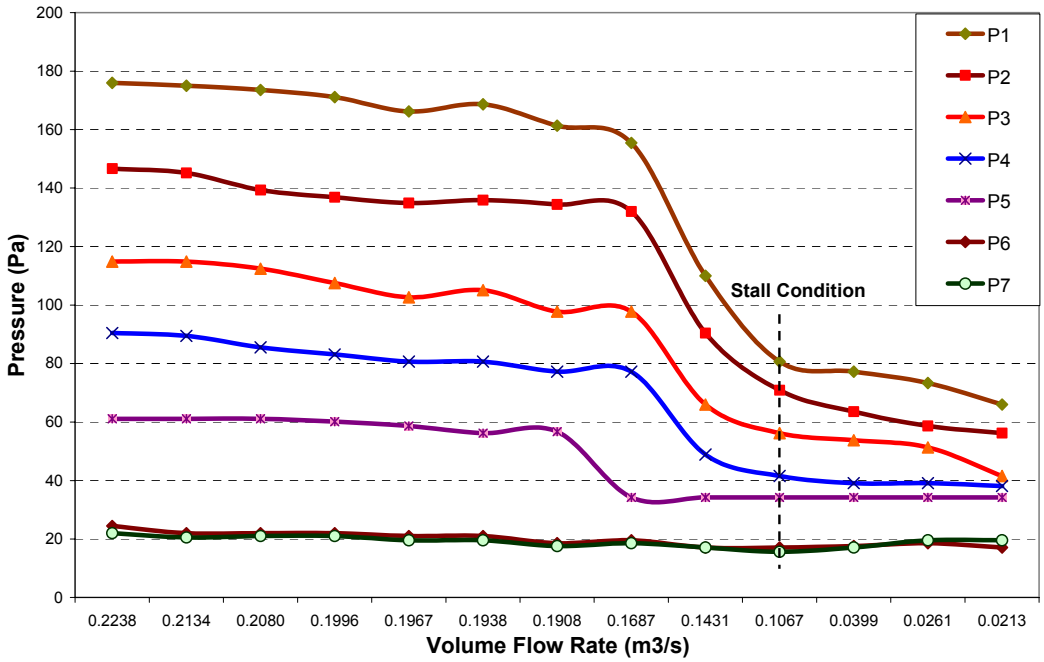

Figure 4.22: Pressure Distribution on Shroud Wall with Volumetric Flow Rate, $b / D_i = 0.055$ & $D_o / D_i = 1.5$ & N = 2000 RPM

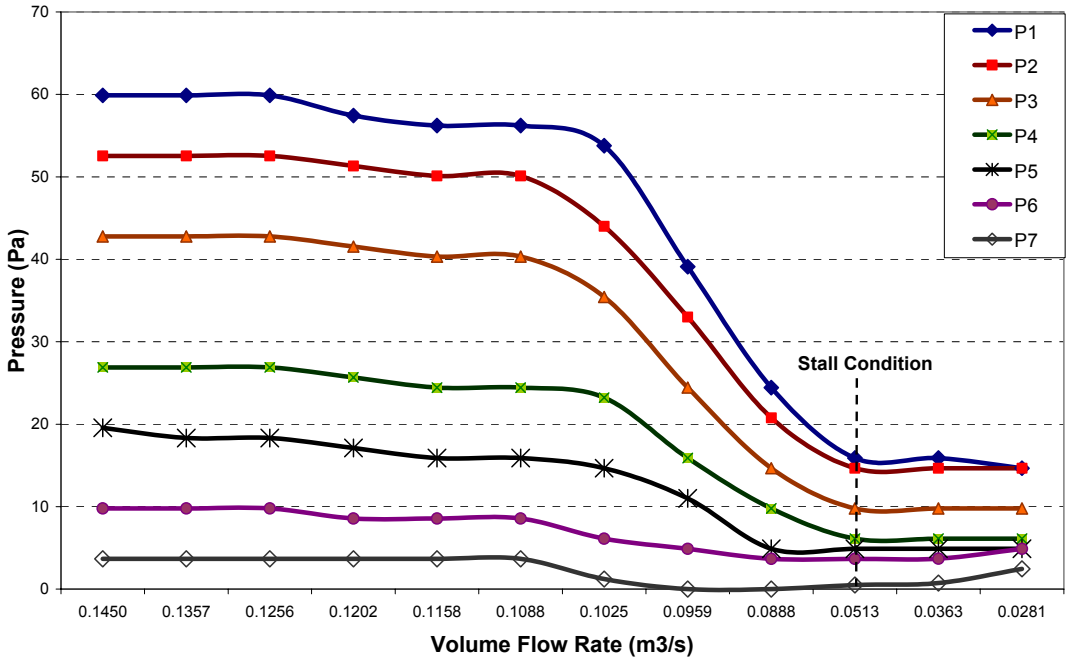

Figure 4.23: Pressure Distribution on Shroud Wall with Volumetric Flow Rate, $b / D_i = 0.055$ & $D_o / D_i = 1.75$ & N = 1000 RPM

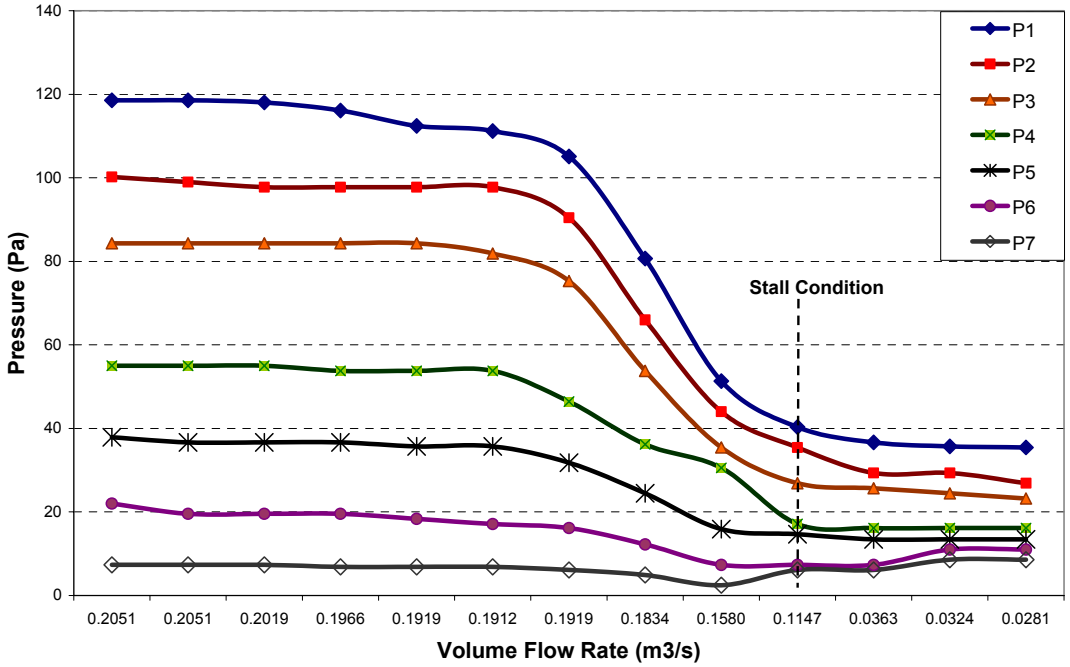

Figure 4.24: Pressure Distribution on Shroud Wall with Volumetric Flow Rate, $b / D_i = 0.055$ & $D_o / D_i = 1.75$ & N = 1500 RPM

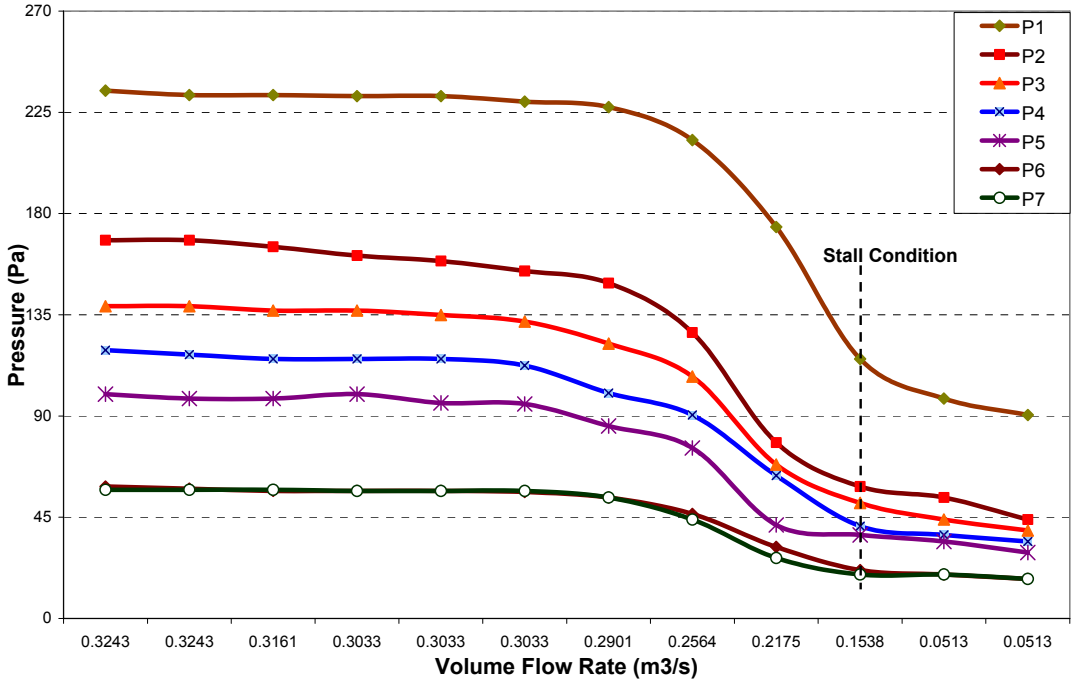

Figure 4.25: Pressure Distribution on Shroud Wall with Volumetric Flow Rate, $b / D_i = 0.055$ & $D_o / D_i = 1.75$ & N = 2000 RPM

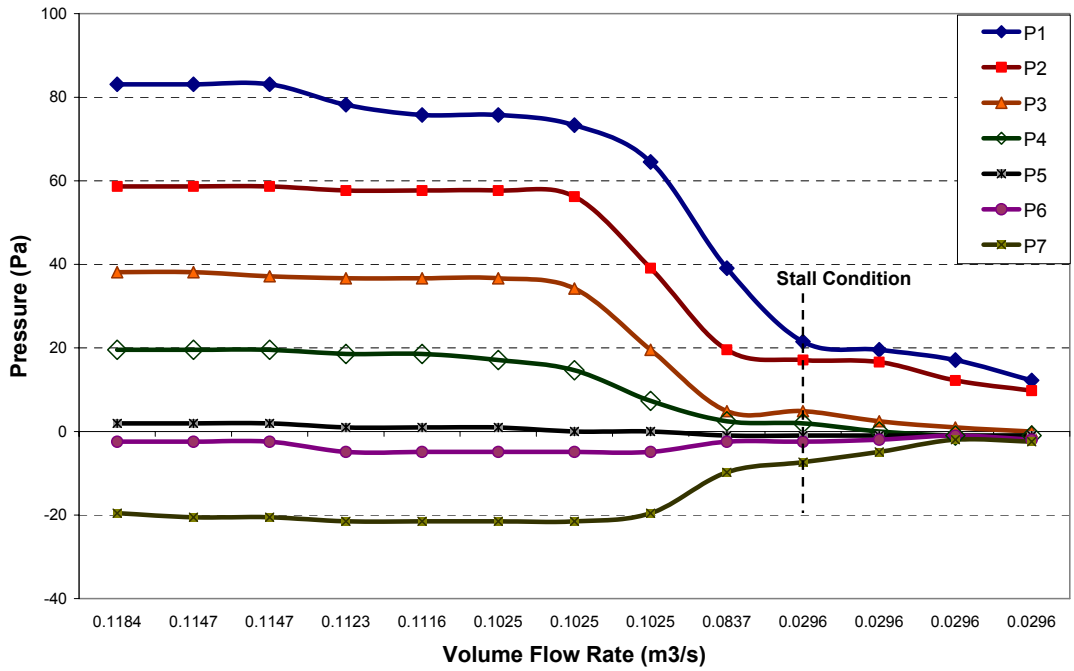

Figure 4.26: Pressure Distribution on Shroud Wall with Volumetric Flow Rate, $b / D_i = 0.055$ & $D_o / D_i = 2.0$ & N = 1000 RPM

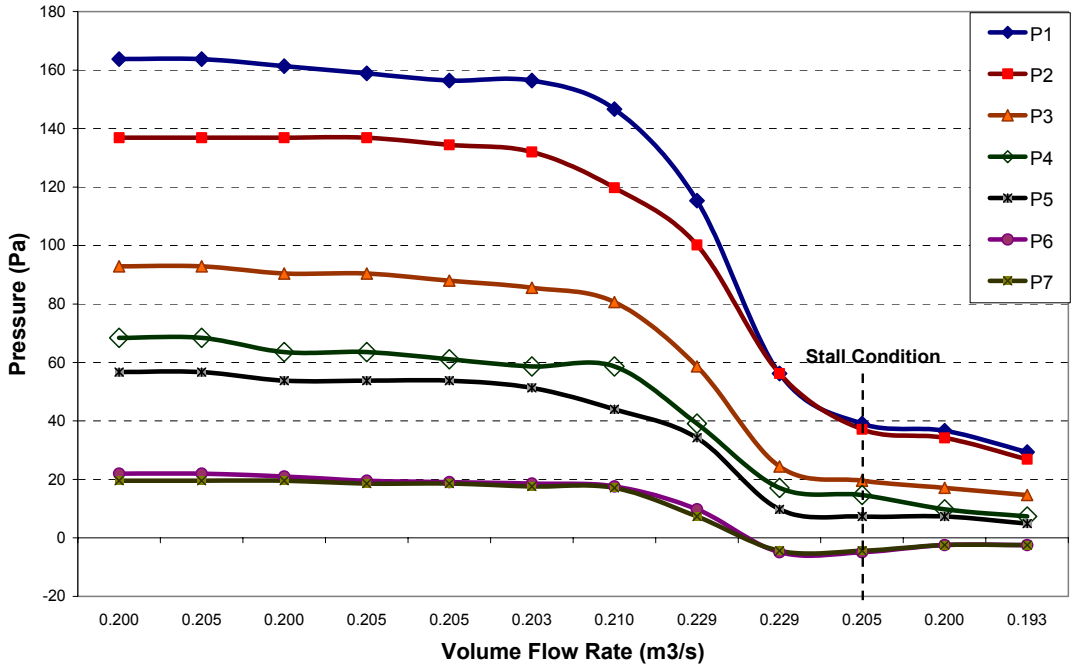

Figure 4.27: Pressure Distribution on Shroud Wall with Volumetric Flow Rate, $b / D_i = 0.055$ & $D_o / D_i = 2.0$ & N = 1500 RPM

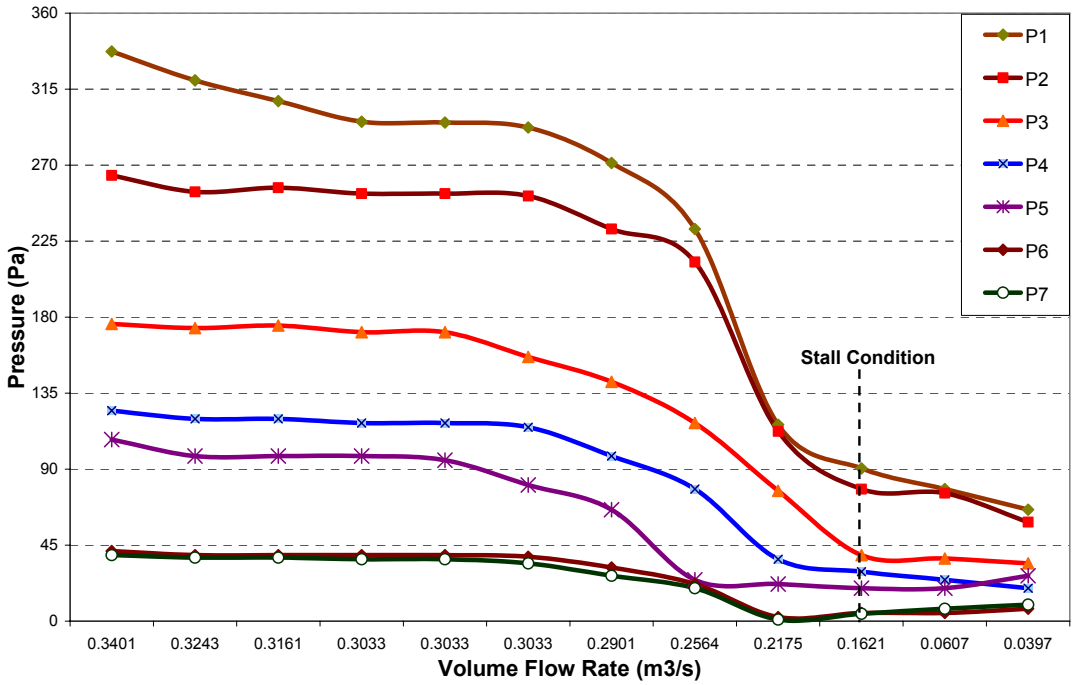

Figure 4.28: Pressure Distribution on Shroud Wall with Volumetric Flow Rate, $b / D_i = 0.055$ & $D_o / D_i = 2.0$ & N = 2000 RPM

CHAPTER 5

ROTATING STALL CHARACTERISTICS

Rotating stall characteristics were measured as a function of flow variables and diffuser geometry. The effects of these variables on rotating stall characteristics are described in this chapter. Before going into the details of how flow variables and diffuser geometry affect the onset and propagation of rotating stall in the vaneless diffuser, it is important to first know whether the stall detected in this study was caused by the impeller or the diffuser. It is logical to assume that the diffuser initiates the flow instability experienced from previous studies as pressure coefficient increases continuously with a decrease in the flow coefficient when the compressor was operated without a diffuser (Kamorudeen, B. and Ahmed, S. (2000)).

5.1 Effects of Impeller Speed

Rotating stall characteristics are reported for one diffuser width ratio ($b / D_i = 0.055$) at three diffuser diameter ratios, (D_o / D_i), of 1.5, 1.75, and 2.0. For each of the diameter ratios, the impeller speed was varied in the range of 1000 to 2000 RPM with an interval of 500 RPM (i.e., three speeds were investigated – 1000, 1500, and 2000 RPM). For each speed, the mass flow rate through the compressor was reduced gradually while recording the pressure values and the mass flow rate. The results were non-dimensionalized and presented in the following sub-sections.

5.1.1 Diameter Ratio Do / Di = 1.5

The characteristic curves for all the impeller speeds tested are shown in Fig. 5.1.

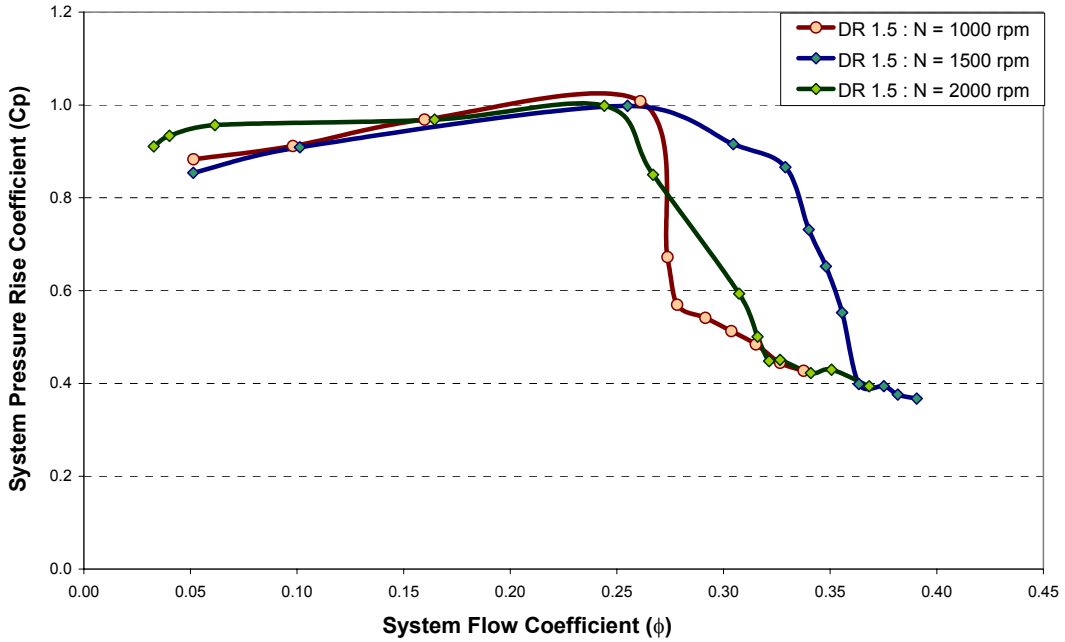

Figure 5.1: Effect of N on System Characteristic Curves, b / D_i = 0.055, D_o / D_i = 1.5

The stability limit of the compressor, which corresponds to the point at which the slope of any curve in Fig. 5.2 changes sign, occurred at ϕ = 0.261, 0.235, and 0.214 for N = 1000, 1500, and 2000 RPM, respectively. As such, these results suggest that the compressor stability increases with increase in the impeller speed. It is important to note here that lower values of the flow coefficient are desirable since they would mean a more stable compressor. The compressor stability limits as determined from the system characteristic curves are not always the onset of rotating stall as shall be shown in the spectral analysis of the signal output from the transducers shortly. Thus, these results are in support of the claim made by Otugen et al. (1988) that the system characteristic curve

is a poor indicator of the onset of diffuser rotating stall. As such, other measurement techniques would have to be employed for the detection of rotating stall in the vaneless diffuser.

Mizuki and Oosawa (1992) used the technique of flow visualization to determine the onset of rotating stall. In this experiment, however, the method used is similar to the one used by Otugen et al. (1988) but with more detailed analysis. The pressure traces from the dynamic pressure transducers at locations 2 and 4 (see Fig. 2.6), which were active low-pass with designed frequency of 100 Hz in order to eliminate frequencies other than the ones associated with rotating stall, were recorded and digitized for further analysis. In particular, the number of rotating stall cells and their speed of rotation relative to the impeller speed were determined from the output of the dynamic pressure transducers at locations 2 and 4. MATLAB was employed for the spectral analyses of the digitized signals from the pressure transducers.

5.1.1.1 N = 1000 RPM

Figures 5.2a-f show the pressure fluctuations from locations 2 and 4 in the time domain for N = 1000 RPM. In general, pressure traces do not show any distinct periodic fluctuation in the flow at high flow coefficients that characterize pre-stall conditions. As the flow coefficient was gradually reduced, periodic patterns were noticed from the pressure signals on the oscilloscope display. The flow coefficient at which these fluctuating patterns were first noticed on both pressure sensors is termed the critical flow coefficient, ϕ_{cr}. A further decrease in the flow coefficient increases the pressure fluctuation amplitude but with no apparent change in the frequency of the signals. Thus, one can define the onset of rotating stall as the first appearance of a clear pattern of

periodic pressure fluctuation. For example, Fig. 5.2d represents the pressure traces at the onset of stall. As such, the critical flow coefficient, ϕ_{cr}, is 0.261. As was noted earlier from the compressor characteristic curve, a precursor to stall in the form of periodic pressure fluctuations occurred at a little higher flow coefficient than ϕ_{cr}. This pre-stall perturbation is responsible for the drop in the pressure coefficient on the compressor characteristic curve. This periodic pressure fluctuation persisted as the flow coefficient was reduced further, but was overshadowed by the stall cell as will be shown in the spectral analysis shortly.

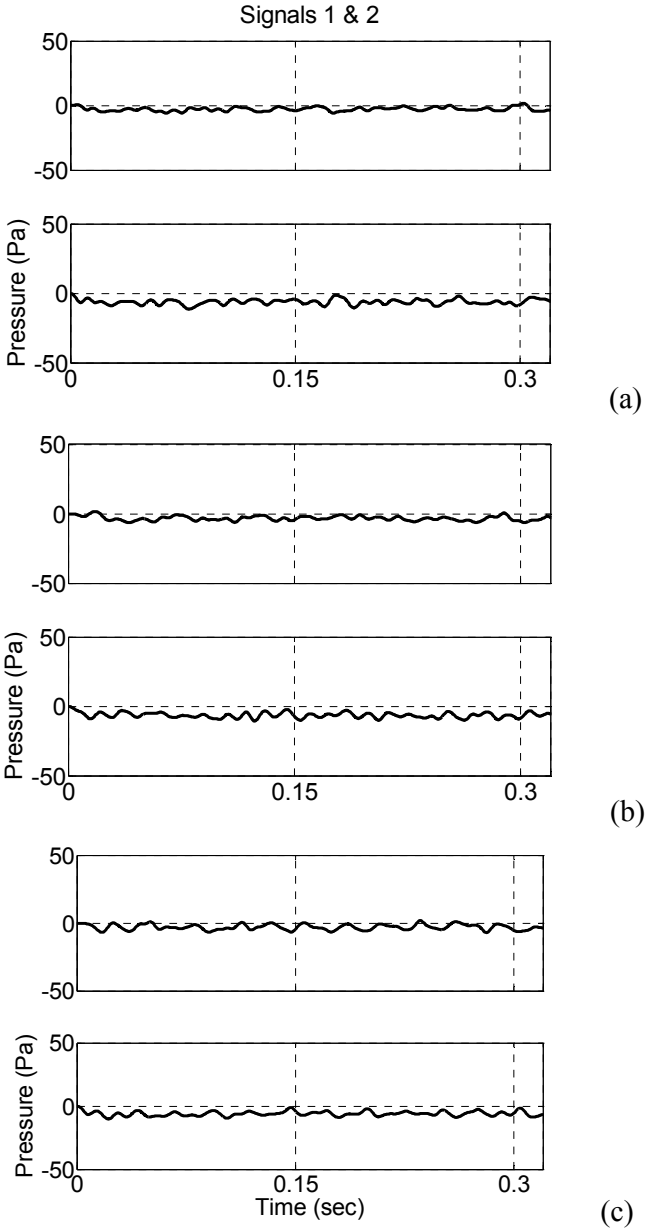

Figures 5.2a-c: Pressure Traces at Different ϕ's, DR = 1.5, N = 1000 RPM
a) ϕ = 0.337 b) ϕ = 0.315 c) ϕ = 0.261

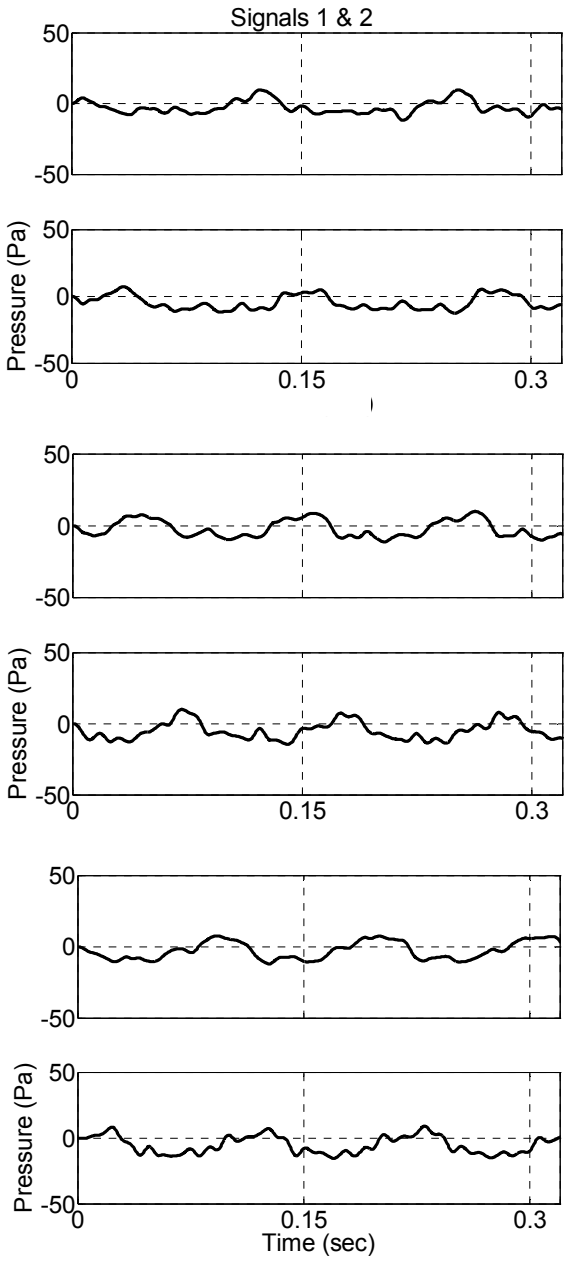

Figures 5.2d-f: Pressure Traces at Different ϕ's, DR = 1.5, N = 1000 RPM
d) ϕ = 0.159 e) ϕ = 0.109 f) ϕ = 0.051

The spectral analysis of these signals accurately revealed the propagating frequencies and their phase angles. Figures 5.3a-f and 5.4a-f show the CSD, phase angles and PSD (respectively) of the output signals from the pressure transducers at locations 2 and 4. Just before stall inception (Figs. 5.3c and 5.4c), the spectral densities showed that there are no propagating frequencies in the diffuser. Figure 5.3c represents the point of maximum pressure coefficient on the flow characteristic curve. Hence, the point of maximum pressure coefficient on the compressor characteristic curve is not the onset of rotating stall but rather the compressor stability limit. At stall inception (Figs. 5.3d and 5.4d), two periodic patterns emerged with lobe numbers 1 and 2. As the flow coefficient was reduced further, the pattern with lobe number 1 grew in strength as could be discerned from the spectral plots. The relative strength of the periodically propagating frequencies would not be known without the PSD analysis at subsequent flow coefficients after stall inception. Table 5.1 shows the stall characteristics. From this table, all the propagating structures from the two pressure transducers at locations 2 and 4 are highly coherent (see φ values) and, as such, no relative strength information could be deduced without the stall cells strength information under the CSD column. For example, at $\phi = 0.1598$, which corresponds to the onset of rotating stall, the CSD value of the stall cell propagating at 5.495 Hz (m = 1) is 48.19 while it is 1.849 for the stall cell of periodicity 2 and propagating at a frequency of 10.27 Hz. Hence, the harmonic-numbers with m = 1 is stronger or relatively more dominant when compared with the harmonic-numbers with m = 2. As the flow coefficient was decreased further, the harmonic-number with m = 1 increases in strength and become more dominant over its multiples with m = 2. Thus, the stall cell with m = 1 was dominant at lower flow coefficient than the critical flow coefficient. Effects of impeller speed on the propagating frequency of the stall cells shall be presented later in another chapter.

Therefore, the structures with n = 1 (or m = 1), which grew in strength as the flow coefficient is reduced, is the primary rotating stall cell with periodicity 1 and rotating in the same direction as the impeller (negative phase angle). The fluctuating patterns with periodicity 2 are better described as the pre-stall symptom (or secondary stall cell) as it is gradually being overshadowed by the primary stall cell at lower flow coefficients than ϕ_{cr}. Finally, Abdelhamid and Bertrand (1980) also reported that the values of Ns / N are independent of ϕ (a further reduction of ϕ_{cr} would not change the value of Ns / N).

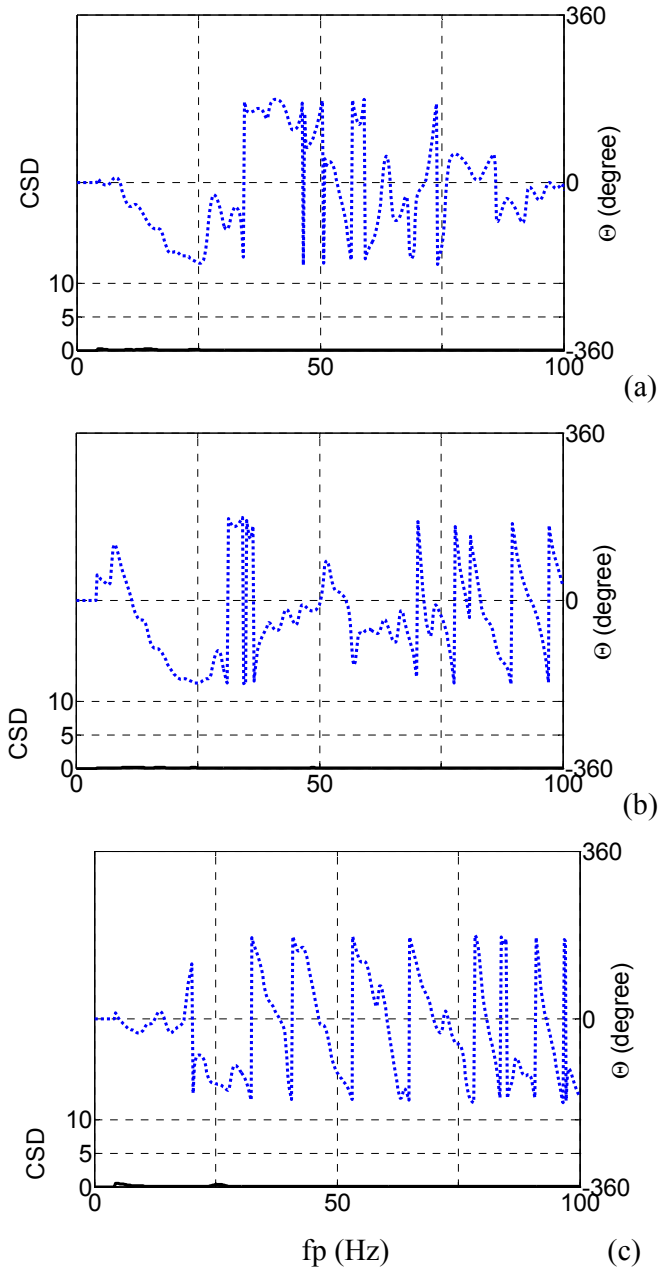

Figures 5.3a-c: Spectra of Pressure Fluctuations (CSD) at Different ϕ's, DR = 1.5 & N = 1000 RPM

a) ϕ = 0.337 b) ϕ = 0.315 c) ϕ = 0.261

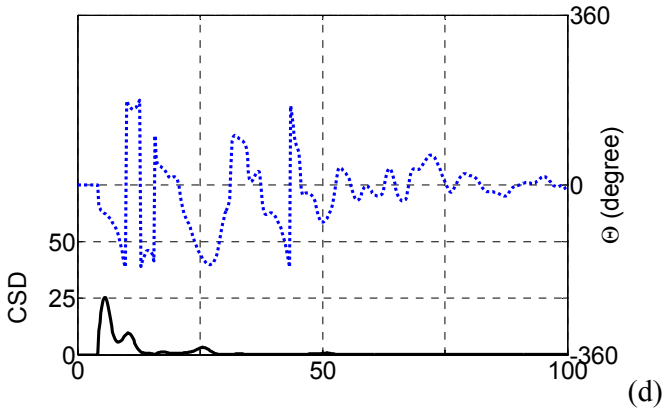

(d)

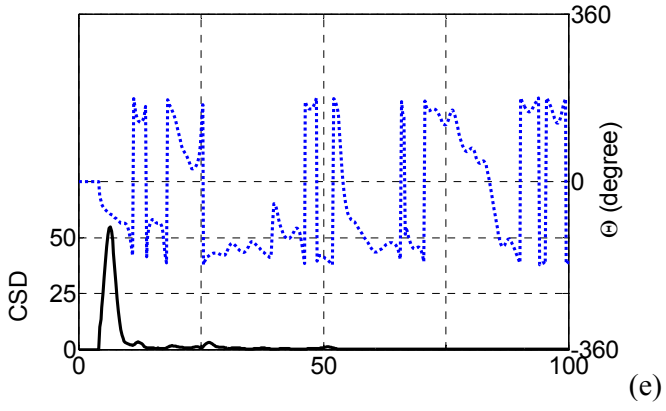

(e)

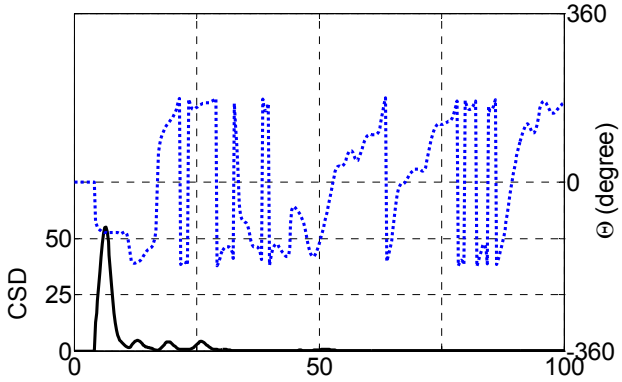

fp (Hz) (f)

Figures 5.3d-f: Spectra of Pressure Fluctuations (CSD) at Different ϕ's, DR = 1.5 & N = 1000 RPM

d) ϕ = 0.159 e) ϕ = 0.109 f) ϕ = 0.051

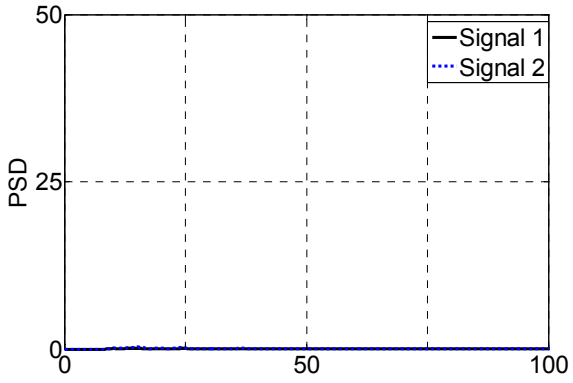

(d)

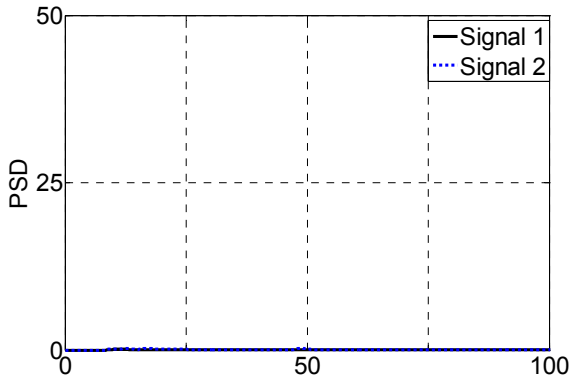

(e)

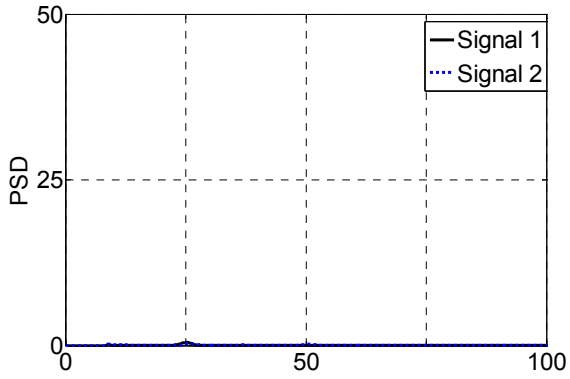

fp (Hz) (f)

Figures 5.4a-c: Spectra of Pressure Fluctuations (PSD) at Different ϕ's, DR = 1.5 & N = 1000 RPM

a) ϕ = 0.337 b) ϕ = 0.315 c) ϕ = 0.261

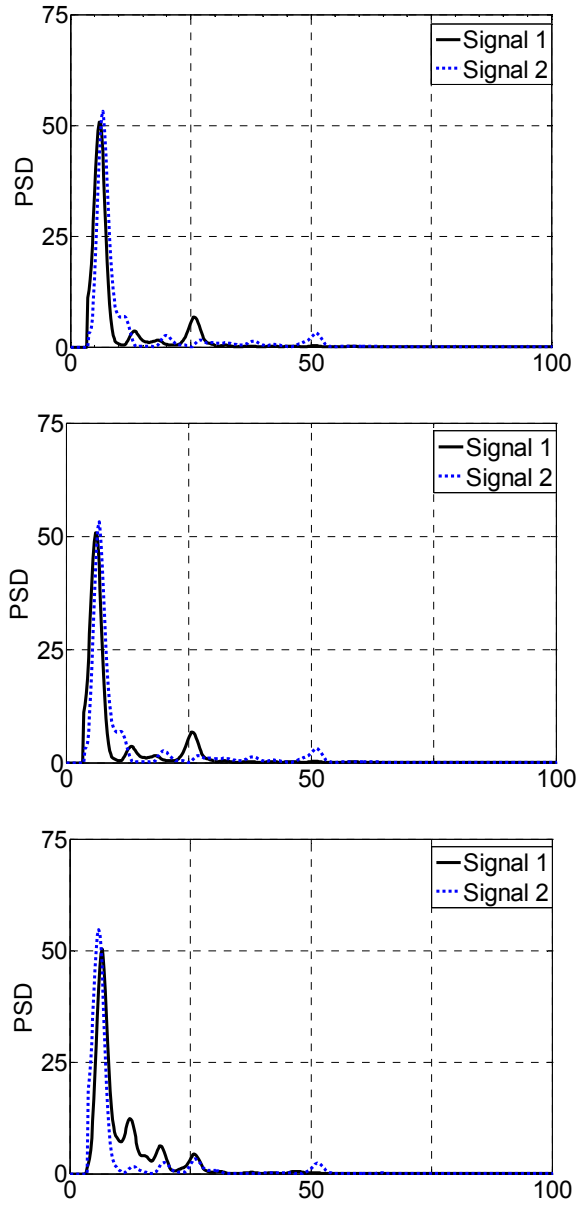

Figures 5.4d-f: Spectra of Pressure Fluctuation (PSD) at Different ϕ's, DR = 1.5 & N = 1000 RPM

d) ϕ = 0.159 e) ϕ = 0.109 f) ϕ = 0.051

5.1.1.2 N = 1500 RPM

Figures 5.5a-d show the pressure traces at different ϕ's for the same diffuser geometry under consideration (i.e., b / D_i = 0.055). No distinct periodic pattern was noticed from Figs. 5.5a-b. However, when the flow coefficient was decreased further, periodic pressure patterns begin to emerge as shown in Fig. 5.5c. Further reduction of the flow coefficient features an increase in the amplitude of the periodically fluctuating pressure pattern. Therefore, the pressure traces in Fig. 5.5c represent the output of the dynamic pressure sensors at the onset of rotating stall. As such, the critical flow coefficient, ϕ_{cr}, is 0.235.

The propagating frequency of the stall cells and other rotating stall cell features were determined as discussed earlier. Figures 5.6a-d and 5.7a-d show the PSD, phase angles, and CSD of the pressure traces shown in Figs. 5.6a-d. The absence of any distinguished spike in the CSD and PSD plots of Figs. 5.6a-b and 5.8a-b confirmed that there is no propagating frequency of periodic pattern at these flow rates. The first distinct spike appeared in Fig. 5.6c and 5.7c. Details of the stall cell features are presented in Table 5.1. This table also confirmed that the first stall cell of periodicity 1 become more dominant than its harmonics as the flow coefficient was reduced further after the onset of rotating stall.

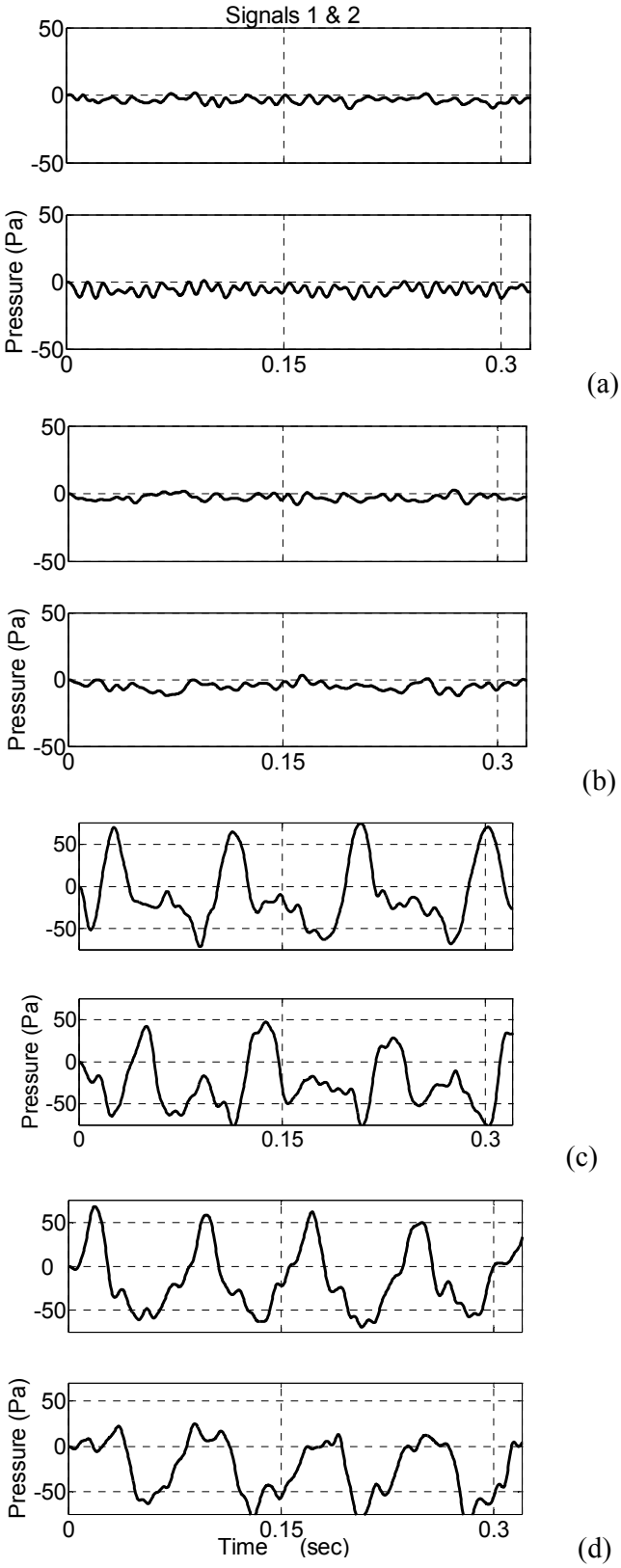

Figures 5.5a-d: Pressure Traces at Different ϕ's, DR = 1.5, N = 1500 RPM
a) ϕ = 0.32 b) ϕ = 0.304 c) ϕ = 0.255 d) ϕ = 0.051

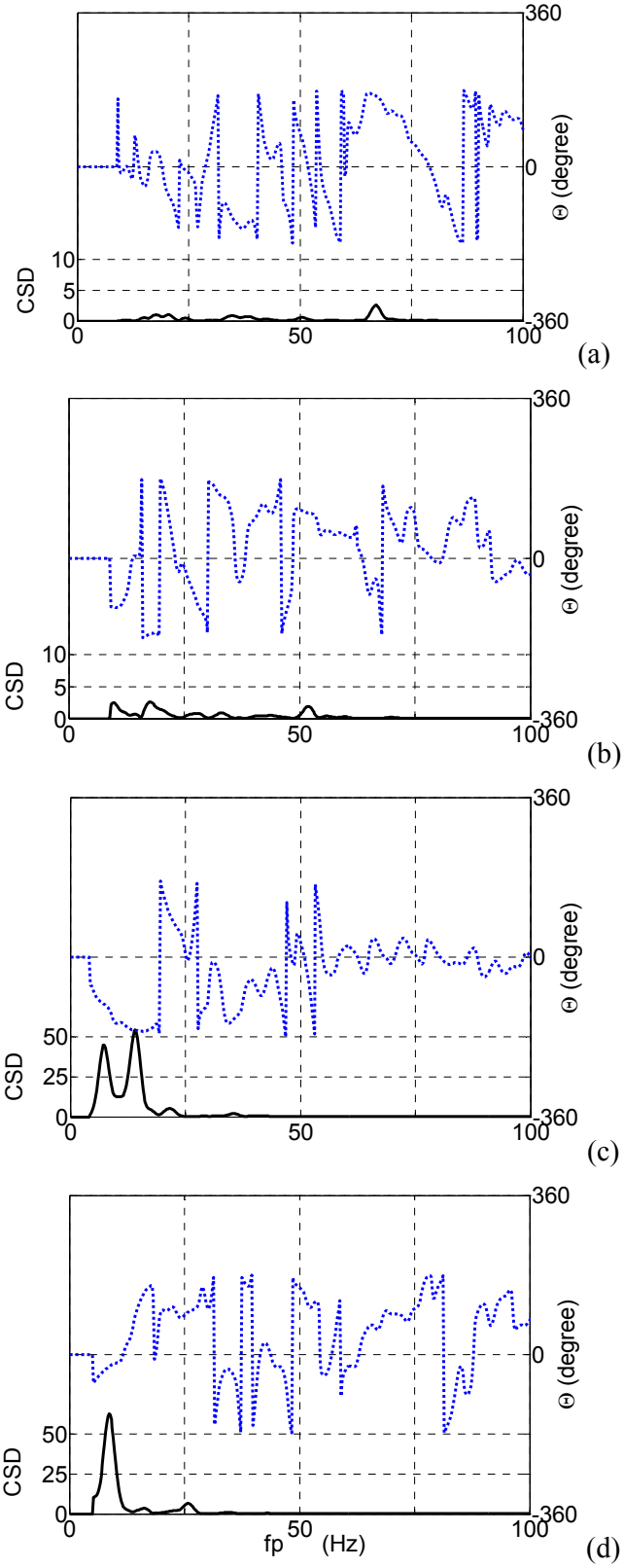

Figures 5.6a-d: Spectra of Pressure Fluctuation (CSD) at Different ϕ's, DR = 1.5 & N = 1500 RPM

a) ϕ = 0.32 b) ϕ = 0.304 c) ϕ = 0.255 d) ϕ = 0.051

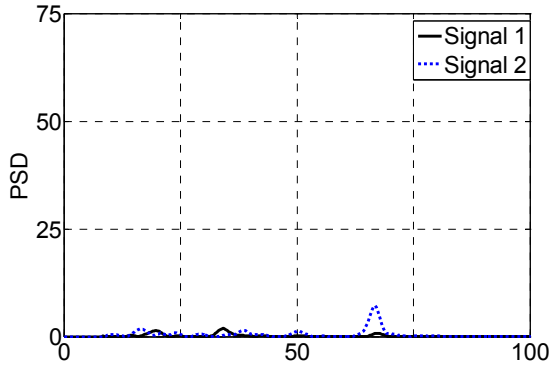

(a)

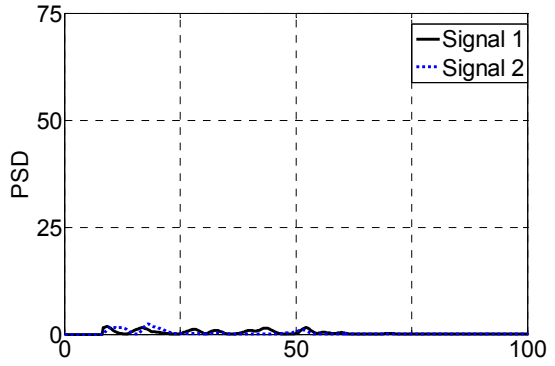

(b)

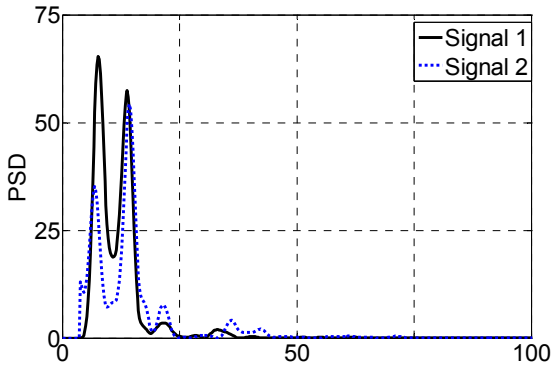

(c)

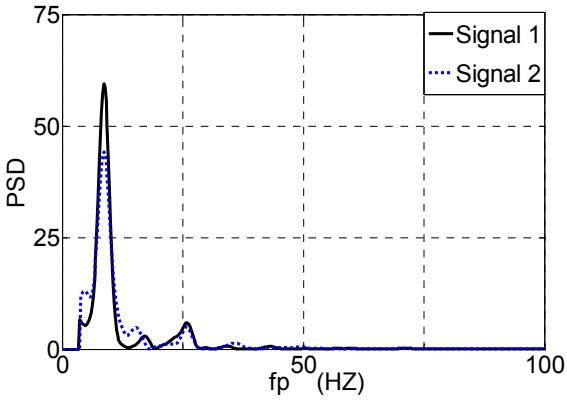

(d)

Figures 5.7a-d: Spectra of Pressure Fluctuation (PSD) at Different ϕ's, DR = 1.5 & N = 1500 RPM

a) ϕ = 0.32 b) ϕ = 0.304 c) ϕ = 0.255 d) ϕ = 0.051

5.1.1.3 N = 2000 RPM

The time-series of the output signal from the pressure transducers at different flow coefficients are shown in Figures 5.8a-d The critical flow coefficient, based on its earlier definition, is $\phi_{cr} = 0.214$ which corresponds to Fig. 5.8c. The primary stall cell grows in strength as the flow coefficient was reduced from 0.214 to 0.051, which was the minimum flow coefficient at which data were taken for this impeller speed.

Figures 5.9a-d and 5.10a-d show the spectra of the pressure fluctuations in Figs. 5.8a-d. The distinct spike in Figs. 5.10a-b with a value of 25.22 Hz is the resonant frequency of the system as it persisted throughout the flow coefficients tested. That is, it was present before and after rotating stall inception. It is not a stall cell as its phase angle is in the order of 14^o, much smaller than the physical angle, 45^o, between the two pressure transducers whose spectra are shown in the figures. Mizuki and Oosawa (1992) made similar observation when they concluded that the 27 Hz structure, which was observed to occur irrespective of the variation of the flow rate, is the system resonant frequency. This type of frequency is present at all the impeller speeds tested.

At the onset of rotating stall, which corresponds to Figs. 5.9c and 5.10c, the CSD and PSD plots show the sudden emergence of the stall cells. These stall cells persisted as the flow coefficient was reduced further. Table 5.1 shows the stall cells features measured at this impeller speed of 2000 RPM. As was noted earlier, the negative phase angle between the two pressure transducers indicates that the stall cells were propagating in the same direction as the impeller (see Abdelhamid (1983a)). The table indicates that the stall cell of periodicity 1 became more dominant as the flow coefficient was reduced, in concordance with the trend discussed earlier. The table also shows that this stall cell was

propagating at an angular speed of about 40% of the impeller angular speed at the beginning of the instability (ϕ_{cr} = 0.214). At much lower flow coefficient, the angular speed of the primary stall cell was about one-third of the impeller angular speed (e.g., at ϕ = 0.051). These results are in good agreement with the experimental results of Kinoshita and Senoo (1985) who reported stall cell angular speed of about one-third of the impeller angular speed. The primary stall cell is 10.27 Hz at the onset of rotating stall (ϕ_{cr} = 0.214). It has second and third harmonics, featuring at $\phi \leq$ 0.214, of 21.02 Hz, and 32.25 Hz, respectively. Thus, this range of flow coefficient features, essentially, one stall cell propagating at a frequency of 10.27 Hz with its three harmonics. It is important to note that the two harmonics, though highly coherent as shown in the table, have very small amplitudes (CSD values in Table 5.1) when compared to the amplitude of the fundamental frequency.

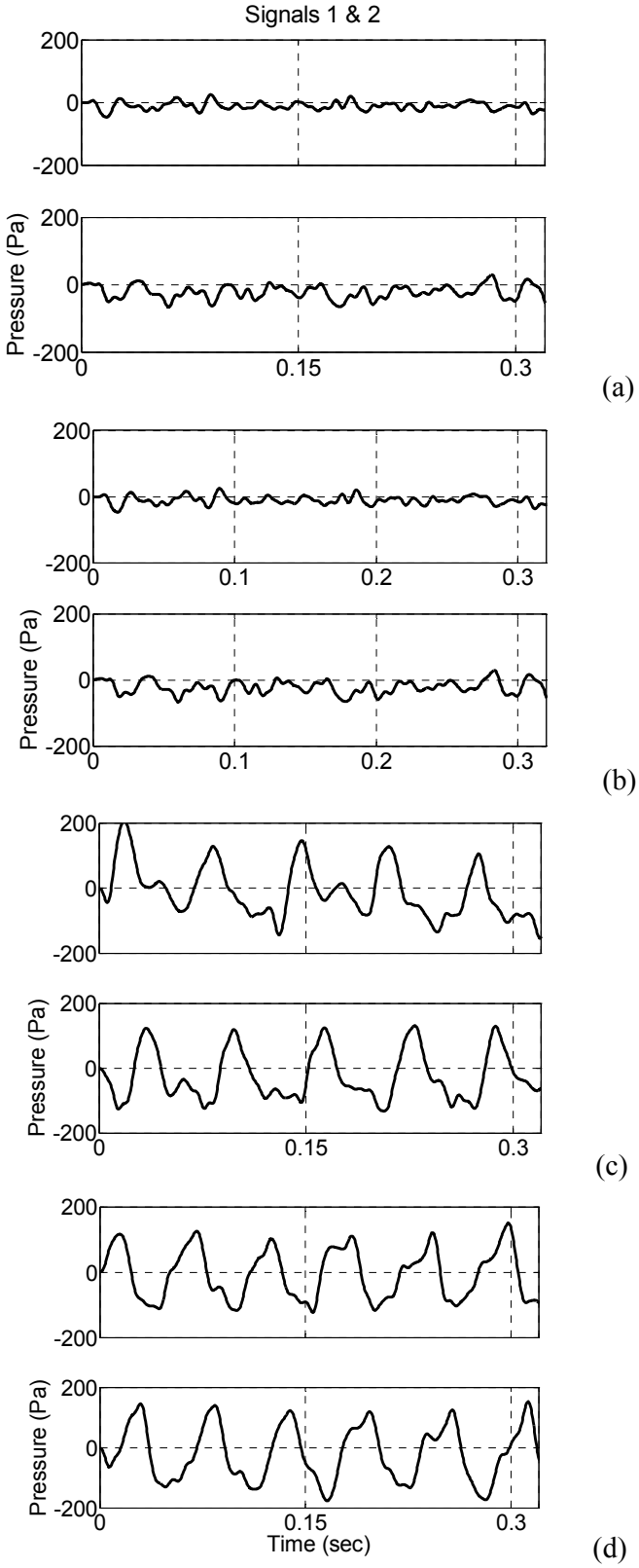

Figures 5.8a-d: Pressure Traces at Different ϕ's, DR = 1.5, N = 2000 RPM
a) ϕ = 0.308 b) ϕ = 0.267 c) ϕ = 0.214 d) ϕ = 0.033

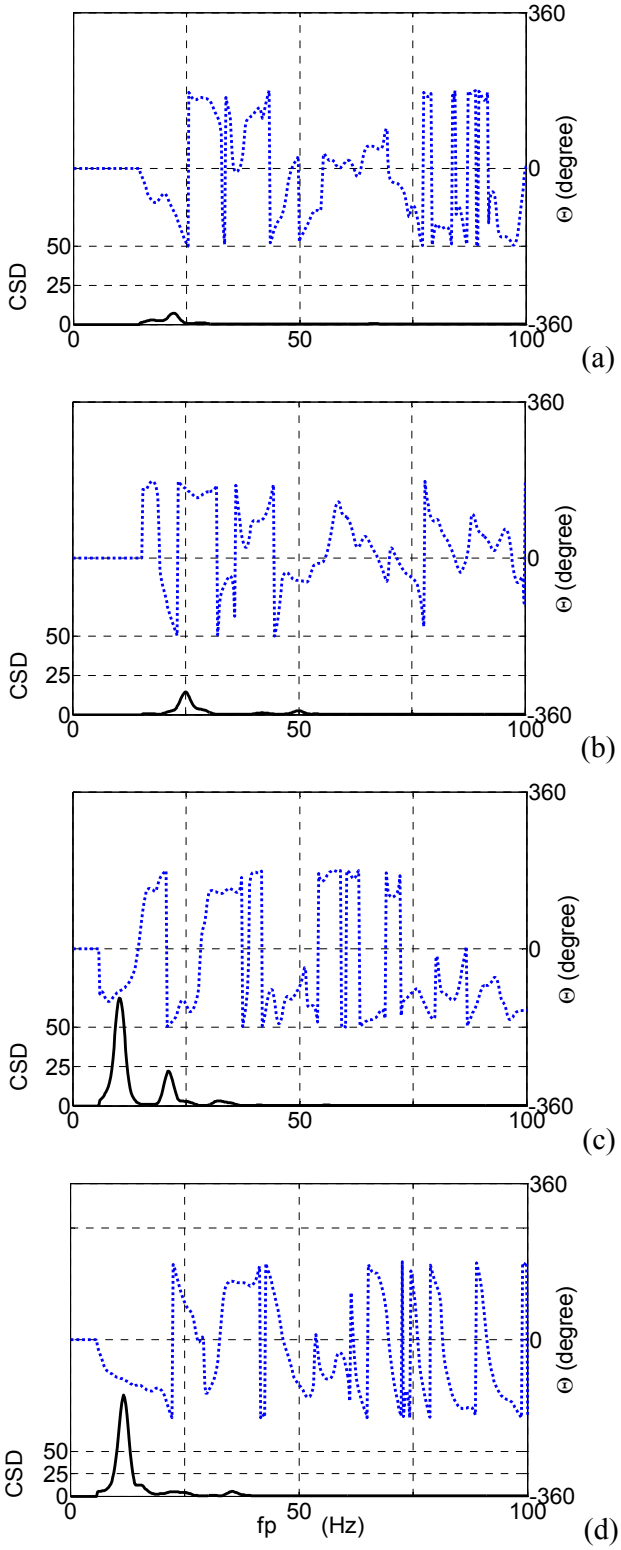

Figures 5.9a-d: Spectra of Pressure Fluctuation (CSD) at Different ϕ's, DR = 1.5 & N = 2000 RPM

a) ϕ = 0.308 b) ϕ = 0.267 c) ϕ = 0.214 d) ϕ = 0.033

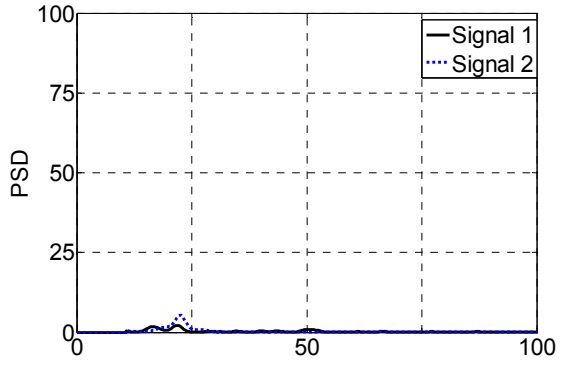

(a)

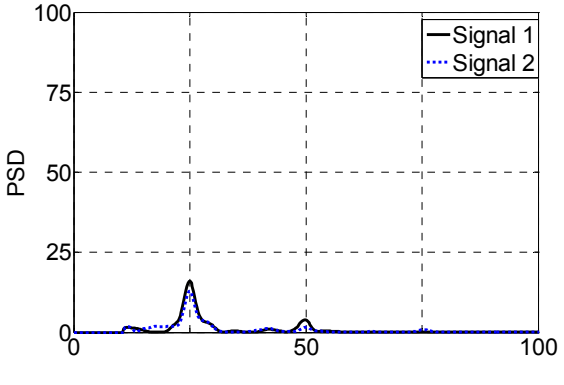

(b)

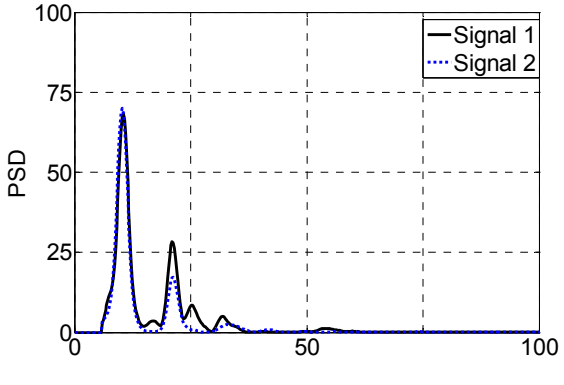

(c)

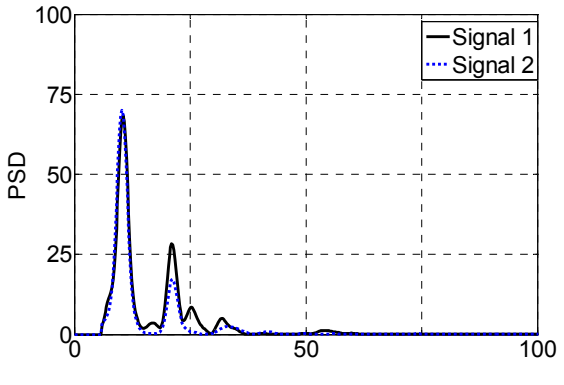

(d)

Figures 5.10a-d: Spectra of Pressure Fluctuation (PSD) at Different ϕ's, DR =1.5 & N = 2000 RPM

a) ϕ = 0.308 b) ϕ = 0.267 c) ϕ = 0.214 d) ϕ = 0.033

5.1.2 Diameter Ratio $D_o / D_i = 1.75$

The system characteristic curves of the compressor for all the impeller speeds tested at $D_o / D_i = 1.75$ is shown in Fig. 5.11. This figure confirms the trend of the compressor stability limit as a function of impeller angular speed suggested by the diffuser geometry discussed in the previous subsection. For example, values of the flow coefficient at which Cp is a maximum for impeller speeds of 1000 RPM, 1500 RPM, and 2000 RPM, are 0.2551, 0.2362, and 0.2274, respectively. Therefore, confirming that the flow coefficient at the stability limit decreases with increase in impeller angular speed at a fixed vaneless diffuser diameter ratio.

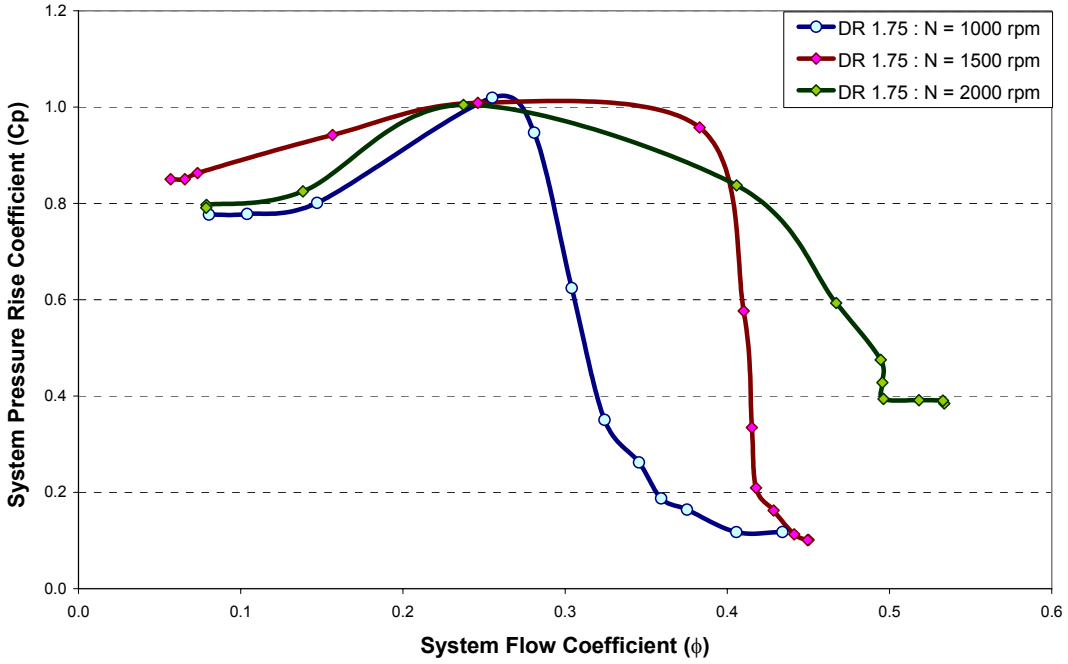

Figure 5.11: Effect of N on System Characteristic Curves, $b / D_i = 0.055$, $D_o / D_i = 1.75$

For the reasons mentioned earlier, the flow coefficient at the onset of rotating stall does not necessarily coincide with the ϕ values at the compressor stability limit. The

same approach described earlier was employed to determine the onset and propagation of rotating stall at this diffuser diameter ratio.

5.1.2.1 N = 1000 RPM

The pressure fluctuations at different flow coefficients are shown in Figs. 5.12a-f. The pressure signal at the onset of rotating stall corresponds to what is shown in Fig. 5.12d. Therefore, the critical flow coefficient, ϕ_{cr}, is 0.1472. As the flow coefficient was reduced further, the strength of the stall cells increased as expected. The details of the propagating frequencies of the stall cells and other stall characteristics were obtained with the help of the spectral analysis of the pressure traces from the dynamic pressure transducers. The spectra of the pressure fluctuations at different ϕ's are shown in Figs. 5.13a-f and 5.14a-f. The non-periodic frequency of 25.08 Hz, which occur irrespective of the flow coefficient, is visible in these figures. The reason why this type of frequency is not considered as a stall cell has been mentioned earlier. At the critical flow coefficient of 0.1472, stall cells begin to emerge as shown in Figs. 5.13d and 5.14d. Figures 5.13d-f and 5.14d-f illustrate that the strength of primary stall cell increases, as expected, as the flow coefficient was reduced further below 0.1472.

The detailed characteristics of the stall cells are tabulated in Table 5.1. The propagating frequency of the primary stall cell changes from 4.061 Hz, at the onset of stall inception, to 8.27 Hz as the flow coefficient was reduced further.

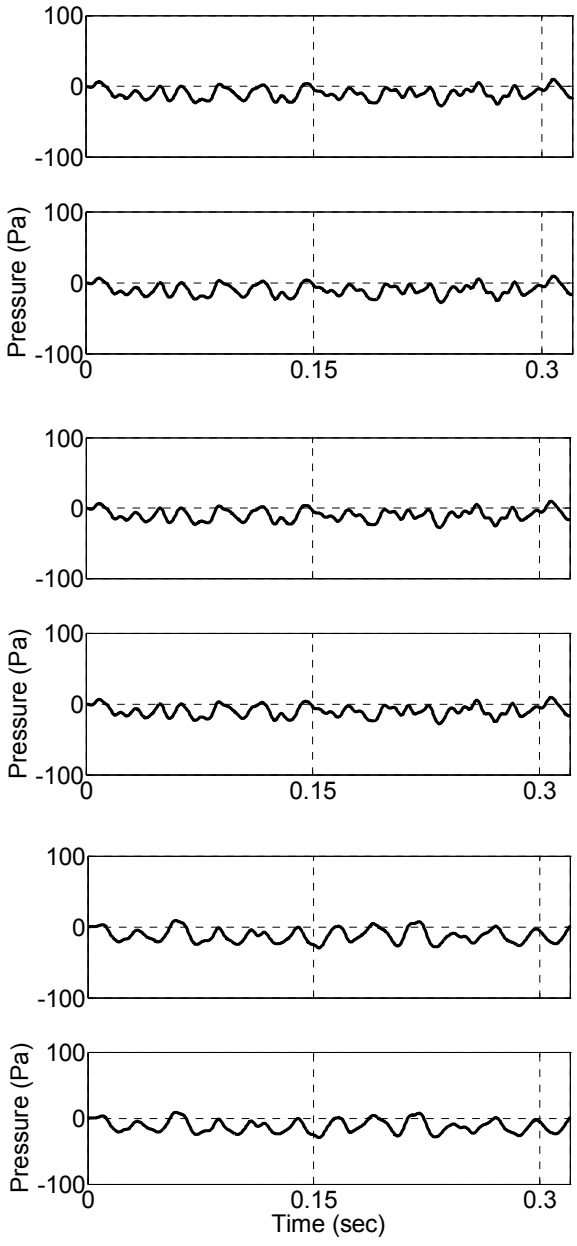

Figures 5.12a-c: Pressure Traces at Different ϕ's, DR = 1.75, N = 1000 RPM
a) ϕ = 0.434 b) ϕ = 0.359 c) ϕ = 0.255

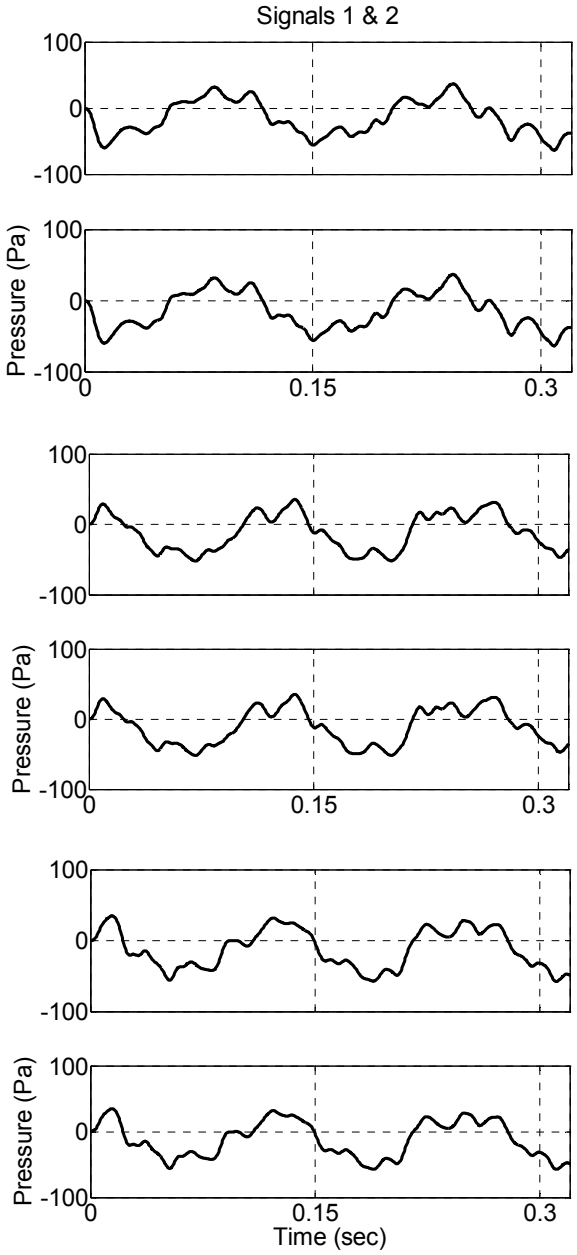

(d)

(e)

(f)

Figures 5.12d-f: Pressure Traces at Different ϕ's, DR = 1.75, N = 1000 RPM
d) ϕ = 0.147 e) ϕ = 0.104 f) ϕ = 0.081

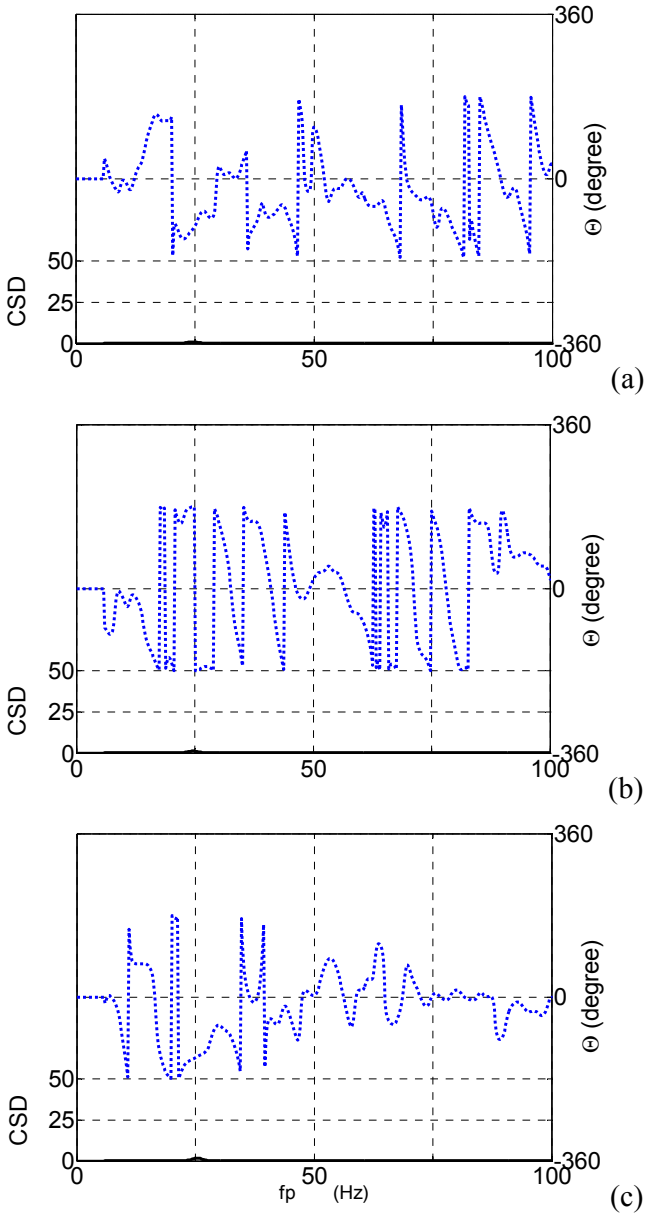

Figures 5.13a-c: Spectra of Pressure Fluctuations (CSD) at Different ϕ's, DR = 1.75 & N = 1000 RPM

a) ϕ = 0.434 b) ϕ = 0.359 c) ϕ = 0.255

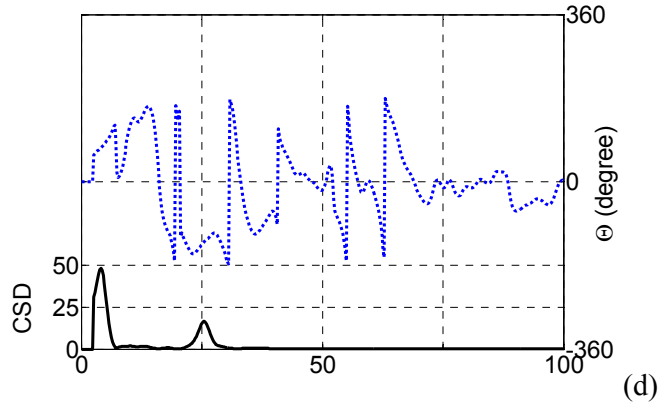

(d)

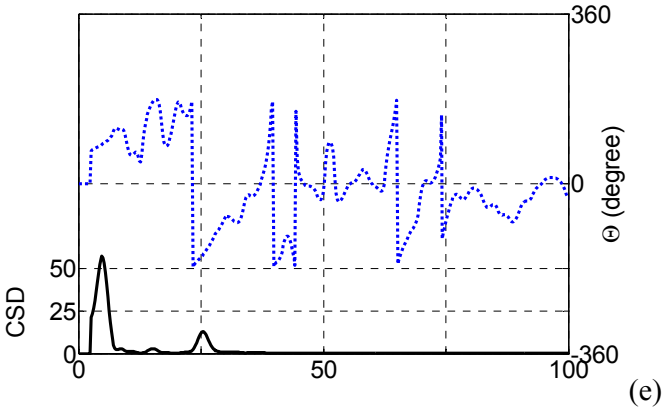

(e)

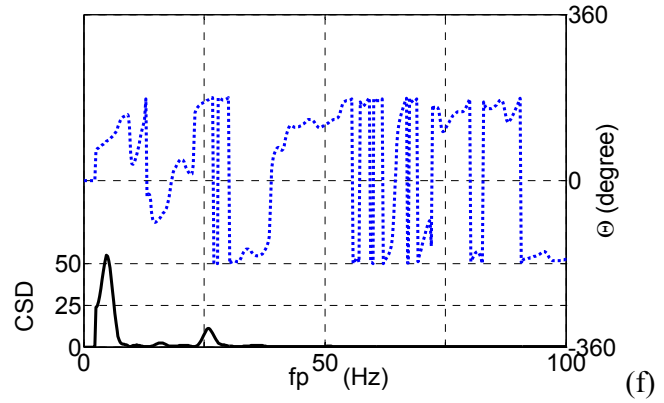

(f)

Figures 5.13-f: Spectra of Pressure Fluctuations (CSD) at Different ϕ's, DR = 1.75 & N = 1000 RPM
d) ϕ = 0.147 e) ϕ = 0.104 f) ϕ = 0.081

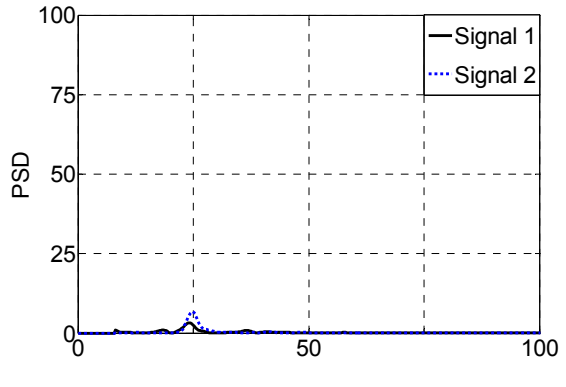

(a)

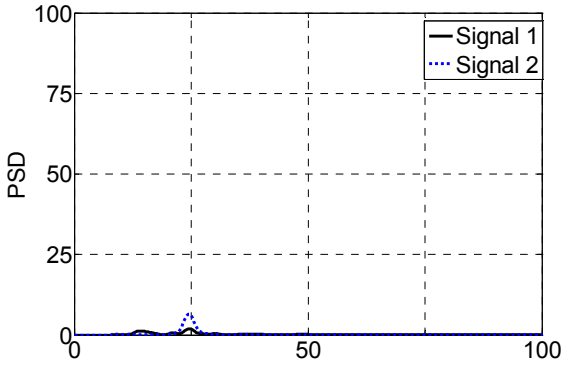

(b)

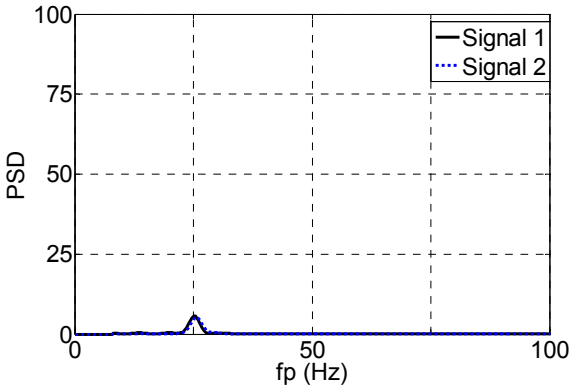

(c)

Figures 5.14a-c: Spectra of Pressure Fluctuations (PSD) at Different ϕ's, DR = 1.75 & N = 1000 RPM

a) ϕ = 0.434 b) ϕ = 0.359 c) ϕ = 0.255

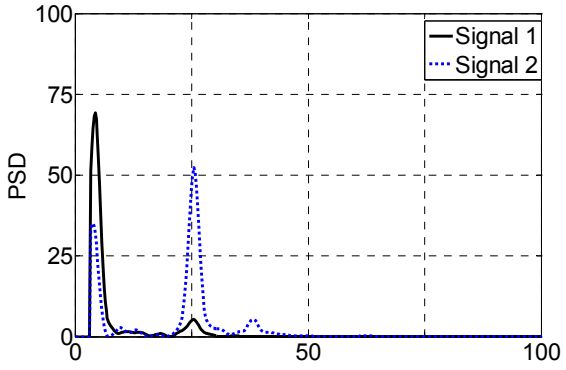

(d)

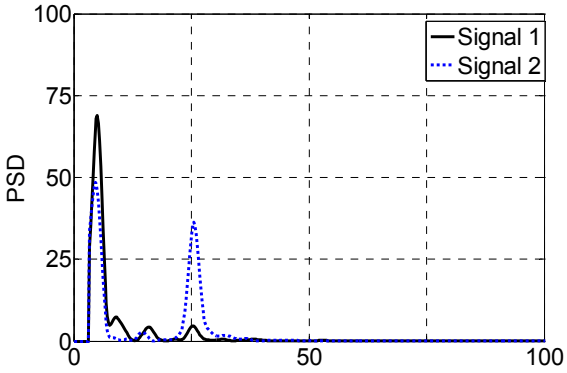

(e)

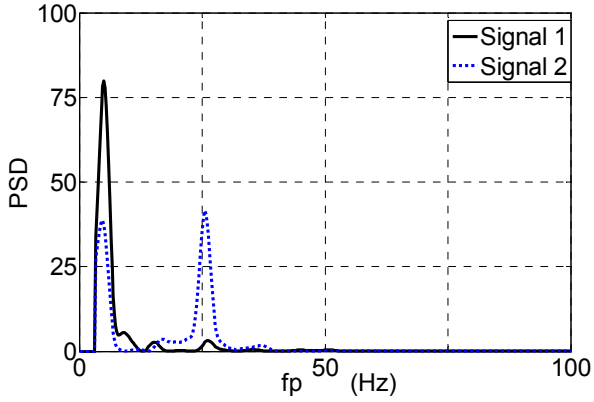

(f)

Figures 5.14d-f: Spectra of Pressure Fluctuation (PSD) at Different ϕ's, DR = 1.75 & N = 1000 RPM

d) ϕ = 0.147 e) ϕ = 0.104 f) ϕ = 0.081

5.1.2.2 N = 1500 RPM

The first periodic flow fluctuation was first noticed at ϕ = 0.1566, which corresponds to Fig. 5.15c. Thus, the critical flow coefficient at impeller speed of 1500 RPM and D_o / D_i = 1.75 is 0.1566. Figure 5.16c and Fig. 5.16d show that the strength of the stall cell increases as the flow coefficient is decreased further. The spectral plots of Figs. 5.16a-b are shown in Figs. 5.16 a-b. No distinguishable spike is noticed from the spectral plots until ϕ = 0.1566. Table 5.1 shows the stall properties extracted from Figs.5.17c-d. In particular, the table shows that the strength of the primary stall cell, with propagating frequency of 6.684 Hz, increases with a decrease in the flow coefficient. The third harmonic of the primary stall cell also occurred at ϕ = 0.0568 and at the inception of rotating stall, respectively.

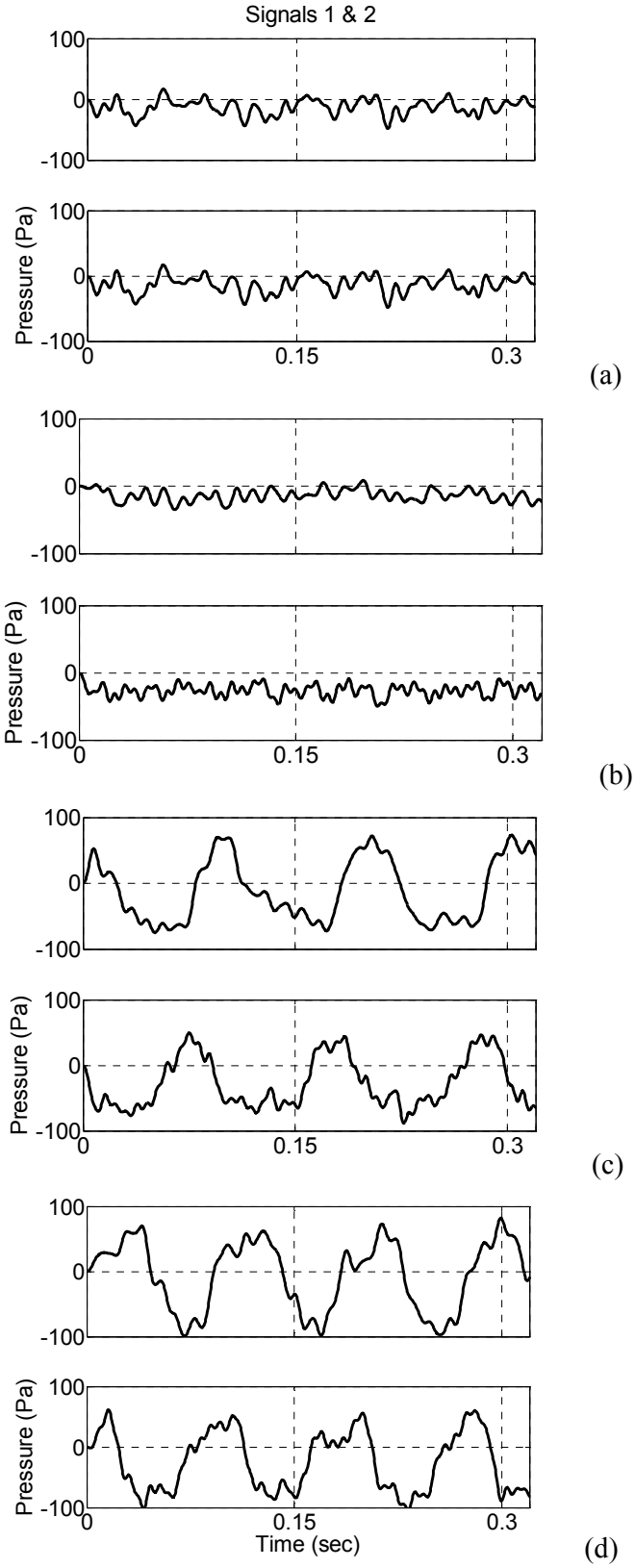

Figures 5.15a-d: Pressure Traces at Different ϕ's, DR = 1.75, N = 1500 RPM
a) ϕ = 0.451 b) ϕ = 0.246 c) ϕ = 0.156 d) ϕ = 0.057

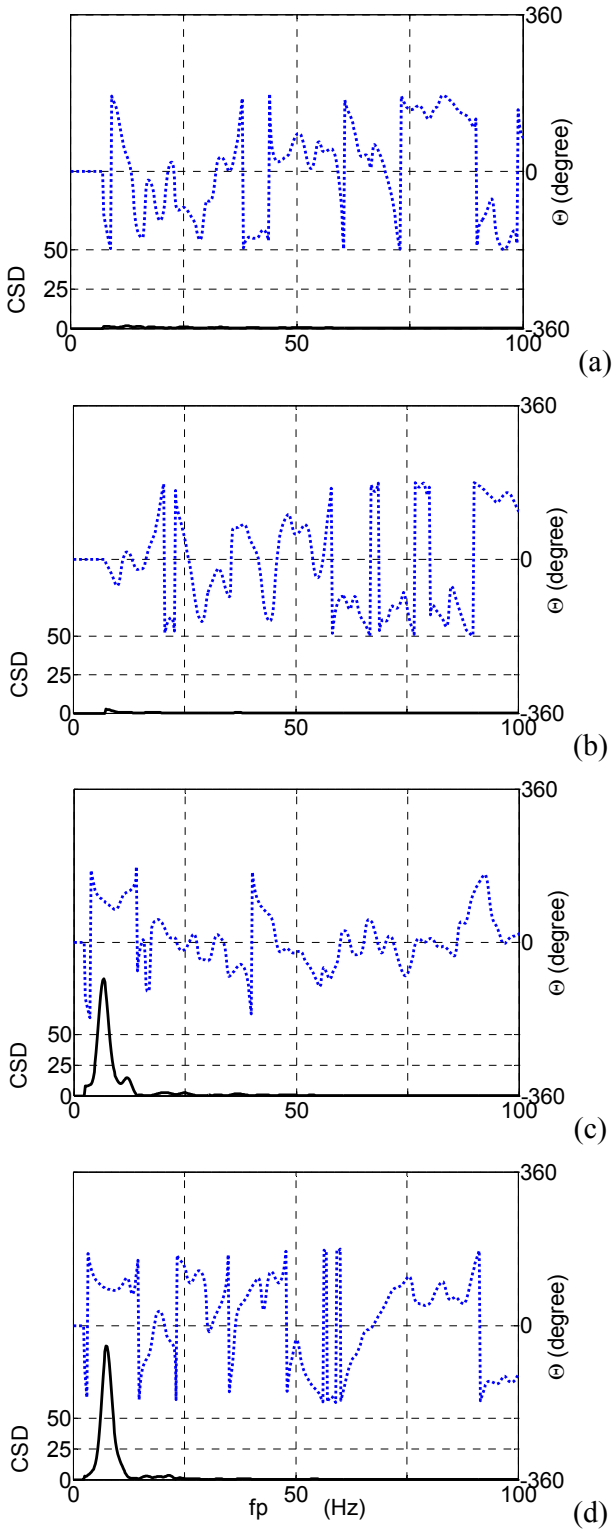

Figures 5.16a-d: Spectra of Pressure Fluctuations (CSD) at Differentϕ's, DR = 1.75 &N=1500 RPM

a) ϕ = 0.451 b) ϕ = 0.246 c) ϕ = 0.156 d) ϕ = 0.057

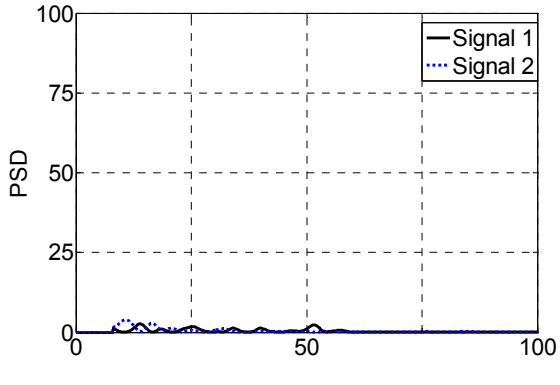

(a)

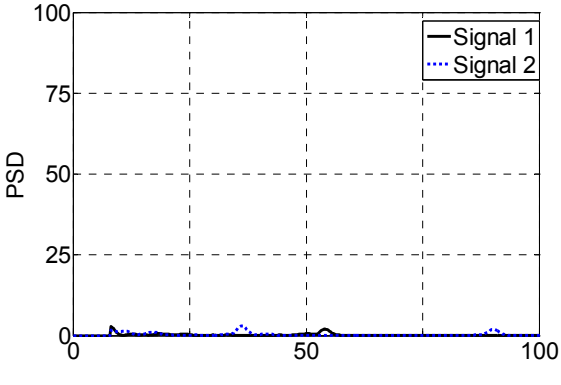

(b)

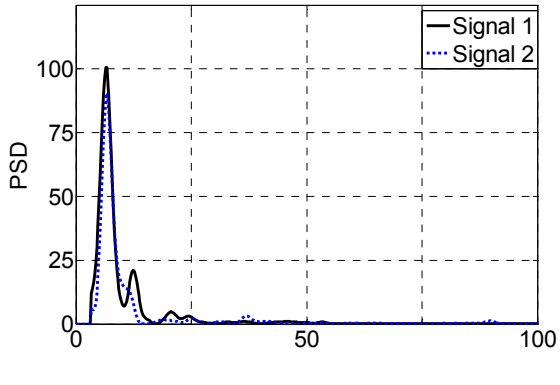

(c)

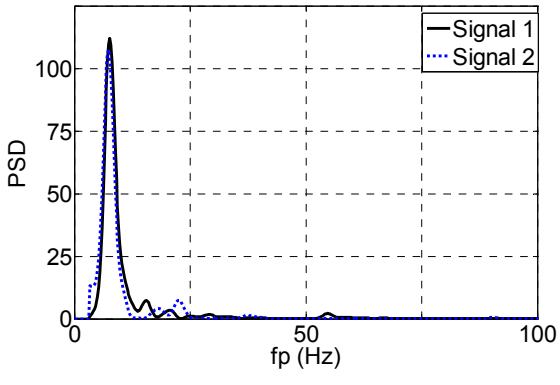

(d)

Figures 5.17a-d: Spectra of Pressure Fluctuations (PSD) at Differentϕ's, DR = 1.75 & N=1500 RPM

a) ϕ = 0.451 b) ϕ = 0.246 c) ϕ = 0.156 d) ϕ = 0.057

5.1.2.3 N = 2000 RPM

The output signals from the dynamic pressure transducers at different flow coefficients are shown in Figs. 5.18a-d. Fig. 5.18c represents the output signal from the pressure transducers at the onset of rotating stall. As such, the critical flow coefficient at impeller speed of 2000 RPM, $b / D_i = 0.055$ and $D_o / D_i = 1.75$ is 0.1384. As the flow coefficient was reduced further after the inception of rotating stall, the strength of the flow perturbation increased as can be discerned from Figs. 5.19c-d. The spectral plots in Figs. 5.19a-d and Figs. 5.20a-d show a clearer picture of the strength of the rotating structures. The emergence of the stall cells is clearly noted in Figs. 5.19c, the spectra of Fig. 5.20c. The spectral plots at higher flow coefficients than $\phi_{cr} = 0.1384$. The frequency of 22 Hz that occurred at all the flow coefficients before $\phi = 0.1388$ is not a stall cell as explained earlier.

Table 5.1 shows the detailed features of the rotating stall. The dominance of the primary stall cell, $f_p = 9.078$ Hz, over the secondary harmonic-number, $f_p = 18.87$ Hz, increases as the flow coefficient is reduced. Going by the amplitude information provided by the CSD column of Table 5.1, the periodic pattern with three harmonic-numbers is relatively insignificant compared to the primary stall cell. This is also obvious from Figs. 5.21c-d. As shown in the coherency column (φ column) of Table 5.1, all the propagating structures are highly coherent. It is interesting to note that the second harmonic of the primary stall cell emerged as ϕ decreases further.

Aside from the one and two harmonic-numbers structures that appeared at the onset of rotating stall, whose spikes are obvious from the CSD plot of Fig. 5.19d, the 3 harmonic-number structures shown at this same flow coefficient (see Table 5.1). These 3

harmonic-number structures, with frequencies of pressure fluctuation of 18.87 Hz and 26.28 Hz, are highly coherent (φ = 0.939 and 0.863, respectively). Without the strength information provided by the spectral densities, the coherence values would not suffice for an adequate description of the stall cells. Similarly, the three harmonic-number structures with propagating frequency of 9.078 Hz, which appeared as the flow coefficient was reduced below the critical value, is hardly visible from the spectral plots but is highly coherent as shown in Table 5.1.Tthe relative strength of these harmonic-numbers need to be evaluated before they could be considered as stall cells. For example, the stall cell with m = 1 has strength (CSD values in Table 5.1) of between 25 and 50 times the strength of the three harmonic-number structures. Finally, the speed of the primary stall cell, 29.4% of impeller angular speed, shown in Table 5.1 is in good agreement with earlier published data as expatiated in the previous subsection.

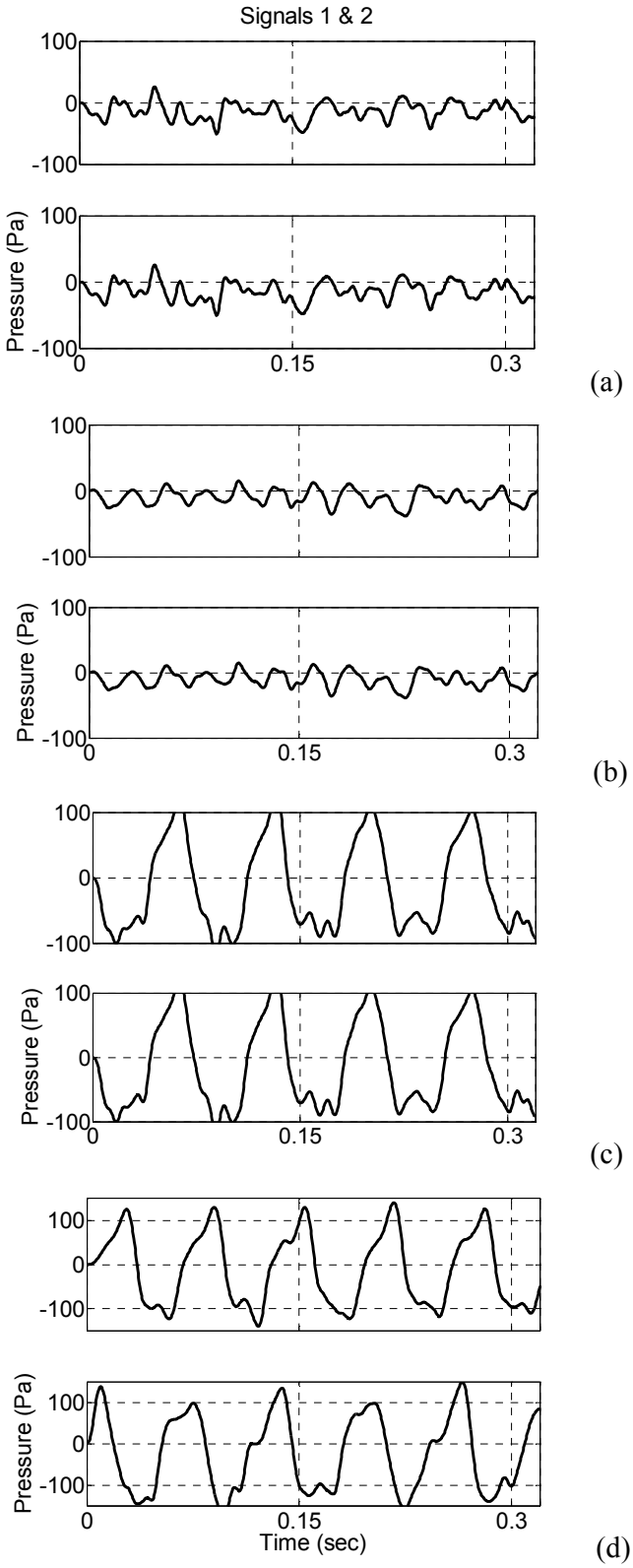

Figures 5.18a-d: Pressure Traces at Different ϕ's, DR = 1.75, N = 2000 RPM
a) ϕ = 0.5337 b) ϕ = 0.237 c) ϕ = 0.138 d) ϕ = 0.078

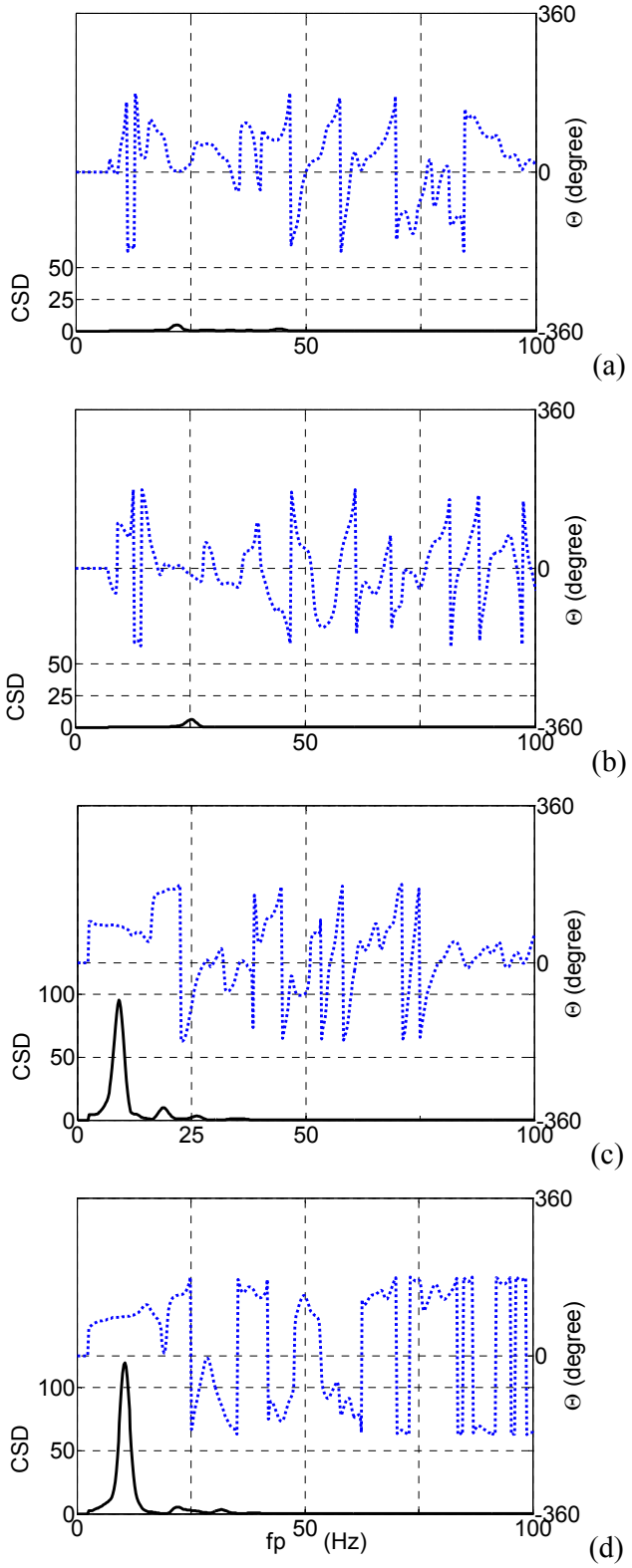

Figures 5.19a-d: Spectra of Pressure Fluctuation (CSD) at Different ϕ's, DR = 1.75 & N = 2000 RPM

a) ϕ = 0.533 b) ϕ = 0.237 c) ϕ = 0.138 d) ϕ = 0.078

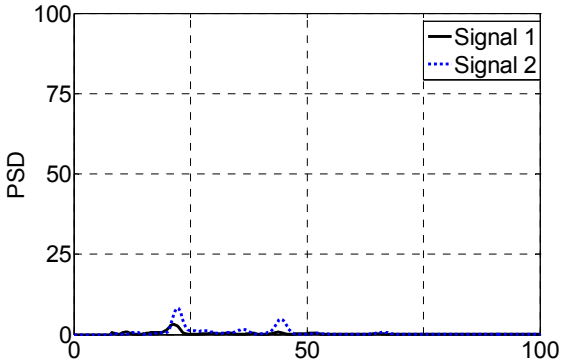

(a)

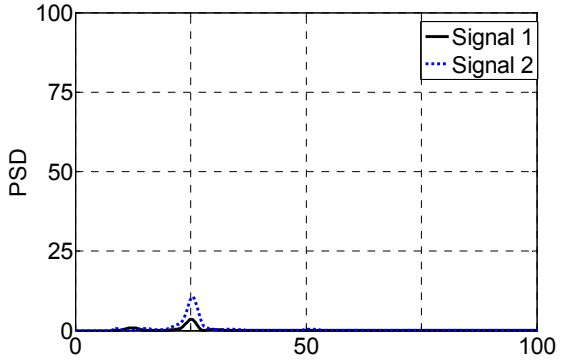

(b)

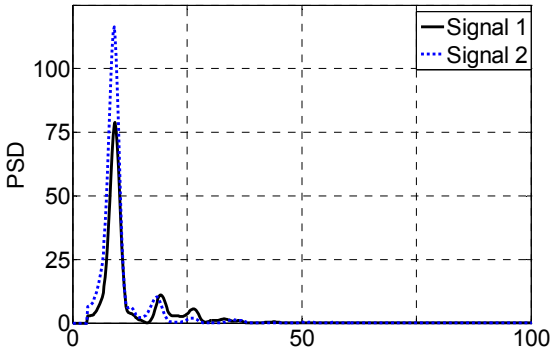

(c)

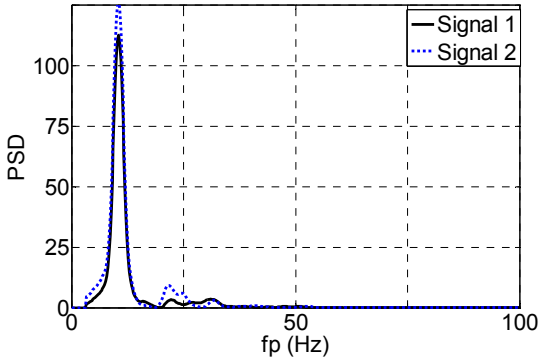

(d)

Figures 5.20a-d: Spectra of Pressure Fluctuation (PSD) at Different ϕ's, DR = 1.75 & N = 2000 RPM

a) ϕ = 0.533 b) ϕ = 0.237 c) ϕ = 0.138 d) ϕ = 0.078

5.1.3 Diameter Ratio D_o / D_i = 2.0

The stability limit of the compressor under the current diameter ratio is deducible from the system characteristic curves of the compressor for all the impeller speeds tested. This is shown in Fig. 5.21. The flow coefficients at which Cp is maximum, which is essentially the compressor stability limit, are ϕ = 0.2408 at N = 1000 RPM, ϕ = 0.2084 at N = 1500 RPM, and ϕ = 0.198 at N = 2000 RPM. Thus, confirming the trend of the compressor stability limit as a function of impeller angular speed suggested by diameter ratio discussed in the previous subsections.

The flow coefficient at the compressor stability limit is better described as the flow coefficient at which any perturbation in the flowfield occur as a precursor to the inception of rotating stall.

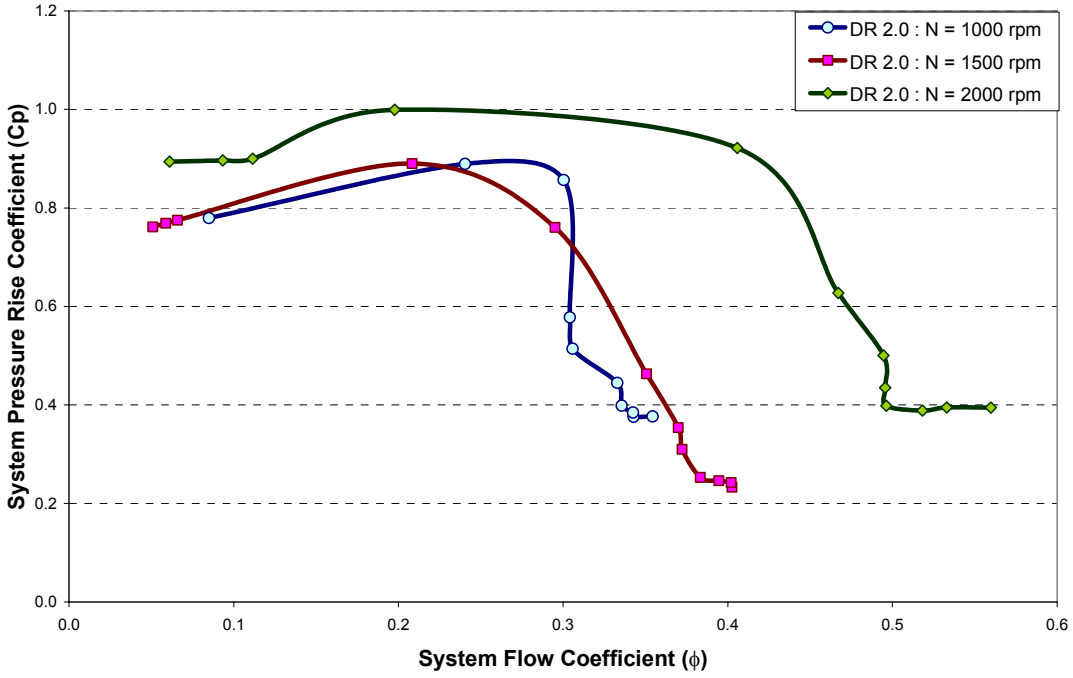

Figure 5.21: Effect of N on System Characteristic Curves, b / D_i = 0.055, D_o / D_i = 2.0

5.1.3.1 N = 1000 RPM

The pressure fluctuations at different flow coefficients are shown in Figs. 5.22a-d. Figs. 5.23c and 2.24c show the output signal from the pressure transducers at the onset of rotating stall. Therefore, the critical flow coefficient, ϕ_{cr}, is 0.2408. As the flow coefficient was reduced further, the strength of the propagating structure is seen to increase (Figs. 5.23d and 5.24d). The emergence of the stall cell is clearly noticed in Figs. 5.23c-d. The transition of the flow from non-stall to stall condition is very swift at this impeller speed (ϕ reduces from 0.2405, just before stall inception, to 0.085 at stall inception). This trend is similar to what obtains at the same impeller speed for the other two diameter ratios discussed earlier. Table 5.1 shows the difference between the ϕ values just before stall inception and at stall inception reduces as the impeller angular speed increases for all diameter ratios.

Table 5.1 shows the stall features at stall inception and two other flow coefficients after stall inception. From this table, the rotating stall cell and its second harmonic occurred at all the flow coefficients shown. Therefore, rotating stall has one cell and is propagating at a frequency of 4.06 Hz.

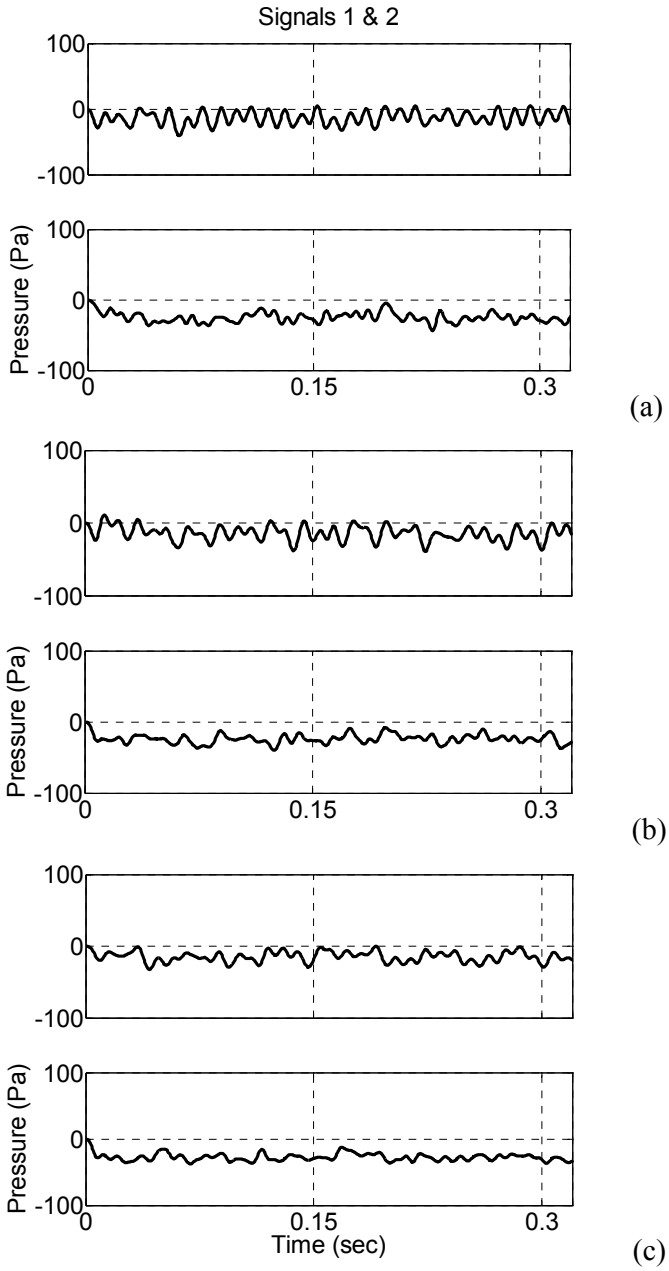

Figures 5.22a-c: Pressure Traces at Different ϕ's, DR 2.0, N = 1000 RPM
a) ϕ = 0.354 b) ϕ = 0.332 c) ϕ = 0.241

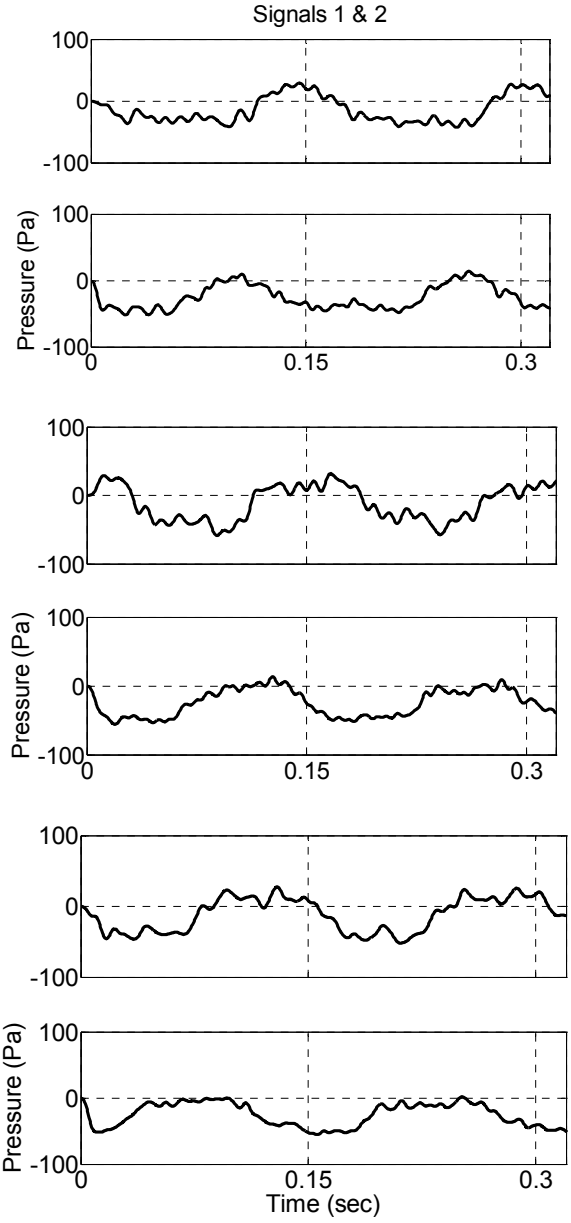

(d)

(e)

(f)

Figures 5.22d-f: Pressure Traces at Different ϕ's, DR = 2.0, N = 1000 RPM
d) ϕ = 0.085 e) ϕ = 0.084 f) ϕ = 0.083

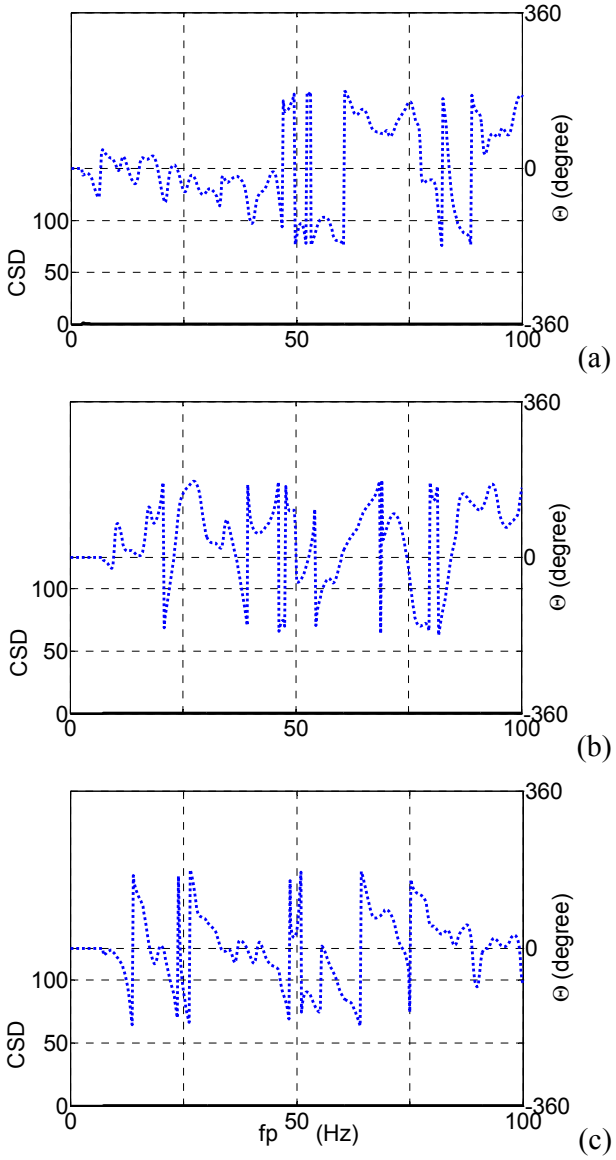

Figures 5.23a-c: Spectra of Pressure Fluctuations (CSD) at Different ϕ's, DR = 2.0 & N = 1000 RPM

a) ϕ = 0.354 b) ϕ = 0.332 c) ϕ = 0.241

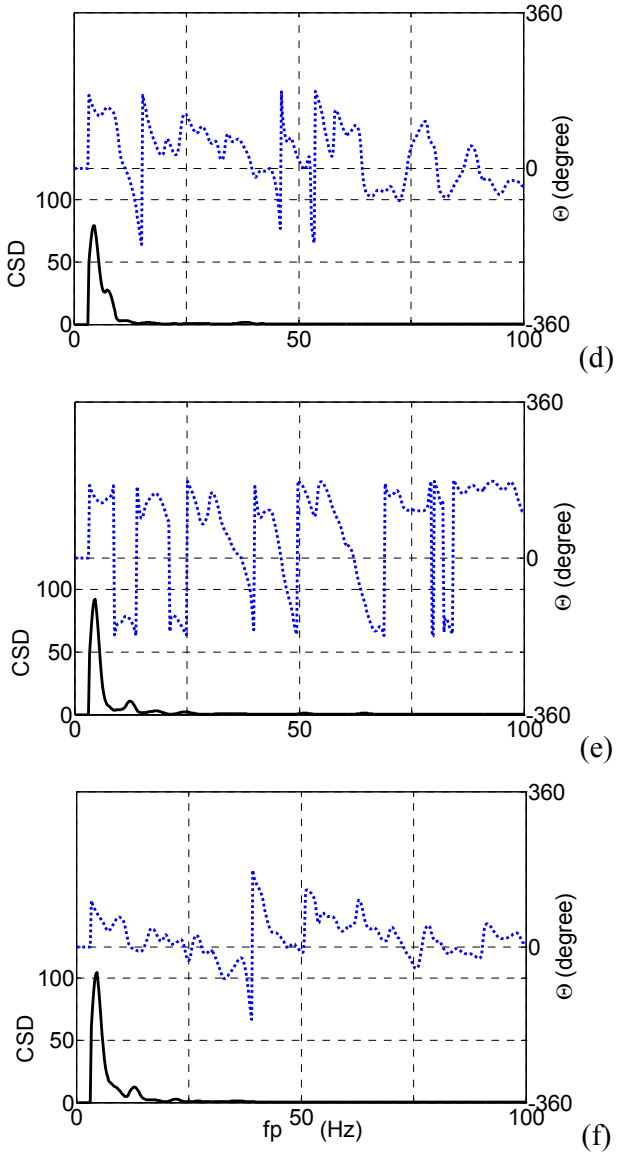

Figures 5.23d-f: Spectra of Pressure Fluctuations (CSD) at Different ϕ's, DR = 2.0 & N = 1000 RPM

d) ϕ = 0.085 e) ϕ = 0.084 f) ϕ = 0.083

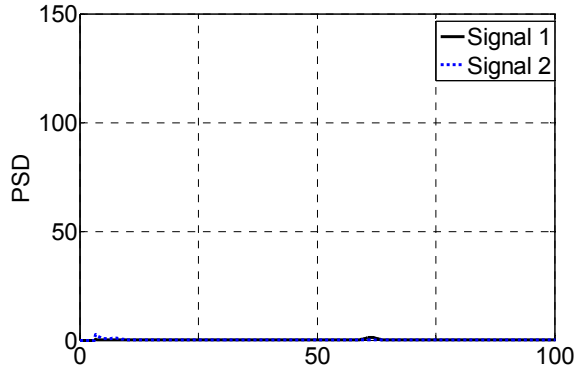

(a)

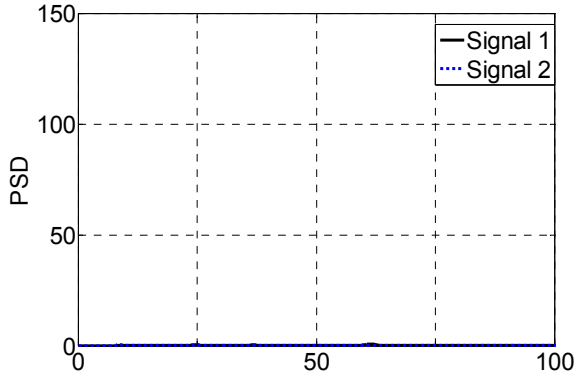

(b)

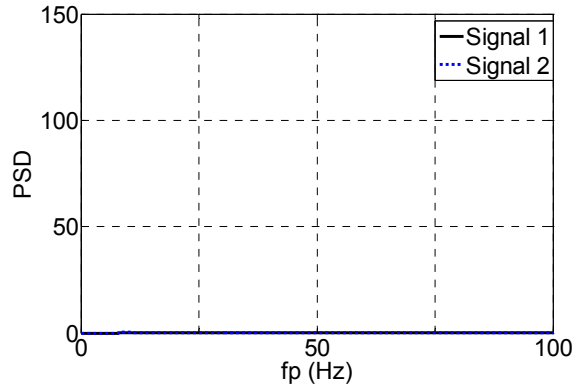

(c)

Figures 5.24a-c: Spectra of Pressure Fluctuations (PSD) at Different ϕ's, DR = 2.0 & N = 1000 RPM

a) ϕ = 0.354 b) ϕ = 0.332 c) ϕ = 0.241

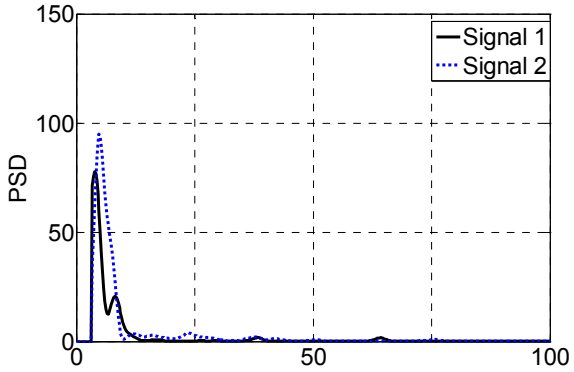

(d)

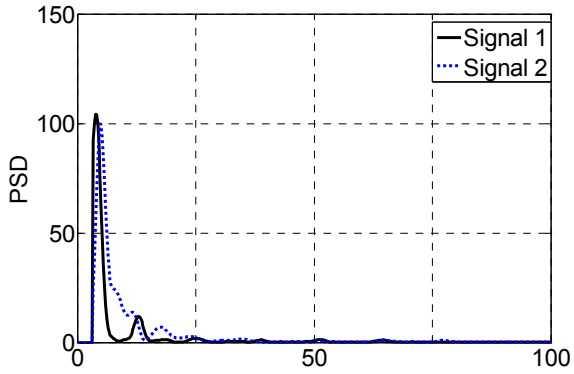

(e)

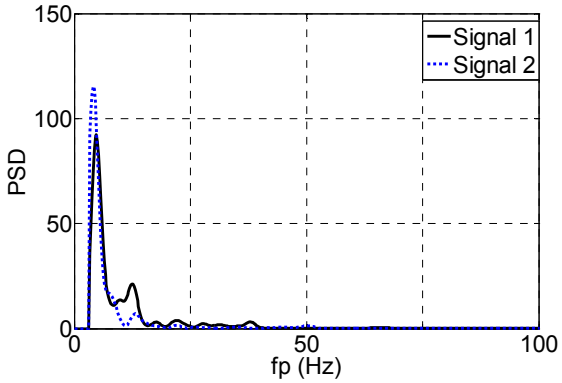

(f)

Figures 5.24d-f: Spectra of Pressure Fluctuation (PSD) at Different ϕ's, DR = 2.0 & N = 1000 RPM

d) ϕ = 0.085 e) ϕ = 0.084 f) ϕ = 0.083

5.1.3.2 N = 1500 RPM

The output signals recorded from the dynamic pressure transducers at different flow coefficients are shown in Figs. 5.25a-d. The onset of rotating stall is distinctly clear from the figures. Figure 5.25c shows the output signals of the pressure transducers at the onset of rotating stall. As expected, perturbation in the flowfield persisted henceforth as it increases in strength. Figures 5.26a-d and 5.27a-d show the spectral plots of the pressure sensor signals. The emergence of the periodic patterns at the onset of stall is clearly indicated in Figs. 5.26c-d and 5.27c-d. The characteristics of the stall cells extracted from Figs. 5.26c-d are shown in Table 5.1. The dominant rotating stall cell is the single cell pattern propagating at a frequency of 6.211 Hz and rotating at an angular speed equal to 24.2% of impeller angular speed. This fundamental frequency has a second and third harmonics at $\phi = 0.085$.

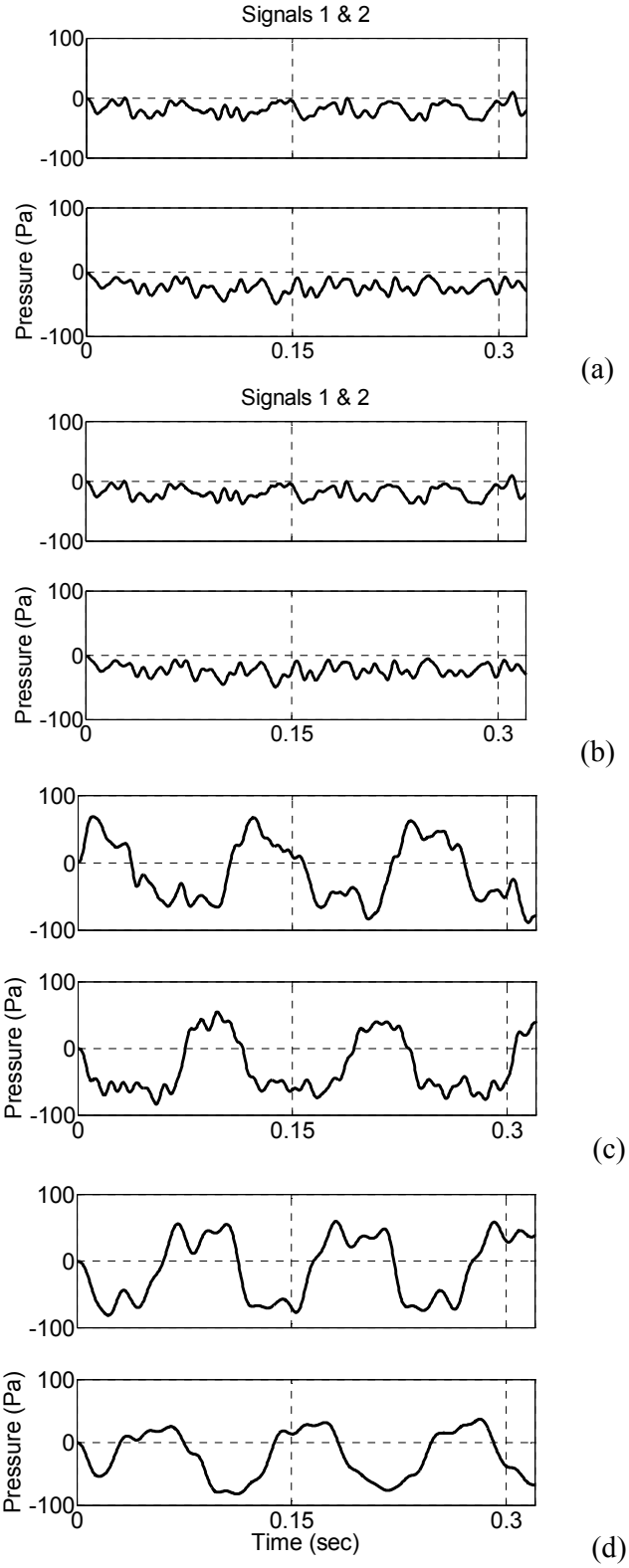

Figures 5.25a-d: Pressure Traces at Different ϕ's, DR = 2.0, N = 1500 RPM
a) ϕ = 0.403 b) ϕ = 0.208 c) ϕ = 0.066 d) ϕ = 0.051

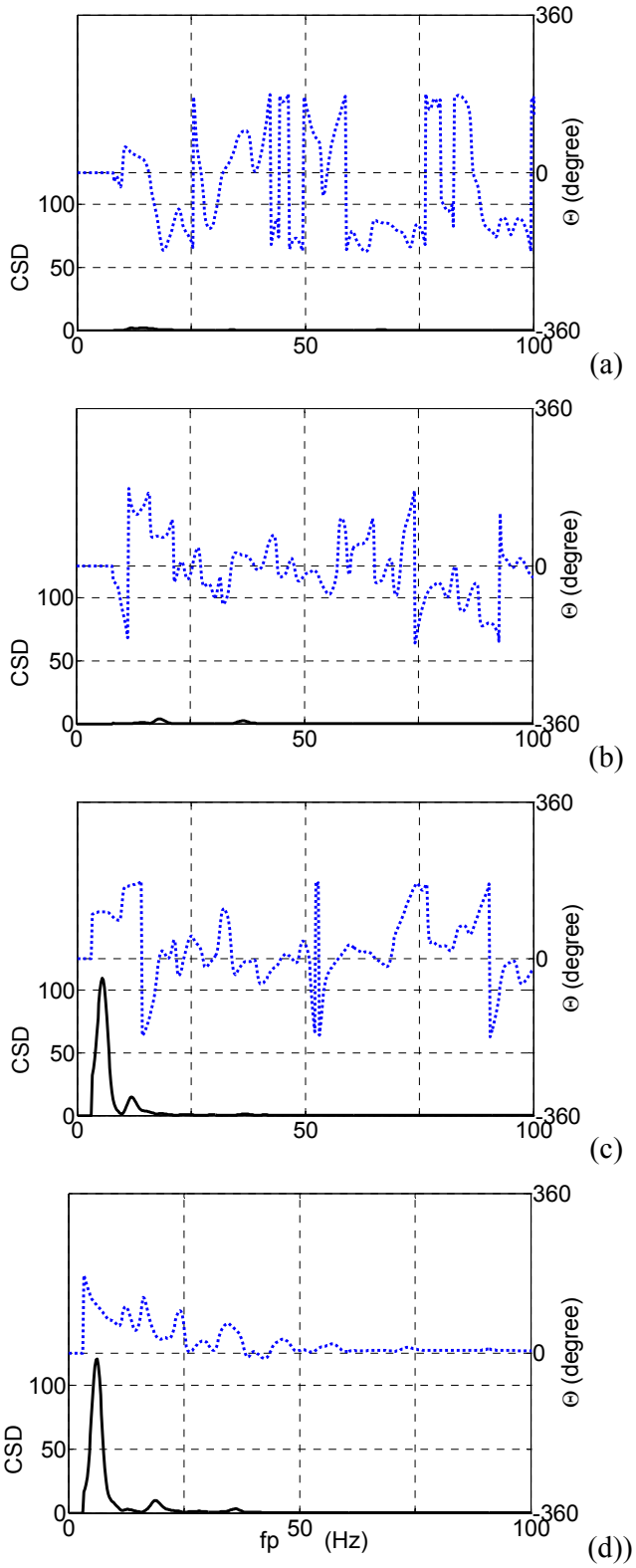

Figures 5.26a-d: Spectra of Pressure Fluctuations (CSD) at Differentϕ's, DR = 2.0 &N=1500 RPM

a) ϕ = 0.403 b) ϕ = 0.208 c) ϕ = 0.066 d) ϕ = 0.051

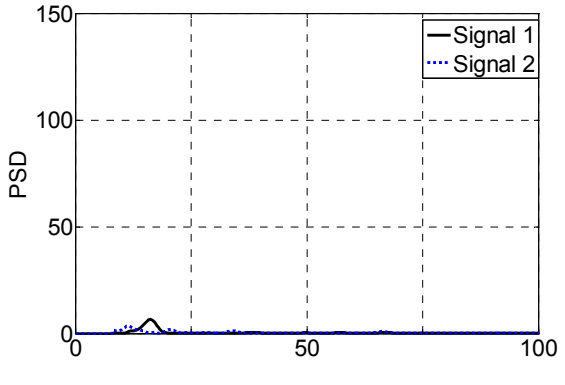

(a)

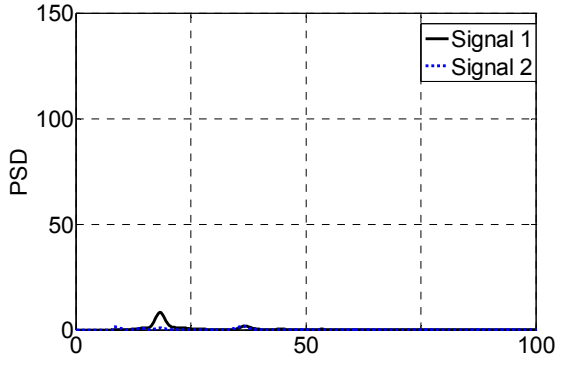

(b)

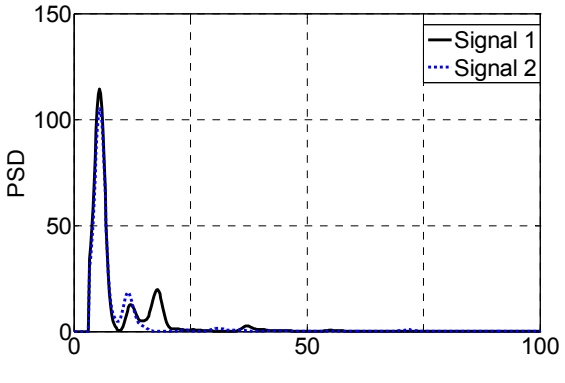

(c)

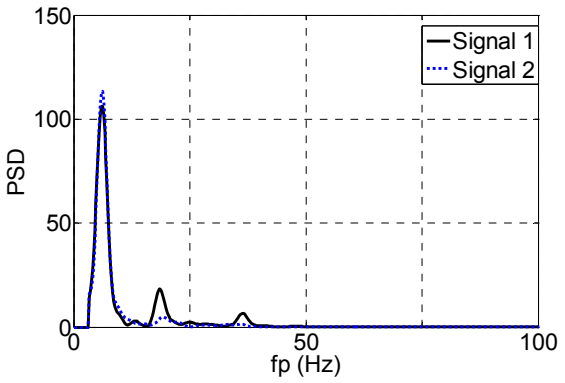

(d)

Figures 5.27a-d: Spectra of Pressure Fluctuations (PSD) at Differentϕ's, DR = 2.0 & N=1500 RPM

a) ϕ = 0.403 b) ϕ = 0.208 c) ϕ = 0.066 d) ϕ = 0.051

5.1.3.3 N = 2000 RPM

The pressure traces at impeller speed of 2000 RPM, for all the flow coefficients at which data samples were taken, are shown in Figs. 5.28a-d. Figure 5.28c shows the pressure traces at the onset of rotating stall. Therefore, the critical flow coefficient is 0.198. The propagating frequencies, their phase angles, and strength are shown in Figs. 5.29a-d and 5.30a-d. Figures 5.29c and 5.30c show the spectral plots at the onset of stall. The stall characteristics are shown in Table 5.1. The primary stall cell is propagating at a frequency of 8.361 Hz. At ϕ = 0.198, its second, and third harmonics appeared. The secondary harmonic number is propagating at a frequency of 16.72 Hz with its second harmonic emerging at ϕ = 0.198. On the other hand, the third-harmonic with f_p =25.56 Hz occurred only at ϕ = 0.198. As discussed earlier, the relatively small strengths of the three stall cells when compared to the primary stall cell suffice as a reason for not considering them as stall cells.

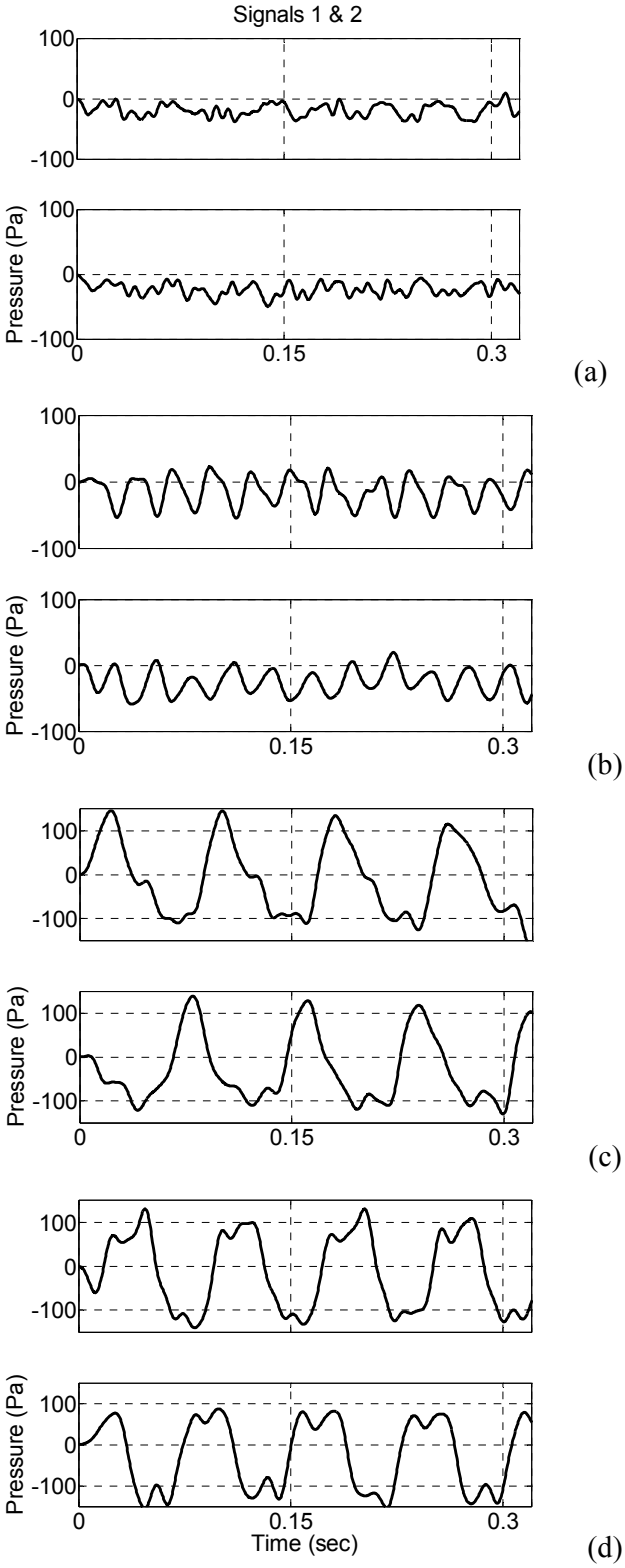

Figures 5.28a-d: Pressure Traces at Different ϕ's, DR = 2.0, N = 2000 RPM
a) ϕ = 0.561 b) ϕ = 0.496 c) ϕ = 0.198 d) ϕ = 0.061

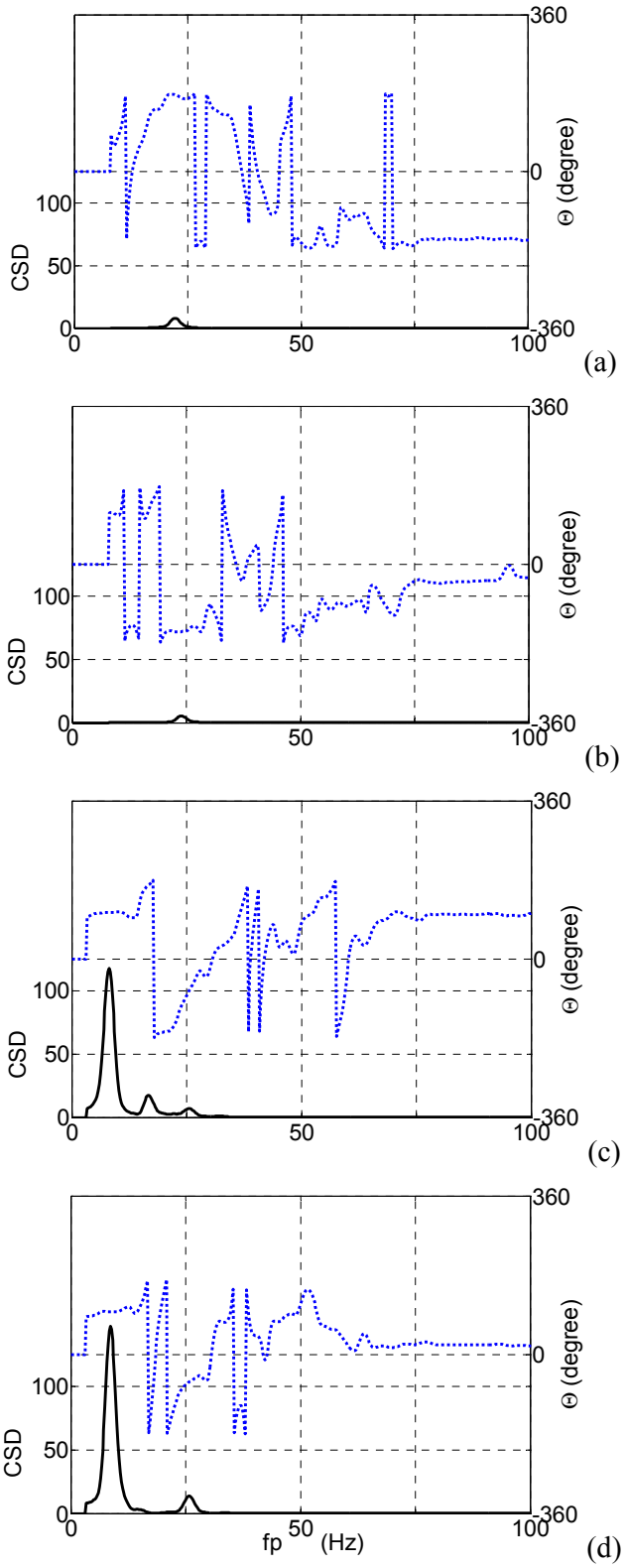

Figures 5.29a-d: Spectra of Pressure Fluctuation (CSD) at Different ϕ's, DR = 2.0 & N = 2000 RPM

a) ϕ = 0.561 b) ϕ = 0.496 c) ϕ = 0.198 d) ϕ = 0.061

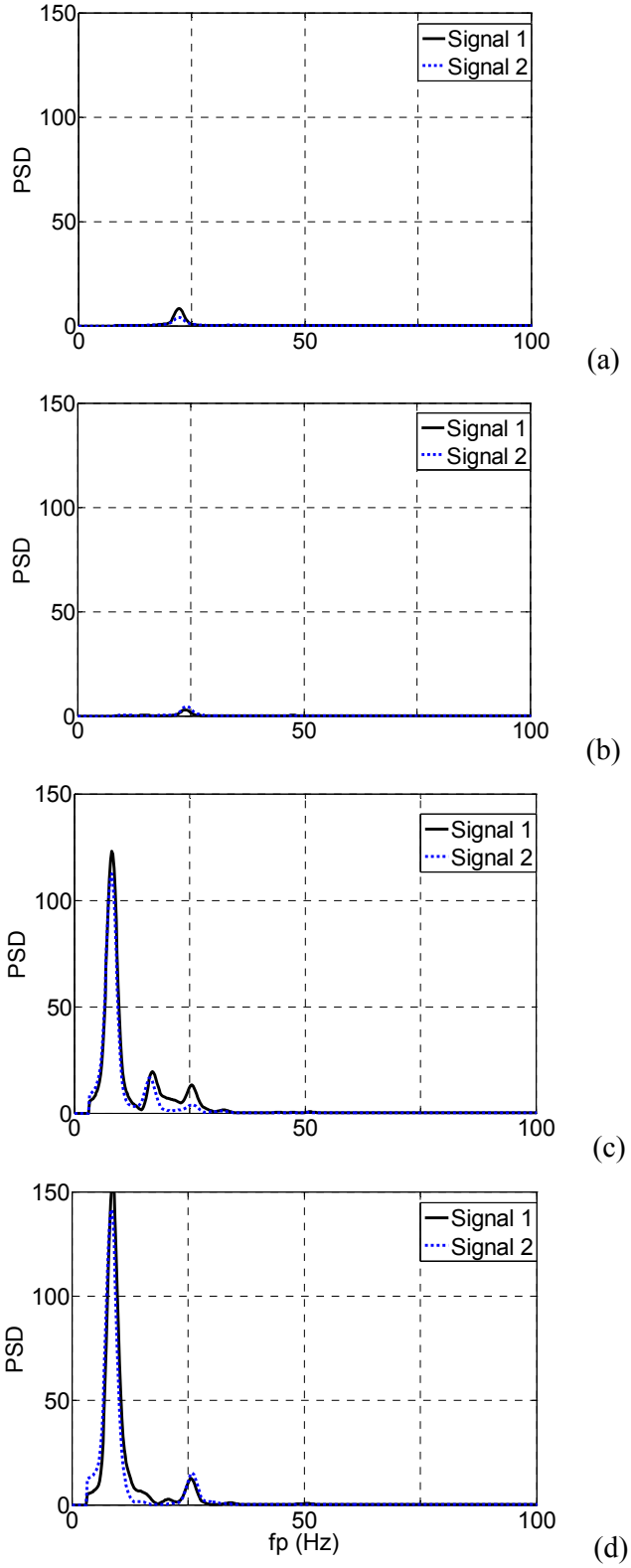

Figures 5.30a-d: Spectra of Pressure Fluctuation (PSD) at Different ϕ's, DR = 2.0 & N = 2000 RPM

a) ϕ = 0.561 b) ϕ = 0.496 c) ϕ = 0.198 d) ϕ = 0.061

Table 5.1: Summery of Stall Characteristics, b / D_i = 0.055

D_o / D_i	N	f_p	CSD	φ	Φ	m	N_s / N
1.5	1000	5.495	25.33	0.983	-59.7	1	0.326
	1000	10.55	10.5	0.962	-165.3	2	0.326
	1000	16.28	3.239	0.922	-140.7	3	0.325
	1500	7.167	44.98	0.964	-104.7	1	0.354
	1500	14.09	54.62	0.924	-174.9	2	0.354
	1500	21.74	5.154	0.957	44.75	3	0.352
	2000	10.27	68.61	0.996	-97.74	1	0.375
	2000	21.02	21.99	0.968	-174.9	2	0.375
	2000	32.25	3.267	0.942	37.7	3	0.374
1.75	1000	4.061	48.19	0.989	48.76	1	0.261
	1000	9.27	1.849	0.945	124.6	2	0.26
	1000	25.56	16.67	0.883	-109	3	0.261
	1500	6.689	95.41	0.973	47.59	1	0.277
	1500	11.95	14.79	0.952	128.2	2	0.277
	1500	20.54	2.532	0.921	69.36	3	0.278
	2000	9.078	95.33	0.927	84.4	1	0.294
	2000	18.87	9.878	0.939	172.9	2	0.294
	2000	26.28	3.279	0.863	-42.05	3	0.293
2.0	1000	3.539	78.8	0.983	135.3	1	0.221
	1000	7.406	27.36	0.964	170.7	2	0.221
	1000	11.71	3.069	0.937	-38	3	0.222
	1500	5.495	109.6	0.963	40.9	1	0.248
	1500	11.94	14.8	0.984	71.8	2	0.248
	2000	8.122	134.2	0.994	45.8	1	0.251
	2000	16.72	19.93	0.895	68.7	2	0.251
	2000	25.56	8.21	0.912	-132.62	3	0.252

CHAPTER 6

ROTATING STALL RESULTS

To summarize the effects of impeller angular speed, diffuser width, and diffuser diameter ratios on the frequency of pressure fluctuations, f_p, and strength, CSD, graphical representations of f_p and CSD as functions of N, b / D_i, and D_o / D_i are necessary.

6.1 Effect of Impeller Angular Speed on the Frequency of Pressure Fluctuations

Figure 6.1 shows the effect of impeller speed, N, on the frequency of fluctuating pressure, f_p. For the same number of stall cells, constant diffuser width and diameter ratio, the figure suggests that the frequency of fluctuating pressure is approximately proportional to the impeller angular speed. Furthermore, for a constant N, the figure suggests that f_p decreases with an increase in the diffuser diameter ratio. This trend is highly visible at all N specified range.

To nullify the effects of number of stall cells, n, and impeller angular speed, N, the frequency of pressure fluctuation was made non-dimensional by dividing it by the product of n and N. The non-dimensional f_p as a function of N is shown in Fig. 6.2. The non-dimensional frequency of pressure fluctuation at a constant impeller speed decreases as D_o / D_i was increased. Thus, it could be concluded that both the dimensional and non-dimensional form of f_p decreases with an increase in the diffuser diameter ratio. Moreover, non-dimensional frequency of pressure fluctuation is fairly dependent of the impeller speed and number of stall cells at a fixed diffuser diameter ratio. This is a confirmation of the linear relationship between f_p and N.

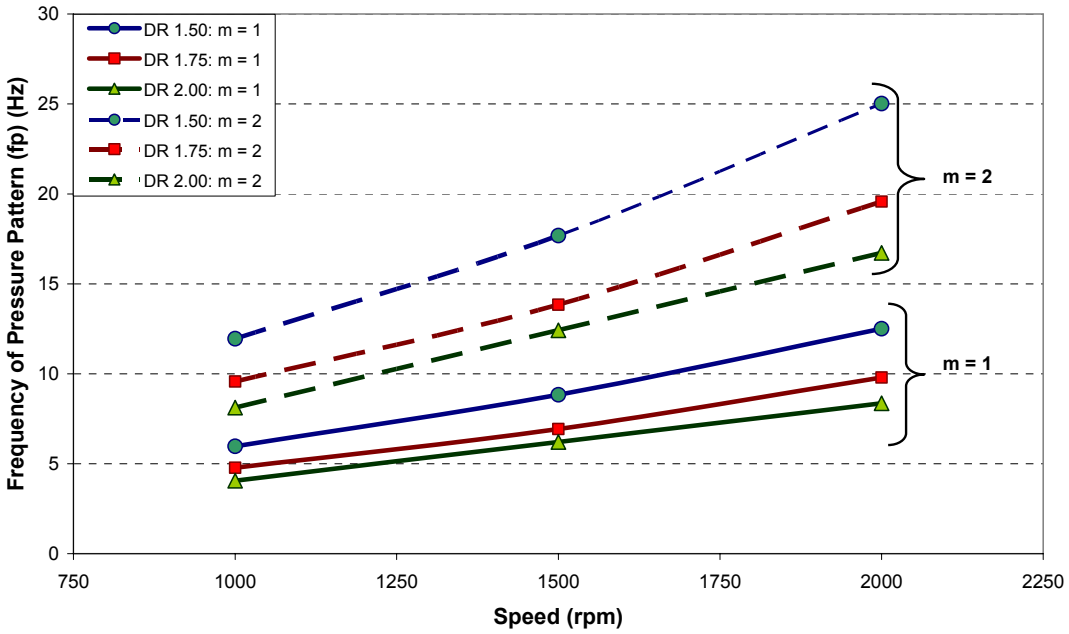

Figure 6.1: Effects of Impeller Angular Speed on the Frequency of Pressure Fluctuations, b / D_i = 0.055

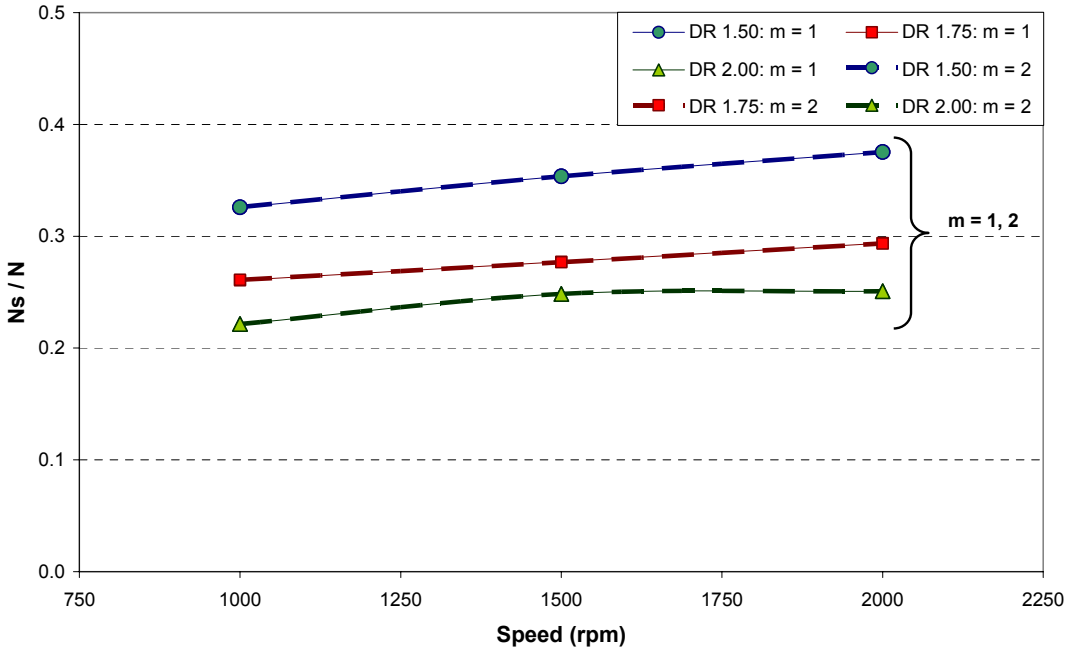

Figure 6.2: Effects of Impeller Angular Speed on Non-Dimensional Frequency of Pressure Fluctuations, b / D_i = 0.055

6.2 Effect of Impeller Angular Speed on the Strength of Rotating Stall Cells

Figure 6.3 shows the effect of the impeller angular speed on the strength of the rotating stall cells for all the diffuser diameter ratios tested. The results indicate that the strength of the stall cells, at a fixed diffuser diameter ratio, increases as the impeller speed is increased. Furthermore, the stall cells with first harmonic number (m = 1) are always stronger than the stall cells with it multiple (m = 2 and 3) at all the impeller speeds shown. It is important to note that the data in Fig. 6.3 was extracted at flow coefficients below ϕ_{cr}.

Abdelhamid and Bertrand (1980) reported that the effect of Re, N, or b / Di on Ns / N values is insignificant while the effect of increasing Do / Di tends to decrease their values. This is probably why the current values of Ns / N are slightly higher than those reported by other investigators [Abdelhamid and Bertrand (1980) or Mizuki and Oosawa (1992)]. Otugen et al. (1988), as well as Abdelhamid and Bertrand (1980), reported that Ns / N is independent of b / Di, but decreases slightly when stall cells increase. Table 6.1 shows no change of the value of Ns / N as the harmonic number value increases (m = 1, 2, and 3). This is exactly similar to Abdelhamid and Bertrand (1980) results, where it shows no changes for Ns / N as the number of lobes increases (only for $b / D_i = 0.054$).

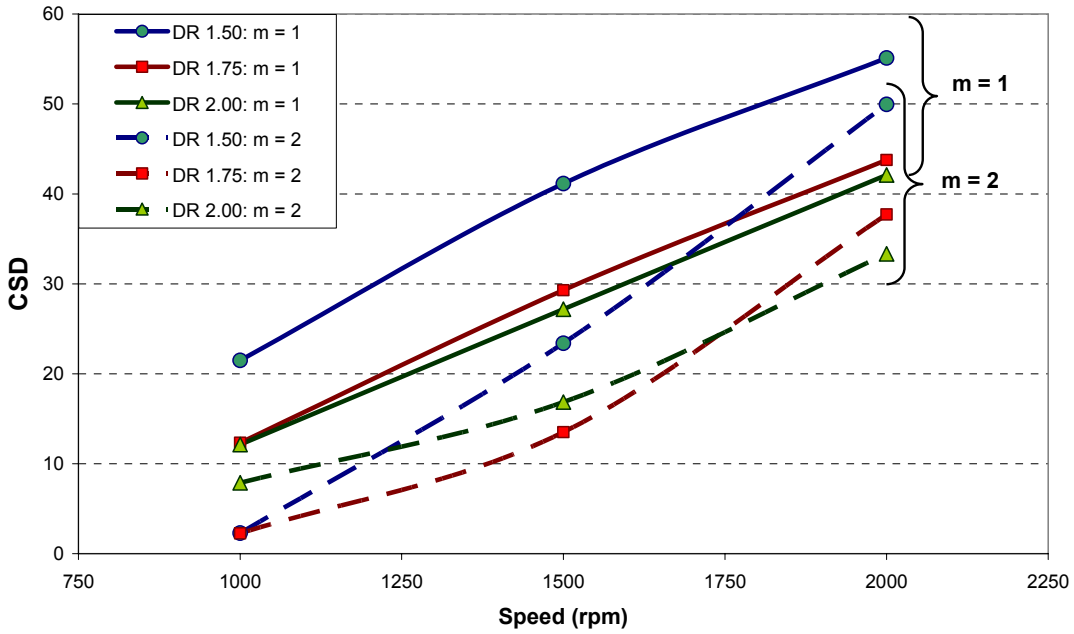

Figure 6.3: Effects of Impeller Speed on the Strength of Rotating Stall Cells, b / D_i = 0.055

Table 6.1: Comparison of Stall characteristic Results

Reference	m	f_p	N	N_s / N
Current Data $D_o / D_i = 1.50$ $b / D_i = 0.055$	1	5.495	1000	0.326
	2	10.55	1000	0.326
	3	16.28	1000	0.325
	1	7.167	1500	0.354
	2	14.09	1500	0.354
	3	21.74	1500	0.352
	1	10.27	2000	0.375
	2	21.02	2000	0.375
	3	32.25	2000	0.374
Ahmed, S. A. (2002) $D_o / D_i = 1.5$ $b / D_i = 0.055$	1	6.10	1000	0.366
	2	13.40	1000	0.403
	1	9.77	1500	0.391
	2	19.53	1500	0.391
	1	13.43	2000	0.403
	2	26.90	2000	0.403
Mizuki and Oosawa (1992) $D_o / D_i = 1.59$ $b / D_i = 0.071$	1	55	10000	0.330
Abdelhamid and Bertrand (1980) $D_o / D_i = 1.55$ $b / D_i = 0.054$	1	27	5000	0.324
	2	54	5000	0.324

6.3 Effect of Diffuser Diameter Ratio on the Frequency of Pressure Fluctuations

The effects of diffuser diameter ratio on stall characteristics are presented in Table 6.2. The table shows the existence of a primary stall cell with one lobe and its second harmonic at all the diffuser diameter ratios tested.

The effect of diffuser diameter ratio on the frequency of pressure fluctuation is shown in Figs. 6.4a-b. For all the impeller speeds shown in the figure, the frequency of pressure fluctuation decreases as the diffuser diameter ratio was increased. It is pertinent to note here that the slope of the curves in the figure under reference increases with increase in the impeller angular speed. In other words, for an increase of 33.33% in the diffuser diameter ratio (from D_o / D_i = 1.50 to 2.0), the decrease in the frequency of pressure fluctuation increases with an increase in the impeller angular speed. For example, the frequency of pressure fluctuations, fp, decreased by 27.4%, 29.73%, and 33.17% for impeller angular speeds of 1000 RPM, 1500 RPM, and 2000 RPM, respectively, when the diffuser diameter ratio was increased by 33.33%.

The effect of diffuser diameter ratio on the non-dimensional speed of the stall cells is shown in Figure 6.5a-b. For all the impeller angular speeds shown, the non-dimensional speed of the stall cells decreases as the diffuser diameter ratio was increased. For example, an increase of 12.5% in the diffuser diameter ratio (from D_o / D_i = 1.75 to 2.0) resulted in a decrease of 14.64% in the non-dimensional rotational speed of the one lobe stall cell when the impeller was operated at N = 2000 RPM. Furthermore, the non-dimensional speed, Ns / N, decreased by 27.4%, 29.73%, and 33.17% for impeller angular speeds of 1000 RPM, 1500 RPM, and 2000 RPM respectively, when the diffuser

diameter ratio was increased by 33.33% (from D_o / D_i = 1.5 to 2.0). This is another confirmation of the linear relationship between fp and N as shown earlier in this chapter.

The results of Saad A. Ahmed et al. (2002) showed similar strong dependence of the stall cell speed on the diffuser diameter ratio. For example, a decrease of 15.3% in the diffuser diameter ratio resulted in about 22.7% increase in the non-dimensional speed of the single lobe stall cell.

In addition, table 6.2 shows the effect of diffuser diameter ratio on the characteristics of the stall cells at a fixed diffuser width ratio (b / D_i) of 0.055. The results show a significant decrease in the non-dimensional speed of the stall cells when the diffuser diameter ratio was increased. From the foregoing analysis, it could be concluded that the non-dimensional speed of the stall cells is strongly dependent on the diffuser diameter ratio.

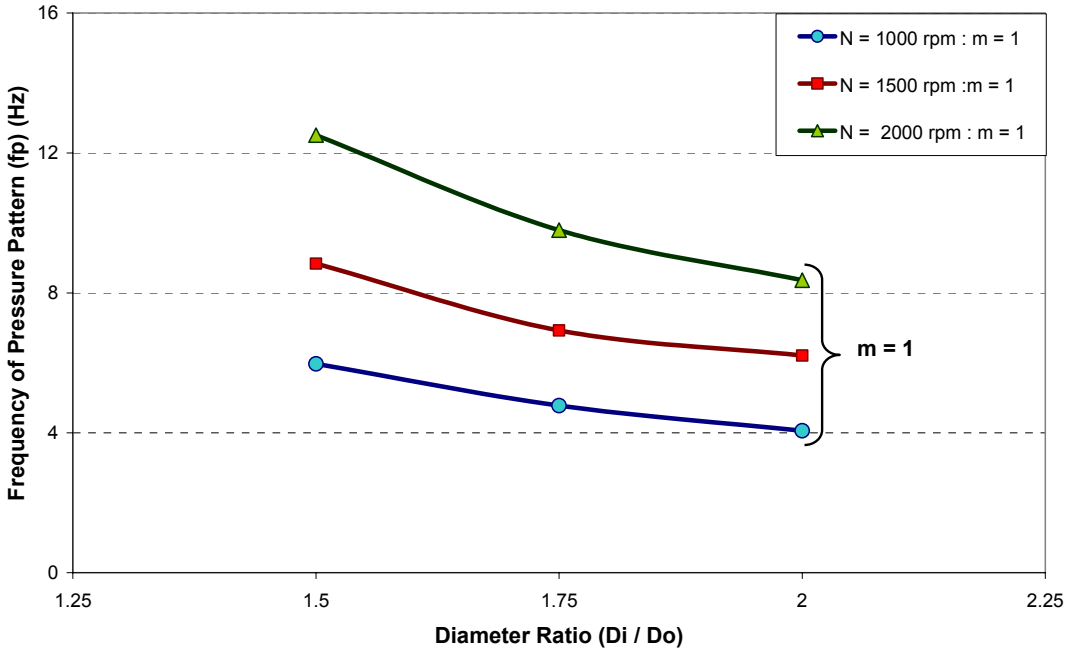

(a) m = 1

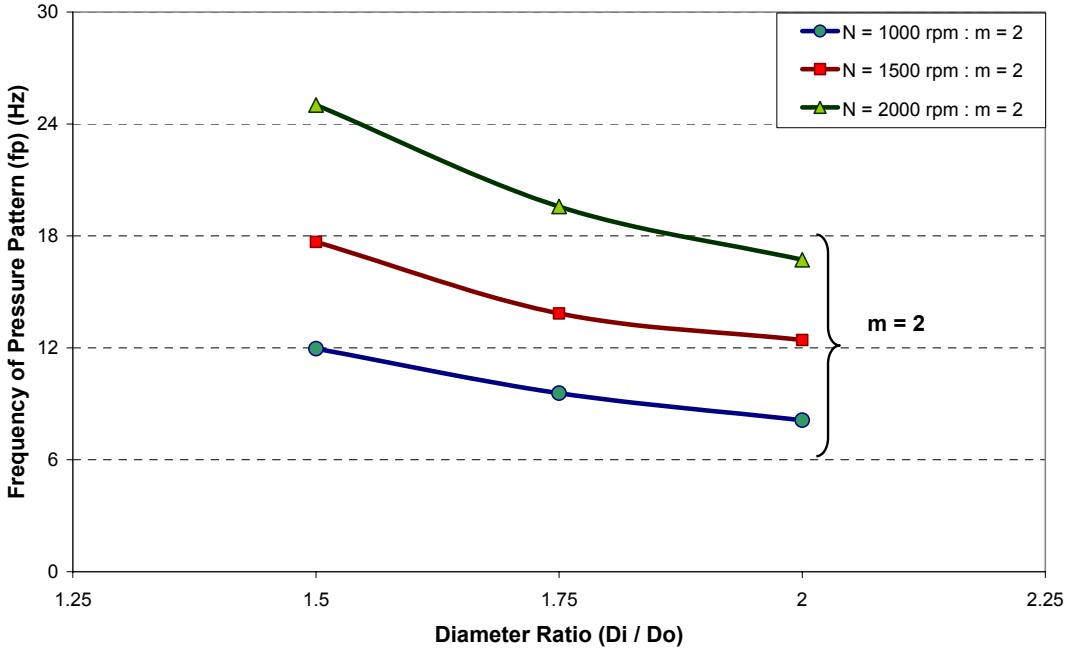

(b) m = 2

Figure 6.4a-b: Effects of Diffuser Diameter Ratio on the Frequency of Pressure Fluctuations, b / D_i = 0.055

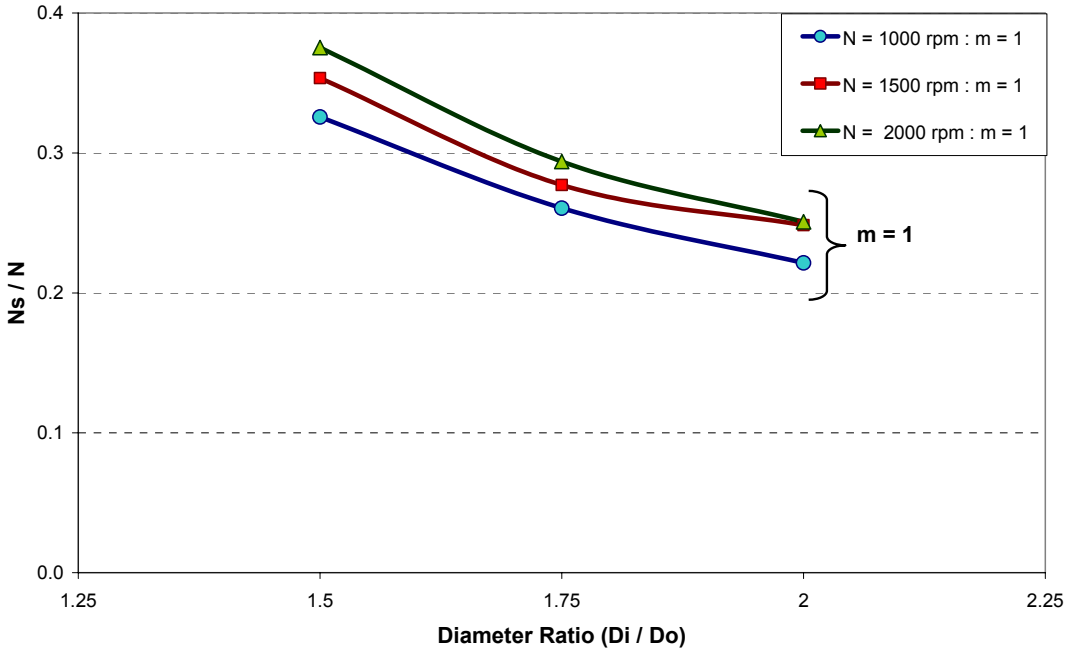

(a) m = 1

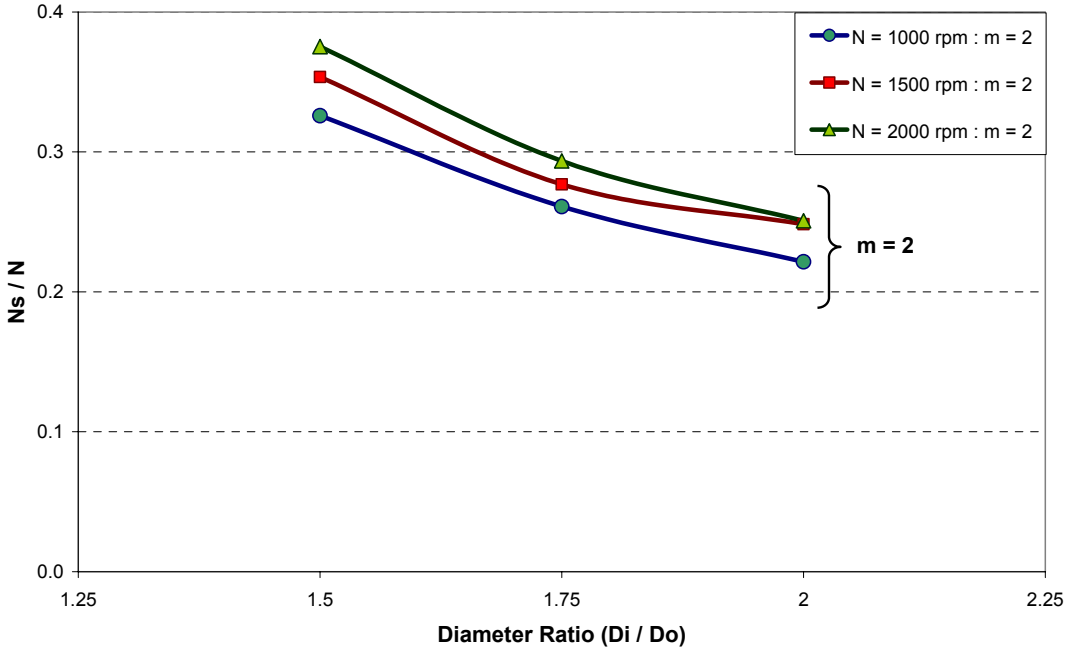

(b) m = 2

Figure 6.5a-b: Effects of Diffuser Diameter Ratio on the Non-Dimensional Speed of the Stall Cells, b / D_i = 0.055

6.4 Effect of Diffuser Diameter Ratio on the Strength of Rotating Stall Cells

Figure 6.6a shows the effect of diffuser diameter ratio on the strength of rotating stall cells. The results indicate that the strength of stall cells, at a fixed impeller speed, decreases as the diffuser diameter ratio is increased. Furthermore, the stall cells with one lobe (n = 1 or m = 1) are always stronger than its harmonic (m = 2 and 3) at all diffuser diameter ratios shown.

In addition, Fig. 6.6a shows that the strength of rotating stall cell (n = 1) has a visible reduction with the increment of the diffuser diameter ratio. For example, the strength of rotating stall cells, CSD, decreased by 23.59%, 32.43%, and 44.51% for impeller angular speed of 1000 RPM, 1500 RPM, and 2000 RPM respectively, when the diffuser diameter ratio was increased by 33.33%.

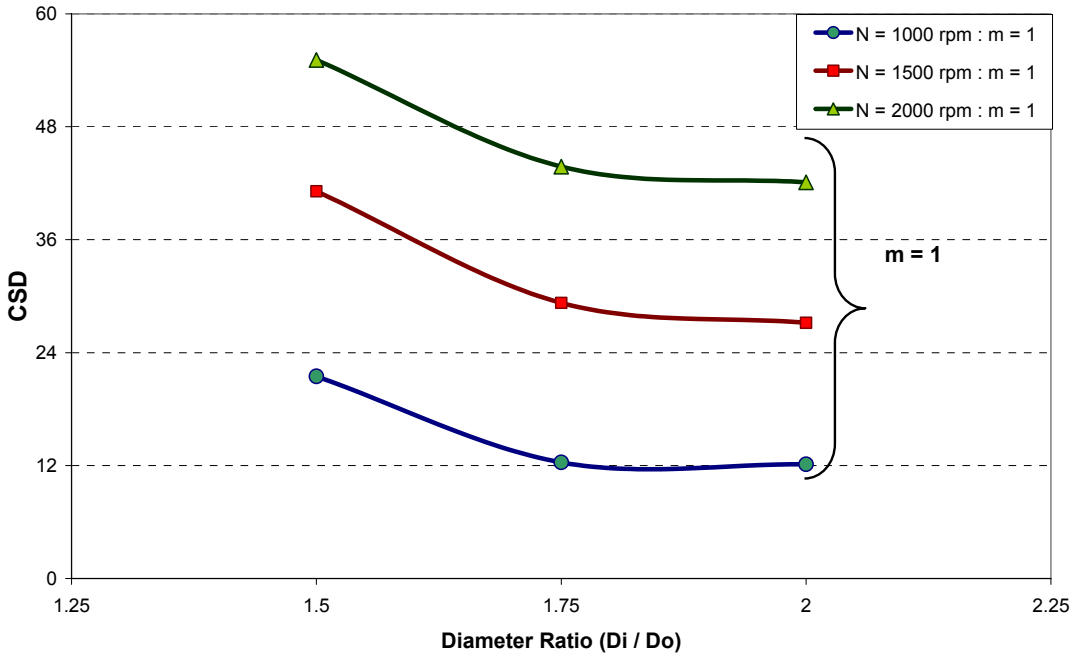

(a) m = 1

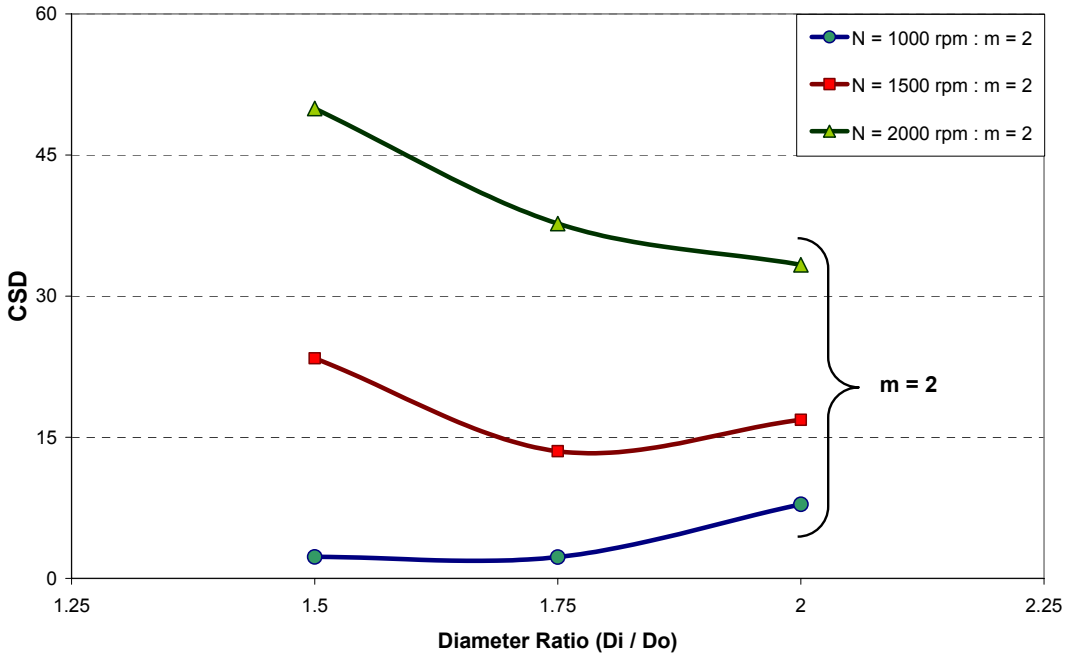

(b) m = 2

Figure 6.6a-b: Effects of Diffuser Diameter Ratio on the Strength of Rotating Stall Cells, b / D_i = 0.055

Table 6.2: Effect of Diffuser Diameter Ratios on Stall Characteristics, b / D_i = 0.055

D_o / D_i	N	f_p	CSD	m	N_s / N
1.5	1000	5.495	25.33	1	0.326
	1000	10.55	10.5	2	0.326
	1000	16.28	3.239	3	0.325
	1500	7.167	44.98	1	0.354
	1500	14.09	54.62	2	0.354
	1500	21.74	5.154	3	0.352
	2000	10.27	68.61	1	0.375
	2000	21.02	21.99	2	0.375
	2000	32.25	3.267	3	0.374
1.75	1000	4.061	48.19	1	0.261
	1000	9.27	1.849	2	0.26
	1000	25.56	16.67	3	0.261
	1500	6.689	95.41	1	0.277
	1500	11.95	14.79	2	0.277
	1500	20.54	2.532	3	0.278
	2000	9.078	95.33	1	0.294
	2000	18.87	9.878	2	0.294
	2000	26.28	3.279	3	0.293
2.0	1000	3.539	78.8	1	0.221
	1000	7.406	27.36	2	0.221
	1000	11.71	3.069	3	0.222
	1500	5.495	109.6	1	0.248
	1500	11.94	14.8	2	0.248
	2000	8.122	134.2	1	0.251
	2000	16.72	19.93	2	0.251
	2000	25.56	8.21	3	0.252

CHAPTER 7

CONTROL OF ROTATING STALL

The occurrence of flow fluctuations leading to rotating stall has been delayed by the use of several methods that can be categorized under active and passive control of rotating stall. Details of these types of control systems have been provided in the introduction to this thesis. The passive control method employed in this study is similar to the method used by Abdelhamid (1983b) and Saad A. Ahmed (2000) to stabilize the flow in the diffuser and improve the static pressure rise coefficient (Cp). This method involves changing the flow area at the diffuser exit with the use of throttling rings attached to either the diffuser shroud, or the diffuser hub. Simultaneous attachment of the throttle rings to both the diffuser shroud and hub was also made. Schematic of the modes of the diffuser exit area blockage used in this investigation is shown in Fig. 7.1. The diffuser exit area blockage ratios used are 25%, 50%, and 75%. For the simultaneous blockage of the diffuser exit area, the following blockage ratios were used: 25% from both walls, 25% from the diffuser shroud and 50% from the diffuser hub, and vise versa. The effects of these blockage ratios on the stability of the compressor are presented under the flowing subsections. The blockage ratios are identified by, for example, BR = 0.25S, which means a blockage ratio of 25% with the throttling ring attached to the diffuser shroud.

Similarly, BR = 0.5H means a blockage ratio of 50% with the throttling ring attached to the diffuser hub, while BR = 0.25S/.25H indicates that 25% of the diffuser exit flow is simultaneously blocked from both the diffuser shroud and hub. If no throttling ring is attached to the diffuser walls, the label NB /or/ 0BR, meaning no blockage, is used.

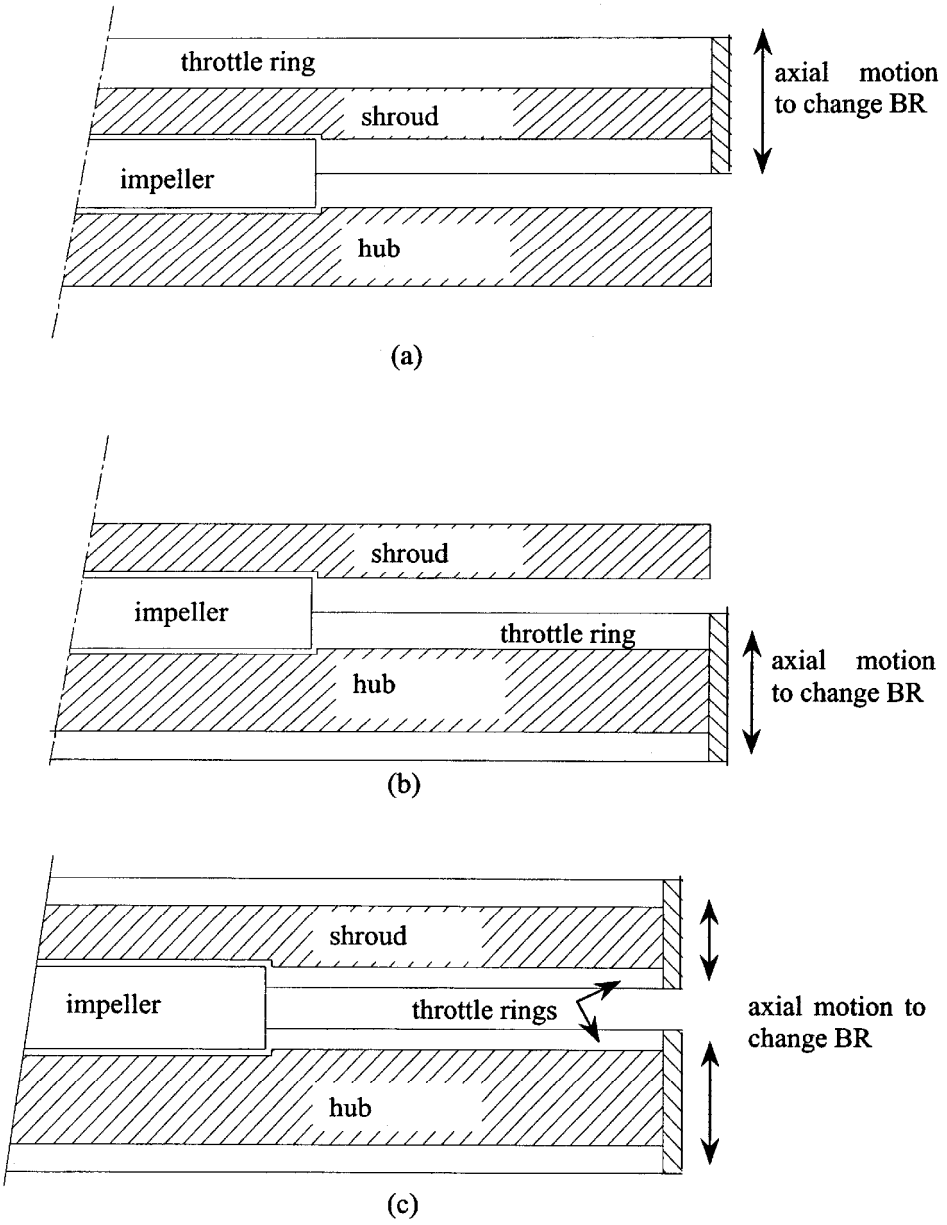

Figure 7.1: Modes of Diffuser Exit Blockage Used Throttle Rings

Used: (a) Throttle Ring attached to Shroud Wall,
(b) Throttle Ring Attached to Hub Wall,
(c) Throttle Ring Attached to Both Hub & Shroud Walls

7.1 Effects of Blockage Ratio on the Performance of the Compressor

The diffuser exit flow area was reduced by 25%, 50%, and 75% by attaching the rings to the diffuser walls. The effects of these blockage ratios on the performance of the compressor are presented in the following subsections. Since the effect of impeller angular speed on the stability of the compressor has been discussed extensively in the preceding chapter, it will not be repeated here. The main reason is that the effect of the impeller angular speed on the flowfield in the diffuser is the same with and without diffuser exit flow area blockage. Therefore, the effects of diffuser exit flow area blockage are discussed for selected impeller speeds.

7.1.1 25% Blockage Ratio

The effects of reducing the diffuser exit flow area by 25% on the performance (stability) of the compressor was checked by attaching the throttling ring to either the diffuser shroud or hub with the impeller running at constant angular speed (N = 2000 RPM) at fixed diffuser width ($b / D_i = 0.055$) on different diffuser diameter ratios (D_o / D_i = 1.5, 1.75, and 2.0). Figure 7.2 shows the comparison of the system flow coefficient (ϕ) at impeller speed of 2000 RPM and diameter ratio of 1.5, when no throttle rings are attached and with BR = 0.25S and BR = 0.25H. The figure shows that the flow coefficient at which the system become unstable was successfully delayed by both blockage ratios, suggesting, as expected, that the system is more stable with the introduction of the flow exit area blockage. In other words, with the introduction of diffuser exit flow area blockage, no flow oscillations occurred at the critical flow coefficient of the compressor when no rings are attached to the diffuser walls. This, in turn, indicates that onset of rotating stall is delayed to a lower flow coefficient when the throttle rings are attached as

has been extensively discussed in chapter 5. There is a remarkable difference between the effects of the two blockage ratios on the stability of the compressor. For the instant, the difference between the critical flow coefficients for compressor stability, ϕ_{crb}, between the two blockage ratios is less than 15.87% as shown in Fig. 7.2.

In addition, further work done to analyze the performance of the compressor characteristics by experiencing different diffuser ratios with/without the throttle rings on hub, shroud and combinations of both. For 25% blockage ratio, figures 7.2, 7.3, and 7.4 illustrate a consistency in the improvement of delaying the occurrence of rotating stall by increasing the diameter ratio. Results confirm that using throttle rings attached to hub wall is better than to shroud wall, for example, the flow coefficient, ϕ, decreased by 15.87%, 29.79%, and 30.8% for impeller angular speed of 2000 RPM, as the diameter ratio increased from 1.5 to 2.0 (throttle rings attached to hub wall).

7.1.2 50% Blockage Ratio

Figures 7.2, 7.3 and 7.4 show the compressor characteristics with and without blockage. It is interesting to note that the use of throttle ring leads to better performance of the compressor at flow coefficients higher than ϕ_{crb} of a system without rings. For 0.5% blockage ratio (shroud, hub, and a combination), all the blockage ratios have shown a lower flow coefficient at which the system becomes unstable, for example, the flow coefficient decreases by 31.58%, 36.85%, and 40.33% when diffuser diameter ratio was increased by 33.33% (D_o / D_i = 1.5, 1.75, and 2.0 respectively). These results match well with those of Saad A. Ahmed (2002), Abdelhamid (1983b) and Watanabe et al. (1994). In addition, these figures show the relative performance of the different combinations of 50% blockage ratio used. The figure shows that 50% blockage from hub side has best

performance. In other words, BR = 0.5H will provide the most stable system when compared to the shroud or equivalent combination blockage ratios shown in those figures.

7.1.3 75% Blockage Ratio

The diffuser exit flow area was reduced 75% using various combinations of the throttle rings. The resulting systems characteristic illustrations of blockage ratio combinations were used are shown in Figs. 7.2-4. Since the critical flow coefficient of the system without any blockage is known, measurements were concentrated around this flow coefficient when the throttle rings were fitted to the diffuser walls. Again, it is clear from the figures that the compressor performance was greatly improved when the rings were used after the onset of instability. For example, all the blockage ratios shown in Figs. 7.2-4 delayed system stability limit to a flow coefficient much lower than ϕ_{crb}. An examination of the pressure signal and its power spectral densities at lower flow coefficient than ϕ_{crb} revealed that there is no periodic propagating structure in the diffuser. This is in line with the extensive discussions on this subject in chapter 5.

A comparison of the different modes of blockage ratios used to achieve the 75% blockage ratio is presented in Figs. 7.2-4. The figure suggests that reducing the diffuser exit flow area by 75% with the throttle ring attached to the diffuser hub is the most beneficial in relative terms. In absolutely terms, however, the performance of the compressor is comparable with the use of any of the various combinations shown in the figures.

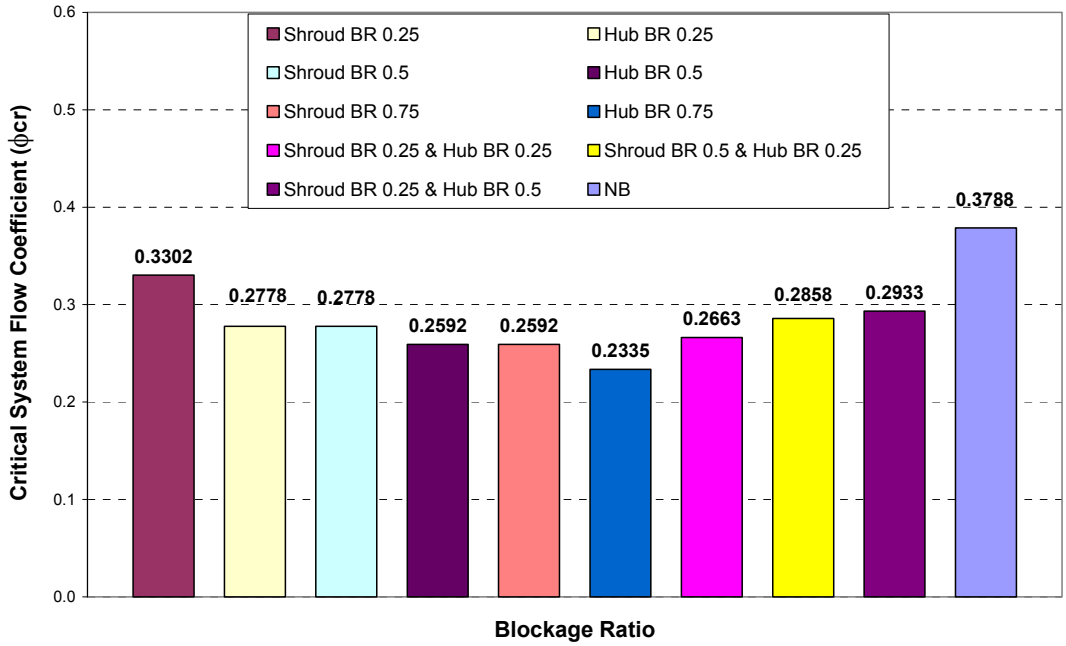

Figure 7.2: Effects of Throttle Ring Attached on Hub, Shroud, and Simultaneous Walls on Compressor Characteristics with $D_o / D_i = 1.5$, N = 2000 RPM & $b / D_i = 0.055$

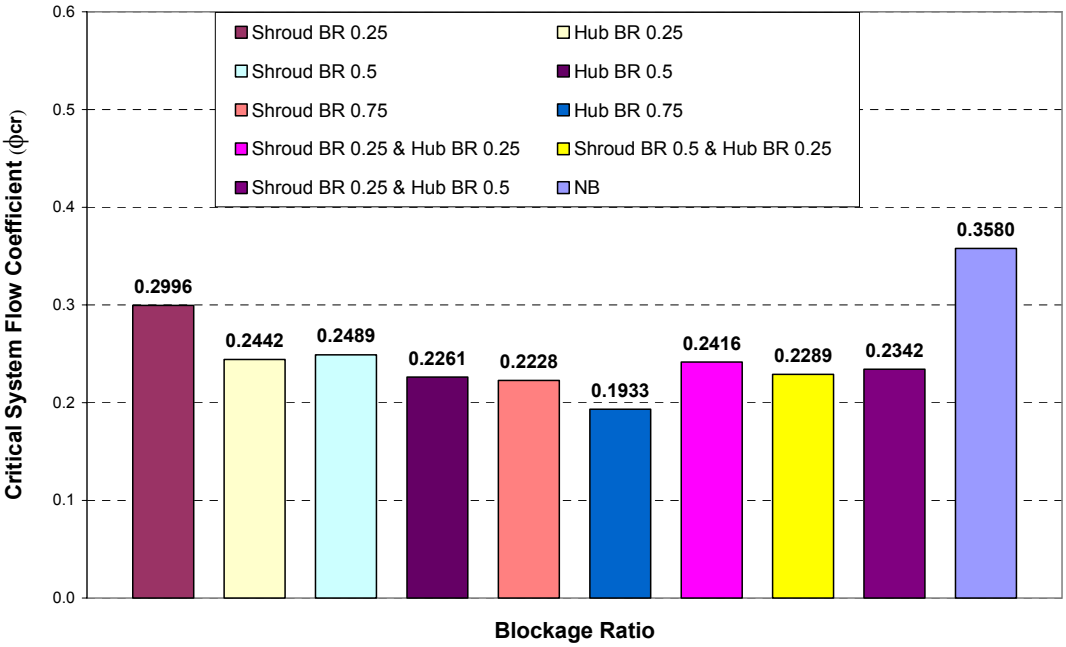

Figure 7.3: Effects of Throttle Ring Attached on Hub, Shroud, and Simultaneous Walls on Compressor Characteristics with $D_o / D_i = 1.75$, N = 2000 RPM & $b / D_i = 0.055$

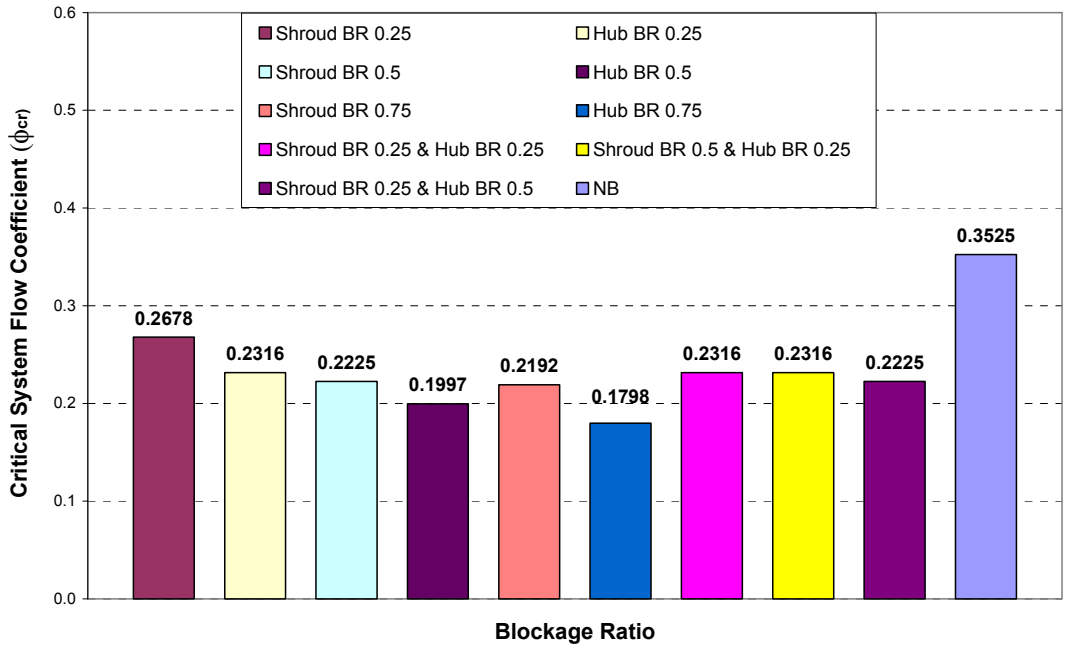

Figure 7.4: Effects of Throttle Ring Attached on Hub, Shroud, and Simultaneous Walls on Compressor Characteristics with D_o / D_i = 2.0, N = 2000 RPM & b / D_i = 0.055

7.2 Effects of Blockage Ratio on the Diffuser Flow Characteristics

It has been shown in the earlier chapters that the flow conditions at the diffuser are the most affected by the presence of any instability in the diffuser. Therefore, any favorable modification to flow conditions at the diffuser inlet will improve the performance characteristics of the diffuser and, in turn, improve the performance of the entire system. Hence, the effects of reducing the diffuser exit flow area on the flow characteristics at the diffuser inlet are examined under the following subheadings.

7.2.1 Effects of Blockage Ratio on Diffuser Stability

The modifications caused to the through flow at the diffuser inlet when a blockage ratio was employed are shown in Figs. 7.5, 7.6, and 7.7. Different blockage ratios are

tested, wherein impeller angular speed is kept constant. With throttle rings attached to hub wall, shroud wall, and their combination, three diffuser diameter ratios are experienced to restore clear analysis of the stall. . From these figures, a comparison between optimal design conditions (No blockage ratio) and attaching throttle rings on diffuser wall is performed. Curves indicate significant improvement in velocity profile as blockage ratio is increased. Also, these figures illustrate that the velocity profile would be better modified with throttle rings attached to hub wall. Results are in line with the outcome of the previous part in this chapter. In addition, studying the effects of diffuser diameter ratio (D_o / D_i) of 1.5, 1.75 and 2.0 are examined as well. For example, calculations show that the velocity ratio (V_p / V_o) decreased by 13.2%, 15.8%, and 16.85% as 25%, 50%, and 75% blockage ratio were used respectively at two diameter ratios of 1.5 and 2.0.

On the average, the stability of the system was improved as the system flow coefficient decreases. A decrease in the flow coefficient indicates that the flow is becoming more radial and thus, improving the stability of the diffuser as shown in Fig. 7.9.

In general, the attachment of the throttle ring to diffuser hub wall increases the static pressure and tendency for reverse flow on the hub side. This hydrodynamic modification of the flow in the vicinity of the diffuser hub wall tend to counterbalance the existing reverse flow, or tendency thereof, on the shroud side resulting in improving the stability of the diffuser (Ahmed, S. A. et al. 2002 and Ishida, M. et al. 2000).

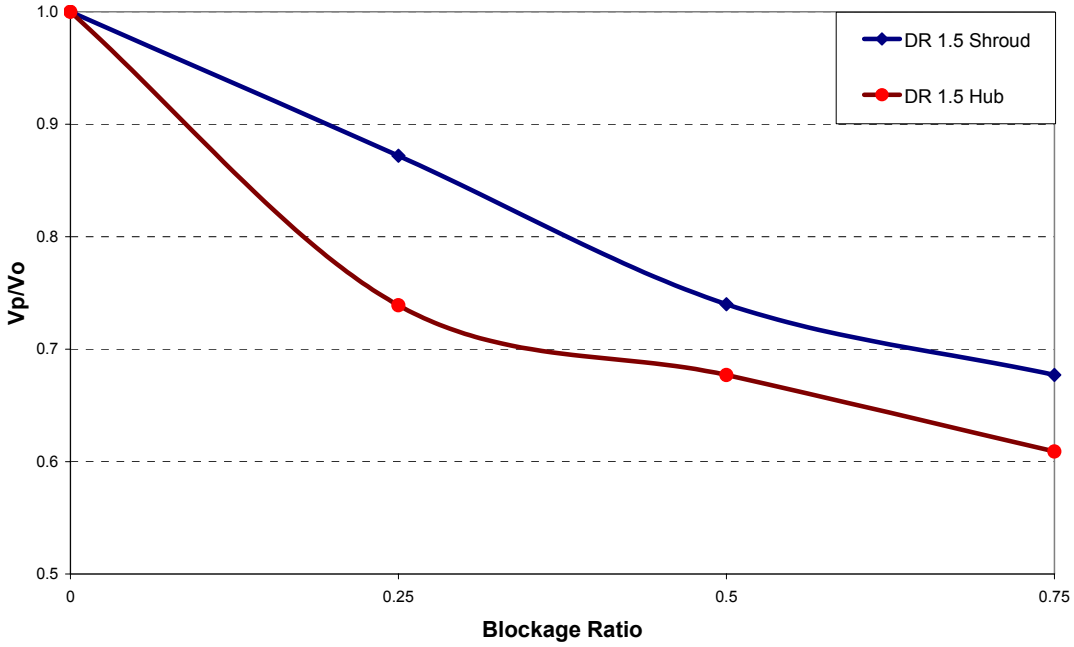

Figure 7.5: Effects of Throttle Ring Attached on Hub & Shroud Walls on Velocity Profile with D_o / D_i = 1.5, N = 2000 RPM & b / D_i = 0.055

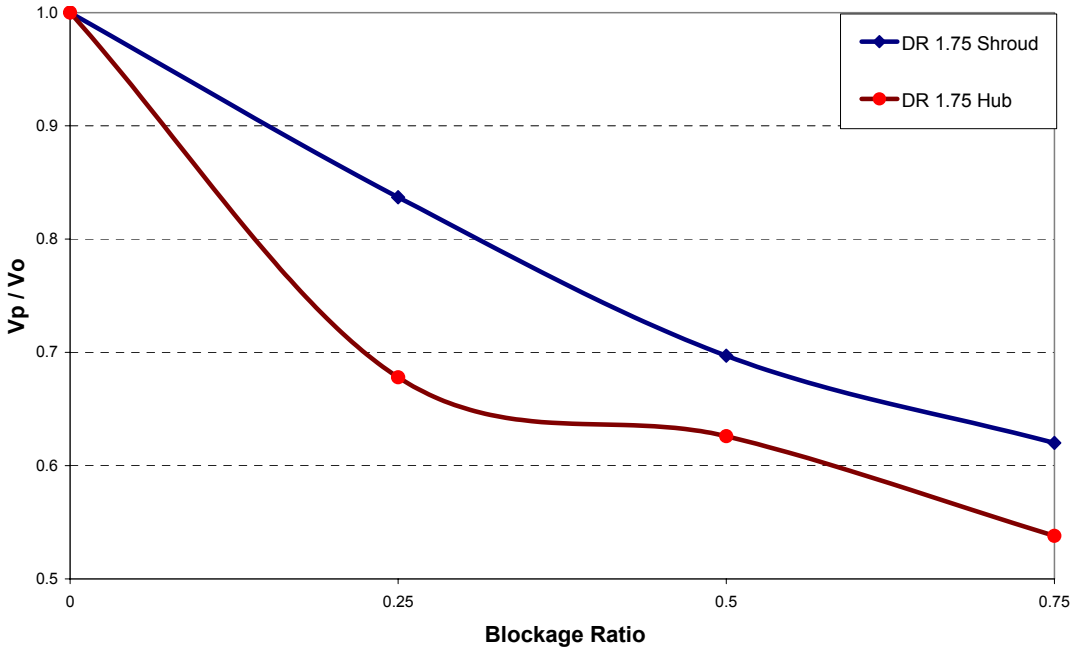

Figure 7.6: Effects of Throttle Ring Attached on Hub & Shroud Walls on Velocity Profile with D_o / D_i = 1.75, N = 2000 RPM & b / D_i = 0.055

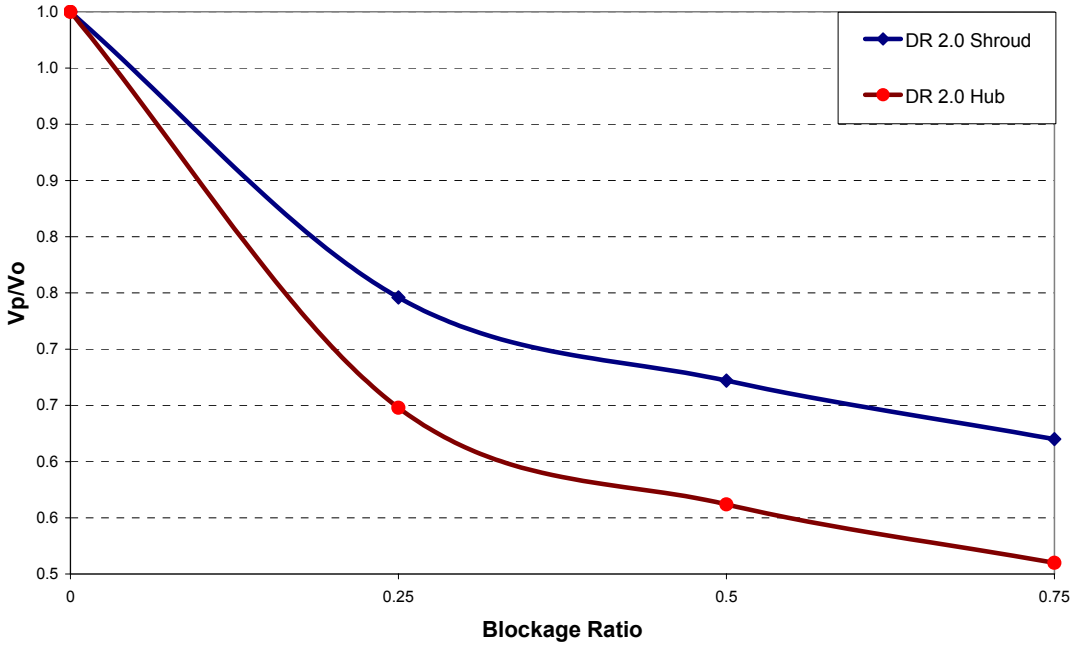

Figure 7.7: Effects of Throttle Ring Attached on Hub & Shroud Walls on Velocity Profile with D_o / D_i = 2.0, N = 2000 RPM & b / D_i = 0.055

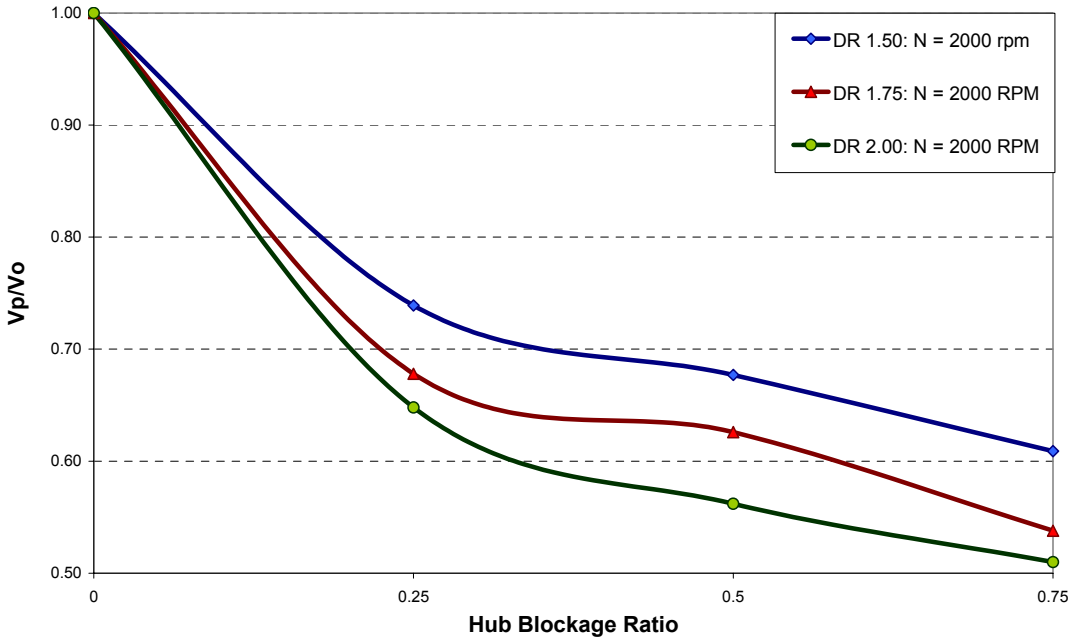

Figure 7.8: Effects of Throttle Ring Attached on Hub Wall on Compressor Characteristics with N = 2000 RPM & b / D_i = 0.055

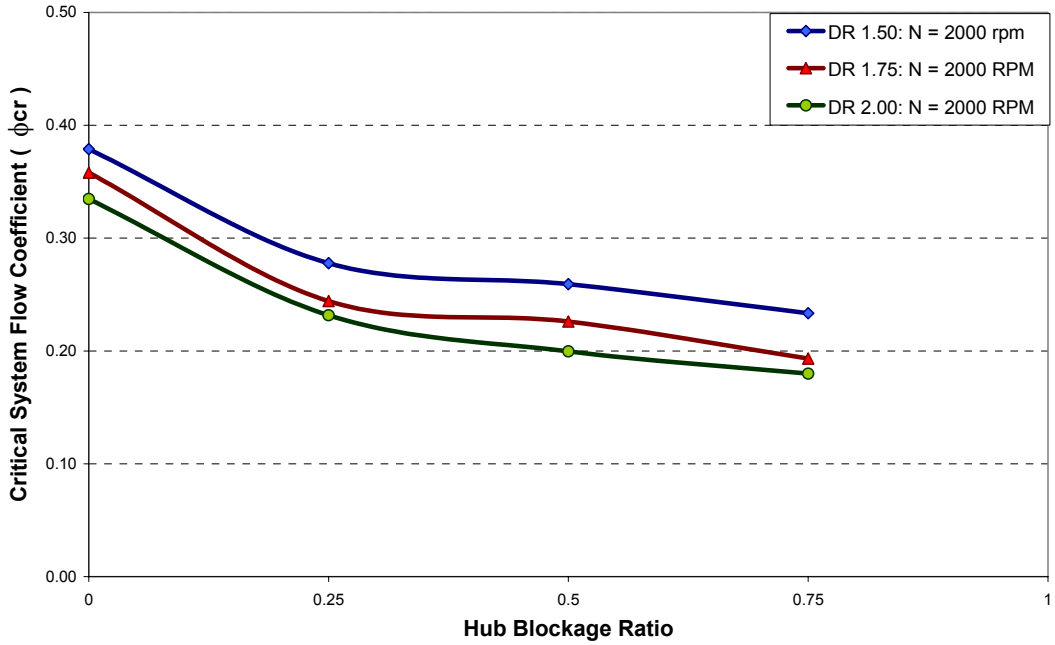

Figure 7.9: Effects of Throttle Ring Attached on Hub Wall on Compressor Characteristics with N = 2000 RPM & b / D_i = 0.055

7.2.2 Effects of Blockage Ratio on the Strength of Rotating Stall Cells

The variations in strength of rotating stall cells, with fixed impeller angular speed and diffuser width ratio at different diffuser blockage ratios, are shown in Fig. 7.10 for n = 1 (m = 1). The figure confirms clearly that the strength of the stall cells increases as the blockage ratios increase. However, the figure does not show any consistent dependence on the stall strength of the diffuser diameter ratio. What could be deduced from the graph is that the inconsistent variation of the stall cell strength increases as the blockage ratio increases. For example, at D_o / D_i = 1.75 and n = 1 (m = 1), the strength of the stall cells increases rapidly as the blockage ratio increased from 25% to 75%. This inconsistent trend was found only at diameter ratio of 1.5, where the strength of rotating stall decreases with the increase of diffuser blockage ratio. However, this inconsistent

trend is limited only to D_o / D_i = 1.5. Thus, it is possible to claim that the strength of the stall cells is dependent on both the diffuser blockage diameter ratios.

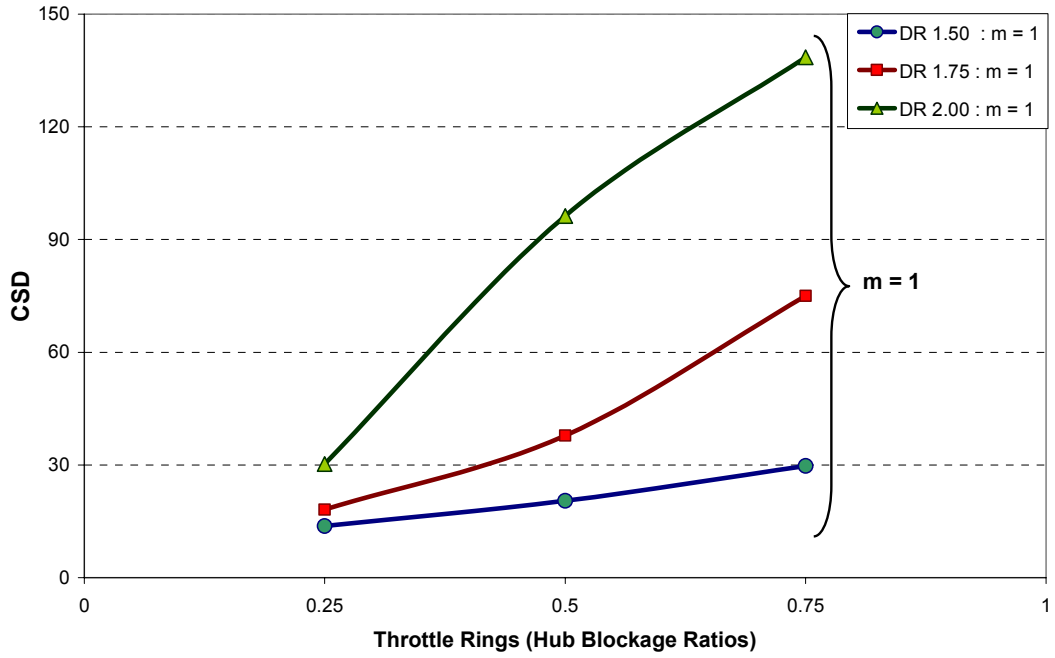

Figure 7.10: Effects of Throttle Rings Attached to Hub Wall on the Strength of Rotating Stall at N = 2000 RPM & b / Di = 0.055

7.2.3 Effects of Blockage Ratio on the Frequency of Pressure Fluctuations

The effect of blockage ratios on the frequency of pressure fluctuation is shown in Figs. 7.11 and 7.12. For the entire diameter ratios shown in the fig. 7.11, the frequency of pressure fluctuations tends to be fixed as the diffuser blockage ratios increase. It is important to note that the frequency of pressure fluctuations decreases with the increase of diameter ratio. However, this is not valid when a comparison between 1.5 and 1.75 diameter ratios is made, where there is no change in the frequency with various blockage ratios. In other words, the frequency of pressure fluctuations is irrelevant to blockage ratio.

Figure 7.12 shows the effects of various diffuser blockage ratios on the frequency of pressure fluctuations. It is clear to note that adding throttle rings on the outlet diffuser with different blockage ratios will decrease the frequency of pressure compared with the optimal diffuser condition, where there is no blockage ratio. It is also obvious that the frequency of pressure fluctuations is independent of all entire blockage ratios attached to diffuser wall at fixed diameter ratio, impeller speed and diffuser width ratio.

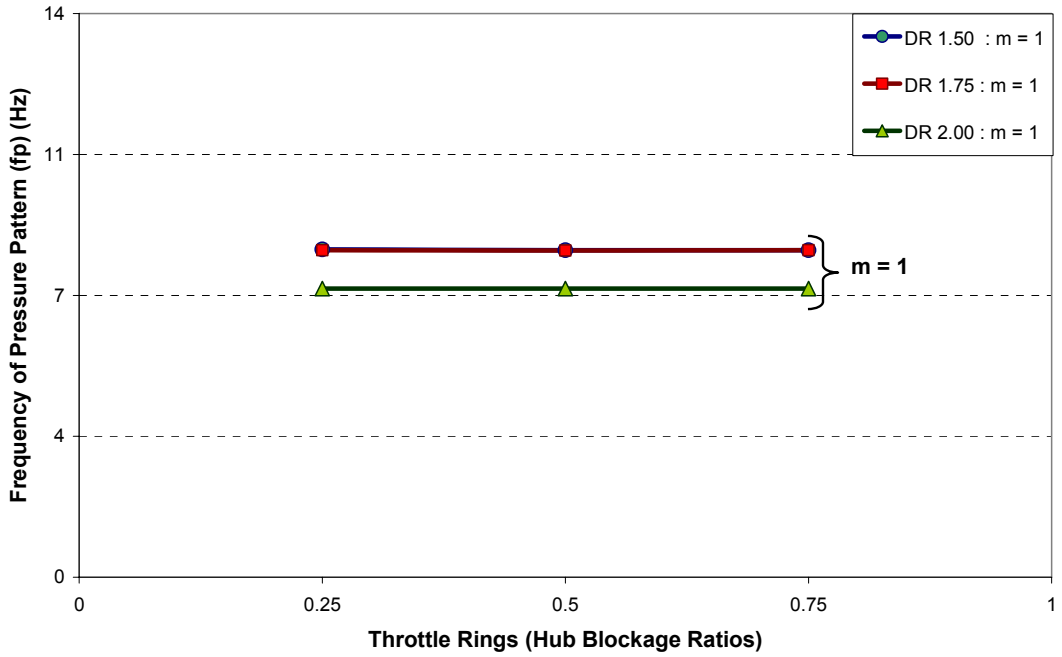

Figure 7.11: Effects of Throttle Rings Attached to Hub Wall on Frequency of Rotating Stall at N = 2000 RPM & b / D_i = 0.055

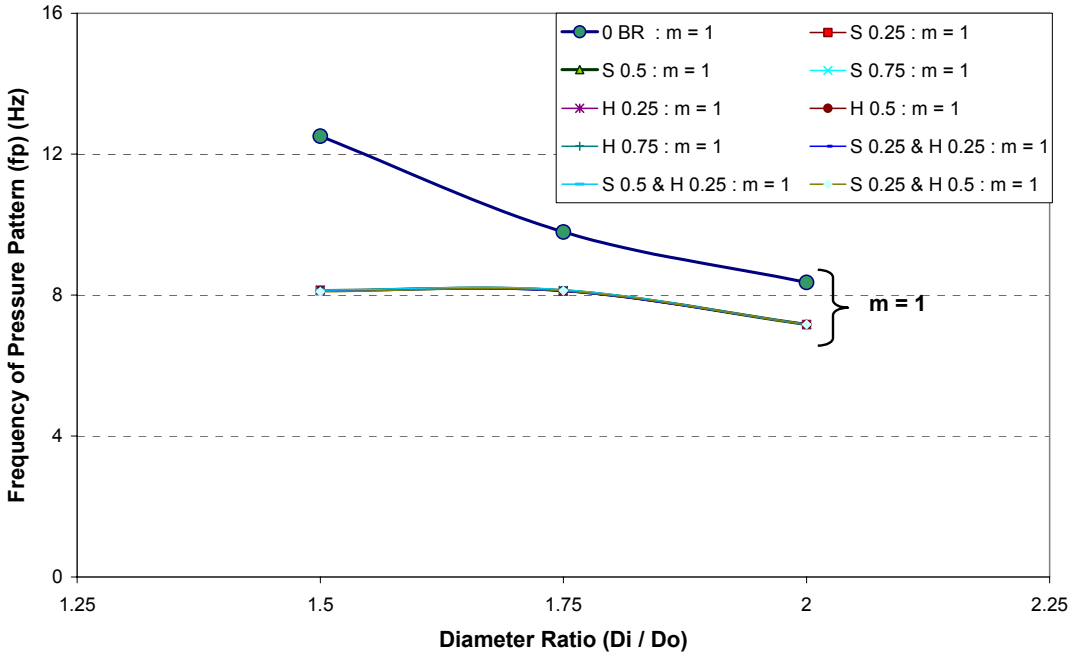

Figure 7.12: Effects of Throttle Rings Attached to Hub Wall, Shroud Wall, & their Combinations on Frequency of Pressure Fluctuations at D_o / D_i = 1.75, N = 2000 RPM & b / D_i = 0.055

CHAPTER 8

CONCULSIONS & RECOMMENDATIONS

8.1 Conclusions

Detailed experimental investigation of rotating stall characteristics in the vaneless diffuser of a centrifugal compressor has been carried out. The results have, to a great extent, successfully clarified the hitherto seemingly contradictory results in the open literature as per the nature and description of rotating stall characteristics in vaneless diffusers of centrifugal compressors and blowers. Furthermore, the data presented in this work are in good agreement with the results of the vast majority of the published works in this field, especially on the hydrodynamic changes that takes place before the onset-, at the onset-, and after the onset of any oscillation in the diffuser. In particular, summary of the results from these experimental measurements of rotating stall characteristics in the vaneless diffuser of a centrifugal compressor is given below:

- It is noticeably revealed that the strength of rotating stall cell is directly proportional to impeller angular speed; On the other hand, the strength of rotating stall cell is inversely proportional to diffuser diameter ratio.
- The performance of the compressor, in terms of stability, is better with a bigger diffuser diameter ratio.
- Although the number of stall cells was not significantly affected by the impeller speed, the results show that the frequency of the stall cells, f_p, increases as the impeller angular speed was increased. The relationship between f_p and N, for constant n, is fairly linear. In addition, the strength of the stall cells, as determined

by the PSD and CSD, increases when the impeller speed is increased, independent of the number of stall cells, m.

- The critical flow coefficient, ϕ_{cr}, decreases with increasing impeller angular speed and decreases as the diffuser diameter ratio was increased at constant impeller angular speed.
- The frequency of the stall cells with m = 1 increases as the diffuser diameter ratio was decreased with a fixed diffuser width. This trend was most consistent for all speeds tested.
- The strength of the rotating stall cells shows consistent trend with a change of the diffuser diameter ratio. Where it decreases as diameter ratio was increased. This trend was the same for all impeller angular speeds tested.
- The results suggest that the instability in the diffuser was delayed to a lower flow coefficient when throttle rings were attached to the diffuser hub wall to reduce its exit flow area.

8.2 Recommendations

There is always the need to improve the quality of a scientific research or discovery however excellent the results might look. In this vein, the author feels that the following enumerated recommendations would go a long way in improving the quality of future research on this subject:

- The construction of the experimental test rig should be improved upon in order to increase its stability at very high impeller speed. For example, the wooden rectangular tops could be replaced with more solid metallic material.
- Since the trend in the change of some of the characteristics of the stall cells, such as fp, was found to be consistent with the change in the diffuser diameter ratio at high impeller speeds, it would be a good idea to equip the experimental test rig with a variable motor whose maximum speed is not less than 10000 RPM. This would enable a more conclusive statement to be made about such properties of the stall cells that show consistent trend at very high impeller angular speed.
- It would be very advantageous too if a panel-mount type tachometer is secured for measuring the impeller angular speed. The hand-held type, currently in use, is laborious to ensure an accurate determination of the impeller angular speed.
- It is a good idea to have the hot wire to complement the measurements for velocity components (radial and tangential). So, a complete enlightenment and observation will be accomplished to understand more about the rotating stall and its characteristics. This tool will be highly resourceful in terms of comparing the measurements from different directions.

- Securing a very good spectrum analyzer for faster extraction of required information from transducer output signals would be very advantageous as a great deal of time and effort will be conserved.
- An upgrade of the Data Acquisition Program (DAP) would not be a bad idea, if such upgrades exist, since the one currently available is bit limited.
- Using two pairs of dynamic pressure transducers be distributed and placed all around the diffuser shroud wall, will be so beneficial to obtain a clear image and observation for the stall occurrence and it is characteristics.

REFERENCES

– Abdelhamid, A. N. and Bertrand, J. (1980) "Distinction between two types of self excited gas oscillations in vaneless radial diffusers," *Canadian Aeronautics and Space Journal,* 26:105-117.

– Abdelhamid, A.N. (1986) "A new technique for stabilizing the flow and improving the performance of vaneless radial diffusers," *ASME Paper # 86-GT-128*.

– Ahmed, S.A. (2002) "Characteristics of Unsteady-Flow Phenomenon in a Channel Radial Diffuser'' *Canadian Aeronautics and Space Journal*, vol. 48, No. 3, September 2002.

– Antonia, R.A., Prabhu, A., and Stephenson, S.E. (1975) "Conditional sampled measurements in a heated turbulent jet," *Journal of Fluid Mechanics*, 72:455-465.

– Arnulfi, G.L., Micheli, D. and Pinamonti, P. (1996) "Experimental investigation on rotating stall in a centrifugal compressor with two and four stages and vaneless diffusers," *ASME Paper # 96-GT-171*.

– Bammert, K., Rautenberg, M., and Wittekindt, W. (1978) "Vaneless diffuser flow with extremely distorted inlet profile," *ASME Paper # 78-GT-47.*

– Bammert, K, Rautenberg, M., and W. Wittekindt (1980) "Matching of turbo-components described by the example of impeller and diffuser in a centrifugal compressor Part I: Aerothermodynamic coupling of impeller and diffuser; Part II: optimized stage efficiency of a centrifugal compressor," *Journal of Engineering for Power*, 102:594-600.

– Chaoqun Nie (2003) "An Experimental Investigation on Different Radial Loading Distribution and Pattern of Stall Inception in a Single-Stage Low-Speed Radial Compressor" *Proceedings of ASME Turbo Expo 2003,* June 16-19, 2003, Atlanta, Georgia, USA.

– Cumpsty, N.A. “Compressor Aerodynamics,” Addison Wesley Longman Limited, Harlow, England (1989).

– Cumpsty, N.A., and Greitzer, E. (1982) “A simple model for compressor stall cell propagation,” *Trans. ASME, Journal of Engineering for Power*, 104:170-176.

– Dean, R.C. and Senoo, Y. (1960) “Rotating Wakes in vaneless diffusers,” *Trans. ASME, Journal of Basic Engineering*, 82:563-574.

– Dou, H.S. (1989) “A method of predicting the energy losses in vaneless diffusers of centrifugal compressors,” *ASME Paper # 89-GT-158*.

– Di Liberti, J.L., Wilmsen, B., and Engeda, A. (1996) “The effect of the vaneless diffuser width on the performance of a centrifugal compressor,” *ASME Fluids Engineering Division Conference,* 237:797-803.

– Dou, H.S., and Cheng, X. D. (1986) “Calculation of three-dimensional turbulent boundary-layers in the vaneless diffuser of a centrifugal compressor,” *Journal of Northeastern university of technology*, 7: 39-48.

– Eckardt, D. (1975) “Instantaneous measurements in the jet wake discharge flow of a centrifugal compressor impeller,” *Trans. ASME, Journal of Engineering for Power*, 97:337-346.

– Eckardt, D. (1976) “Detailed flow investigations within a high-speed compressor impeller,” *Trans. ASME, Journal of Fluids Engineering*, 98:390-402.

– Ferrara, G., Ferrara, L., and Baldassarre, L. (2003) “Rotating Stall in Centrifugal Compressor Vaneless Diffuser Part IV: Impeller Influence on Diffuser Stability” *Proceedings of 2003 ASME Turbo Expo,* June 16-19, 2003, Atlanta, Georgia, USA.

– Ferrara, G., Ferrara, L., and Baldassarre, L. (2004) “Rotating Stall in Centrifugal Compressor Vaneless Diffuser: Experimental Analysis of Geometrical Parameters

Influence on Phenomenon Evolution" *International Journal of Rotating Machinery,* 10 (6): 433-442, 2004.

– Ferrara, G., Ferrara, L., and Baldassarre, L. (2002) "Experimental Investigation and Characteristics of the Rotating Stall in a High Pressure Centrifugal Compressor: Part I: Influence of Diffuser Geometry on Stall Inception" *Proceedings of 2002 ASME Turbo Expo,* June 3-6, 2002, Amsterdam, the Netherlands.

– Fringes, P. and Van Den Braembussche, R. (1984a) "Distinction between different types of impeller and diffuser rotating stall in a centrifugal compressor with vaneless diffuser," *Journal of Engineering for Gas Turbines and Power*, 106:468-474.

– Frigne, P., and Van Den Braembussche, R. (1984) "A theoretical model for rotating stall in the vaneless diffuser of a centrifugal compressor," *ASME Paper # 84-GT-204.*

– Frigne, P., and Van Den Braembussche, R. (1985) "A theoretical model for rotating stall in the diffuser of a centrifugal compressor," *Trans. ASME, Journal of Engineering for Gas Turbine and Power*, 107:507-513.

– Gary J. Shock. (2003) "Experimental Investigation of Centrifugal Compressor Stabilization Techniques" *Proceedings of ASME Turbo Expo 2003,* June 16-19, 2003, Atlanta, Georgia, USA.

– Gergakis, C., Bennette, F., and Lvey, P.C. (2003) "Fast Response Probes Measuring Unsteady Flow in High Speed Research Compressors" *Proceedings of ASME Turbo Expo 2003,* June 16-19, 2003, Atlanta, Georgia, USA.

– Greitzer, E.M. (1981) "The stability of pumping systems – the 1980 freeman scholar lecture," Trans. *ASME, Journal of Fluid Engineering*, 103:193-242.

– Gould, R.D., Stevenson, W.H., and Thompson, H.D. (1990) "Investigation of turbulent transport in an axisymmetric sudden expansion," *AIAA Journal*, 28:276-283.

– Inoue, M. (1983) "Radial vaneless diffusers: A re-examination of the theories of Dean and Senoo and Johnston and Dean," *Journal of Fluids Engineering,* 105:21-27.

– Inoue, M. and Cumpsty, N.A. (1978) "Small perturbation analysis of non-uniform rotating disturbances in vaneless diffuser," *Journal of Engineering for Power,* 100:711-721.

– Ishida, M., Sakaguchi, D., and Ueki, H. (1995) "Detection of rotating stall precursor in vaneless diffuser of a centrifugal blower," *ASME Fluid machinery, Fluids Engineering Division,* 222:155-160.

– Jansen, W. (1964a) "Steady fluid flow in radial vaneless diffuser," *Trans. ASME, Journal of basic Engineering,* 86:607-619.

– Jansen, W. (1964b) "Rotating stall in a radial vaneless diffuser," *Trans. ASME, Journal of basic Engineering,* 86:750-758.

– Japikse, D. (1984) "A critical evaluation of stall concepts for centrifugal compressors and pumps – studies in component performance, Part 7," *ASME Conference on Stall and Surge in Compressors and Pumps*.

– Japikse, D. and Baines, N.C. (1994) "Introduction to turbomachinery Concepts," ETI, Inc. and Oxford University Press, pp. 9-1 to 9-28.

– Jean, Lac Di Liberh (2003) "Effect of the Exit System on the Performance of a Low Specific Speed Industrial Centrifugal Compressor" *Proceedings of ASME Turbo Expo 2003,* June 16-19, 2003, Atlanta, Georgia, USA.

– Jeong-Seek, K. and Shin-Hyoung, K. (2003) "Stall Inception in a Vaneless Diffuser of a Centrifugal Compressor" *Proceedings of ASME Turbo Expo 2003,* June 16-19, 2003, Atlanta, Georgia, USA.

– Jongensen, F.E. (1971) "Directional sensitivity of wire and fiber film probes," *DISA Information*, No. 11:31-37.

– Johnston, J.P. and Dean, R.C. (1966) "Losses in vaneless diffusers of centrifugal compresors and pumps," *Trans. ASME, Journal of Engineering for Power*, 88:49-62.

– Kamordeen B. Abdogun and Ahmed, S.A. (2000) "Detailed Experimental Measurements of the Flowfield Characteristics in a Radial Vaneless Diffuser" Proceedings of 2000 *International Joint Power Generation Conference*, Miami Beach, Florida, July 23-26, 2000.

– Kasagi, N. and Matsunaga, A. (1995) "Three-dimensional particle tracking velocimetry measurement of turbulence statistics and energy budget in a backward-facing step flow," *International Journal of Heat and Fluid Flow*, 16:477-485.

– Kay, S.M. (1988) "Modern spectral estimation," *Englewood Cliffs, NJ; Prentice Hall.*

– Kinoshita, Y., and Senoo, Y. (1985) "Rotating stall induced in vaneless diffusers of very low specific speed centrifugal blowers," *Journal of Engineering for Gas Turbine and Power,* 107:514-521.

– Krain, H. (1981) "A study on centrifugal impeller and diffuser flow," *Journal of Engineering for Power*, 103:688-697.

– Lawless, P.B. and Fleeter, S. (1991) "Active unsteady aerodynamic suppression of rotating stall in an incompressible flow centrifugal compressor with vaned diffuser," *AIAA Paper # 91-1898.*

– Lawless, P.B. and Fleeter, S. (1993) "Prediction of active control of subsonic centrifugal compressor rotating stall," *AIAA Paper # 93-0153.*

– Lawless, P.B. and Fleeter, S. (1999) "Active control of rotating stall in a low-speed centrifugal compressor," *Journal of Propulsion and Power*, 15:38-44.

– Lejvar, S., De Lange, H.C., and Steenhoven, A.A. van (2006) "Two-Dimensional rotating Stall analysis in a Wide Vaneless Diffuser" *International Journal of Rotating Machine,* volume 2006, Article ID 5620, page 1-11.

– Levy, Y. and Pismenny, J. (2003) "The Number and Speed of Stall During Rotating Stall" *Proceedings of ASME Turbo Expo 2003,* June 16-19, 2003, Atlanta, Georgia, USA.

– Ligrani, P.M., Van Den Brembussche, R. and Roustan, M. (1983) "Measurements in the vaneless diffuser of a radial flow compressor," *International Journal of Heat and Fluid Flow*, 4: 103-106.

– Mizuki, S. and Oosawa, Y. (1992) "Unsteady flow within centrifugal compressor channels under rotating stall and surge," *Trans. ASME*, *Journal of Turbomachinery* 114:312-320.

– Moore, J. and Moore, J.G. (1980) "Three dimensional viscous flow calculations for assessing the thermodynamic performance of centrifugal compressors - study of the Eckardt compressor," *AGARD-CP-282*.

– Moore, J., Moore, J.G., and Timmis, P.H. (1984) "Performance evaluation of centrifugal compressor impellers using three dimensional viscous flow

calculations," *Trans. ASME*, *Journal of Engineering for Gas Turbines and Power*, 106:475-481.

– Moore, F.K. (1989) "Weak rotating flow disturbances in a centrifugal compressor with a vaneless diffuser," *Trans. ASME*, *Journal of Turbomachinery*, 111:442-449.

– Moore, F.K. (1991) "Theory of finite disturbances in a centrifugal compression system with a vaneless radial diffuser*," ASME Paper # 91-GT-082.*

– Mounts, J.S., and Brasz, J.J. (1992) "Analysis of the Jet/Wake Mixing in a vaneless diffuser," *ASME Paper # 92-GT-418.*

– Ohashi, H and Shoji, H. (1987) "Lateral fluid forces on whirling centrifugal impeller: experiment in vaneless diffuser," *Trans. ASME*, *Journal of Turbomachinery*, 109:100-106.

– Oleg, D. and Japikse, D. (2005) "Vaneless Diffuser Advanced Model" *Proceedings of GT 2005, ASME Turbo Expo 2005,* June 6-9, 2005, Reno-Tahoe – Nevada, USA.

– Otugen, M.V., So, R.M.C., and Hwang, B.C. (1988) "Diffuser stall and rotating zones of separated boundary layer," *Experiments in Fluids*, 6:521-533.

– Pampreen, R.C. (1993) "*Compressor surge and stall* Concepts" *ETI, Inc., Norwich,* pp. 2-86 to 2-103.

– Rodgers, C. and Mnew, H. (1975) "Experiments with a model free rotating vaneless diffuser," *Journal of Engineering for Power*, 97:p231-244.

– Rothe, P. H. and Johnston, J.P. (1976) "Effects of system rotation on the performance of two-dimensional diffusers," *Trans. ASME, Journal of Fluids Engineering,* 98:422-430.

– Schumann, L.F. (1985) “A three-dimensional axisymmetric calculation procedure for turbulent flows in a radial vaneless diffuser,” *ASME Paper # 85-GT-133.*

– Senoo, Y and Ishida, M. (1975) “Behavior of severely asymmetric flow in vaneless diffuser,” *Journal of Engineering for Power*, 97:375-387.

– Senoo, Y., and Kinoshita, Y. (1977) “Influence of inlet flow conditions and geometries of centrifugal vaneless diffusers on critical flow angle for reverse flow,” *Trans. ASME, Journal of Fluids Engineering*, 99:98-103.

– Senoo, Y., and Kinoshita, Y. (1978) “Limits of rotating stall and stall in vaneless diffuser of centrifugal compressors,” *ASME Paper # 78-GT-19.*

– Senoo, Y., Kinoshita, Y., and Ishida, M. (1977) “Asymmetric flow in vaneless diffusers of centrifugal blowers,” *Trans. ASME, Journal of Fluids Engineering,* 99: 104-114.

– Snyder, P.K., Orloff, K.L, and Reinath, M.S. (1984) “Reduction of flow-measurement uncertainties in laser velocimeters with nonorthogonal channels,” *AIAA Journal*, 22:1115-1123.

– Spakovszky, Z. S. (2004) “Backward Traveling Stall Waves in Centrifugal Compressors” *Journal of Turbomachinery, ASME,* Jan. 2004, vol. 126.

– Starner, S.H., and Bilger, R.W. (1981) “Measurements of scalar-velocity correlations in a turbulent diffusion flame,” *18th Symposium (International) on Combustion, The Combustion Institute,* pp. 921-930.

– Tsujimoto, Y., Yoshida, Y., and Mori, Y. (1996) “Study of vaneless diffuser rotating stall based on two-dimensional inviscid flow analysis,” *Trans. ASME, Journal of Fluids Engineering,* 118:123-127.

– Van Den Braembussche, R., Frigne, P., and Roustan, M. (1980) “Rotating non-uniform flow in radial compressors,” *AGARD CP-282*, paper 12.

– Van Den Braembussche, R. (1984) “Surge and stall in centrifugal compressors,” *VKI lecture series*, 1984-07.

– Van Den Braembussche, R. (1985) “Design and optimization of centrifugal compressors,” *Thermodynamics and Fluid Mechanics of Turbomachinery*, Ucer, A.S. et al., eds., Vol. II, Martinus Nijhoff Publishers, Dordrecht, pp: 829-885.

– Van Den Braembussche, R. (1982) “Rotating stall in vaneless diffusers of centrifugal compressors” *Von Karman Institute for Fluid Dynamics*, Tech.

– Watanabe, H., Konomi, S., and Ariga, I. (1994) “Transient process of rotating stall in radial vaneless diffusers,” *ASME Paper # 94-GT-161*.

– Welch, P.D. (1967) “The use of fast Fourier transform for the estimation of power spectra: A method based on time averaging over short, modified periodograms,” *IEEE Trans. Audio Electroacoust*, AU-15:70-73.

– Whitfield, A, Wallace, F.I., and Atkey, R.C. (1976) “The effects of variable geometry on the operating range and surge margin of a centrifugal compressor,” *ASME Paper # 76-GT-98.*

NOMENCLATURE

A	Diffuser inlet area (mm^2)
b	Diffuser width (mm)
Cp	Pressure Coefficient
CSD	Cross-Spectral Density $(mbar)^2/Hz$
D_i	Diffuser inlet diameter (mm)
D_o	Diffuser outlet diameter (mm)
f_p	Frequency of pressure pattern (Hz)
n	Number of rotating stall
N	Impeller speed (rpm)
Ns	Speed of pressure pattern (rpm)
m	Harmonic number
M_{tip}	Mach number at impeller tip
P_{imp}	Impeller inlet pressure
P_o	System exit Pressure (Pa)
PSD	Power-Spectral Density $(mbar)^2/Hz$
V_{imp}	Impeller tip speed (m/s)

Greek Symbols

θ_p	Physical angular distance between pressure transducers 2 & 4 in Fig2.1
ρ	Density of air
ϕ	Volume flow rate / (A V_{imp})

Subscripts

cr	Critical condition

APPENDIX

A. MATLAB Program

```
close all;
clear
clc
%--------------------------------------------
% Loading data taken from the DAQ
load out1.dat;
out=out1;
t=out(:,1)*10^-6;
x=out(:,2);
y=out(:,3);
%--------------------------------------------
% Specify DSP Parameters
nfft=4096*2;
noverlap=100;
window=hanning(nfft);
fs=1957;
%--------------------------------------------
% Display two signals in term of voltage base
figure(1)
plot(t,x,'--k');
set(gca,'fontsize',14);
title('First Signal');
xlabel('Time (sec)');
ylabel('Voltage (mV)');
grid;
axis([0 0.35 -75 75]);
figure(2)
plot(t,y,'--k');
set(gca,'fontsize',14);
title('Second Signal');
xlabel('Time (sec)');
ylabel('Voltage (mV)');
grid;
```

```
axis([0 0.35 -75 75]);
%-----------------------------------------------
% DESIGN THE DIGITAL FILTER "LOW PASS FILTER ORDER 30th AND
STEP OF O.1 (10 Hz)"
% FIR system to be identified
b  = fir1(30,.01);
% Desired filtered signal 1
d  = (1)*(filter(b,1,x));
% Desired filtered signal 2
s  = (1)*(filter(b,1,y));
%-----------------------------------------------
% Display the two signals as Pressure in Time Domain
figure(3)
subplot(2,1,1);plot(t,(d*tan(86.185))/10);
% The above constant is the convertion factor from calibration curve of DPT
set(gca,'fontsize',14);
title('Signals (1 & 2) "Using Band Pass Digital Filter"');
grid;
set(findobj(gca,'Type','line','Color',[0 0 1]),...
   'Color','black',...
   'LineWidth',3.5);
subplot(2,1,2);plot(t,(s*tan(86.185))/10);
set(gca,'fontsize',14);
xlabel('Time (sec)');
ylabel('Pressure (Pa)');
grid;
set(findobj(gca,'Type','line','Color',[0 0 1]),...
   'Color','black',...
   'LineWidth',3.5);
%-----------------------------------------------
% DESIRED FILTERED SIGNALS
d  = (filter(b,1,x));
s  = (filter(b,1,y));
% power spectral Density for the first filtered signal
[P11,f] = PSD(d,nfft,fs,window,noverlap);
```

```
% power spectral Density for the second filtered signal
[P22,f] = PSD(s,nfft,fs,window,noverlap);
%-----------------------------------------------
% cross power spectrum density
[Pxy,F]=csd(d,s,nfft,fs,window,noverlap);
f=(0:length(Pxy)-1)'/length(Pxy)*fs/2;
% To convert the unit to degree
p=(angle(Pxy))*180/pi;
% phase angle using smoothing function "unwrap"
p1=(unwrap(angle(Pxy)))*180/pi;
%-----------------------------------------------
figure(4)
plot(f,P11/10,'k',f,P22/10,':k','LineWidth',4);
set(gca,'fontsize',14);
grid;
legend('Signal 1','Signal 2');
ylabel('PSD');
xlabel('fp (Hz)');
axis([0 100 0 450]);
figure(5)
[haxes,hline1,hline2]=plotyy(F,abs(Pxy)/10,F,p,'plot');
grid;
xlabel('fp (Hz)');
axes(haxes(1));
ylabel('CSD');
legend('CSD');
ylim([0 650]);
xlim([0 100]);
set(gca,'ytick',[0 100 200]);
axes(haxes(2));
ylabel('\Theta (degree)');
ylim([-360 360]);
xlim([0 100]);
legend('\theta',2);
set(hline1,'color','black','LineWidth',2.5);
```

```
set(hline2,'LineStyle',':','color','black','LineWidth',2.5);
set(gca,'ytick',[-360 0 360]);
%-----------------------------------------------
[Cxy,F]=cohere(d,s);   %coherence
%-----------------------------------------------
figure(6)
plot(F,Cxy,'k');
set(gca,'fontsize',14);
set(gca,'ytick',[0 0.2 0.4 0.6 0.8 1]);
title('Coherence');
ylabel('Power Spectral Density (dB)');
xlabel('Frequency (KHz)');
grid;
%-----------------------------------------------
% EBD OF THE PROGRAM
%-----------------------------------------------
```

B. Statistical Signal Processing

In the following subsections, detailed description of the functions used for spectral analysis in this dissertation is discussed. Examples are provided where necessary.

B.1 Spectral Analysis

Spectral analysis seeks to describe the frequency content of a signal, random process, or system, based on a finite set of data. Estimation of power spectra is useful in a variety of applications, including the detection of signals buried in wide-band noise.

The power spectral density (PSD), P_{xx}, of a stationary random process x_n is related, mathematically, to the correlation sequence by the discrete-time Fourier transforms:

$$P_{xx}(\omega) = \sum_{m=-\infty}^{\infty} \gamma_{xx}(m) e^{-j\omega m} \tag{B.1}$$

This function of frequency has the property that its integral over a frequency band is equal to the power of the signal x_n in that band. The PSD is a special case of the cross-spectral density (CSD) function, defined between two signals x_n and y_n as:

$$P_{xy}(\omega) = \sum_{m=-\infty}^{\infty} \gamma_{xy}(m) e^{-j\omega m} \tag{B.2}$$

As is the case for the correlation and covariance sequences, the MATLAB toolbox estimates the PSD and CSD because signal lengths are finite.

The various methods of PSD estimation can be identified as parametric or nonparametric. The technique used in the MATLAB Signal Processing Toolbox is the popular nonparametric scheme developed by Welch (1967).

B.2 Welch's Method

One way of estimating the power spectrum of a process is to simply find the discrete-time Fourier transform of the samples of the process (usually done on a grid with an FFT (Fast Fourier Transform)) and take the magnitude squared of the result. An example of 1001-element signal xn, which consists of two sinusoids plus noise, is given by:

```
Fs = 1000;       % sampling frequency
t = 0:1/Fs:1;    % one second worth of samples
xn = sin(2*pi*50*t) + 2*sin(2*pi*120*t) + randn(size(t));
```

where pi = π = 3.142 and randn is the noise generation function in MATLAB.

A crude estimate of the PSD of the above function, x_n, is:

$$Pxx = abs(fft(x_n,1024))^2/1001$$

This estimate is called the periodogram. The output of this crude estimate of the PSD is shown in Fig. B.1

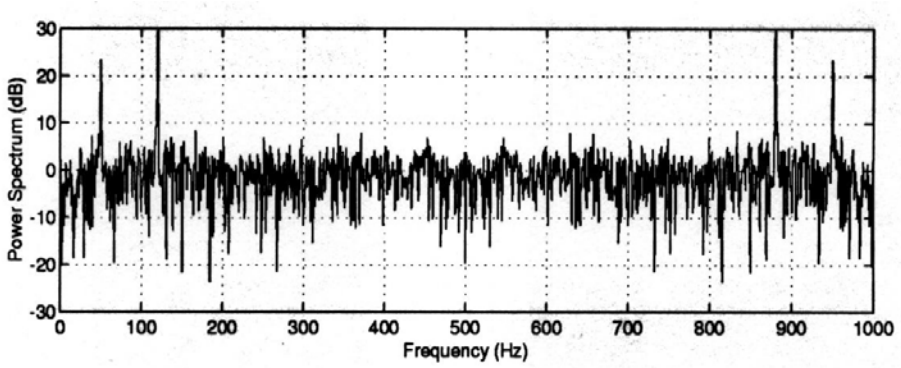

Figure B.1: The Periodogram

To reduce the variance of the PSD estimate, the signal is broken into nonoverlapping sections and averaging the periodograms of these sections. The MATLAB command is:

Pxx = (abs(fft(x_n(1:256)))^2 + abs(fft(x_n(257:512)))^2 + abs(fft(x_n(513:768)))^2) / (256*3);

plot((0:255)/256*Fs,10*log10(Pxx))

The averaged periodogram so obtained is shown in Fig. B.2

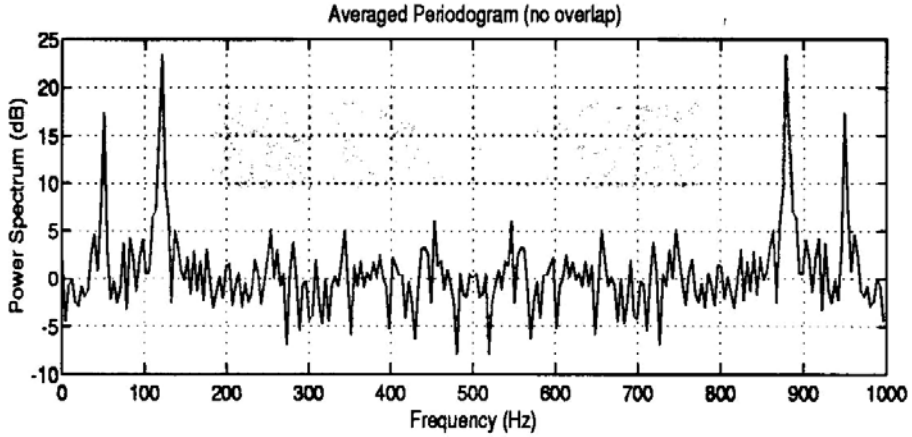

Figure B.2: Averaged Periodogram (no overlap)

This averaged estimate has one-third the variance of the length 256 periodogram shown earlier. The more sections averaged the lower the variance of the result. However, the signal length limits the number of sections possible (to three sections of length 256 in

the previous example). To obtain more sections, the signal is broken into overlapping sections. The result of 128 sample overlap is shown in Fig. B.3

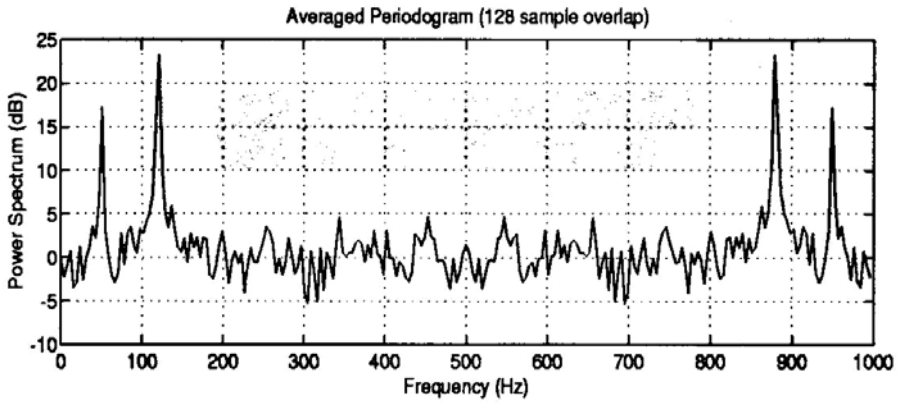

Figure B.3: Averaged Periodogram (128 sample overlap)

In this case the sections are statistically dependent, resulting in higher variance; thus there is a trade-off between the number of sections and the overlap rate.

The periodogram estimate could be improved further by applying a nonrectangular data window to the sections before computing the periodogram, resulting in a modified periodogram. This reduces the effect of section dependence due to overlap, because the window is tapered to 0 on the edges. Also, a nonrectangular window diminishes the side-lobe interference or "spectral leakage" while increasing the width of spectral peaks. With a suitable window (such as Hamming, Hanning, or Kaiser), overlap rates of about half the section length have been found to lower the variance of the estimate significantly.

The application of a Hamming window results in Fig. B.4 below:

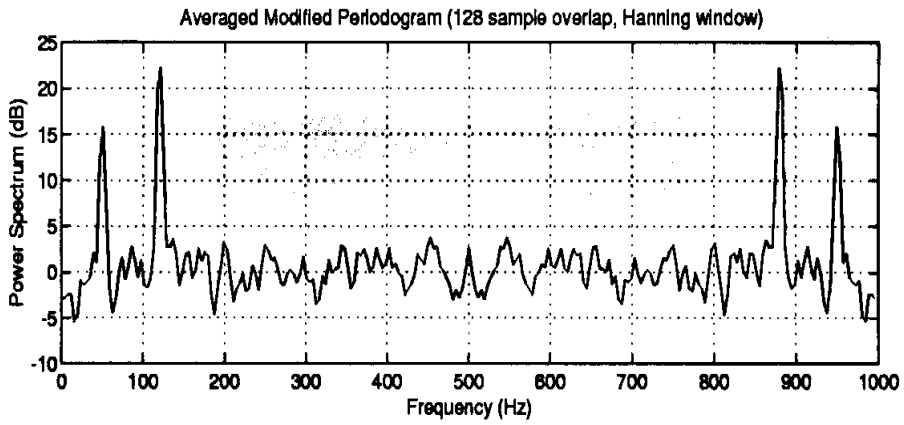

Figure B.4: Averaged Periodogram (128 sample overlap, Hanning window)

It could be easily noticed in this plot that the spectral peaks have widened, and the noise floor, or level of the noise, seems to be the flattest of any estimate so far. This method of averaged, modified periodograms is Welch's method of PSD estimation.

The functions psd and csd provide control over all the parameters discussed so far (FFT length, window, and amount of overlap) in computing the PSD and CSD of one or two signals using Welch's method. For a more detailed discussion of Welch's method of PSD estimation, see Kay (1988) and Welch (1967).

B.3 Power Spectral Density Function

The psd function averages and scales the modified periodograms of detrended sections of a signal. It simply specifies the parameters that control the algorithm as arguments to the function.

An estimate for the PSD of a sequence x_n using psd's (psd is the MATLAB function for calculating the power spectral density) default FFT length (256), window (Hanning of length 256), overlap samples (none), and detrending option (remove best linear fit from sections) is:

Pxx = psd(xn)

If the original sequence xn has units of volts, Pxx has units of volts^2/Hz.

To recreate the last example accurately, the number of samples to overlap is specified as 128 and no detrending:

```
nfft = 256;       %1ength of FFT
Fs = 1000;        %sampling frequency
Window = hanning(256);   % Window function
noverlap = 128;      % number of samples overlap
dflag = 'none'; % detrending option
Pxx = psd(xn,nfft,Fs,window,noverlap,dflag);
```

The order of the inputs to psd is important, except for the dflag string, which can be in any position as long as it is last. The sampling frequency does not affect the PSD estimate but helps psd scale the frequency axis for plotting. psd without any output generates a plot. For example, psd(xn,nfft,Fs,window,noverlap,dflag) generated Fig. B.5.

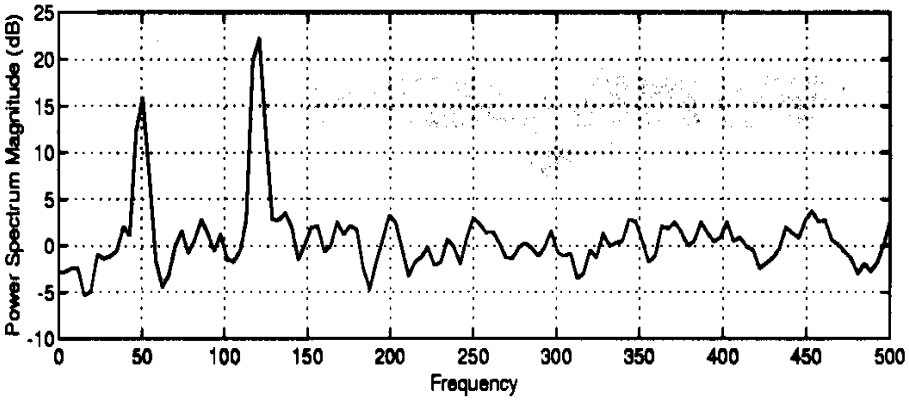

Figure B.5: Plot from psd without an output

B.4 Coherence Function

The magnitude-squared coherence between two signals x(n) and y(n) is

$$C_{xy}(\omega) = \frac{\left|P_{xy}(\omega)\right|^2}{P_{xx}(\omega)P_{yy}(\omega)} \tag{B.3}$$

This quotient is a real number between 0 and 1 that measures the correlation between x(n) and y(n) at the frequency ω. The cohere function takes sequences x and y, computes their PSD and CSD, and returns the quotient of the magnitude squared of the CSD and the product of the PSD. Its options and operation are similar to the csd function.

The coherence function of xn and yn versus frequency is

cohere(xn,yn,256,Fs,256,128,'none')

And the output is shown in Fig. B.6. If the input sequence length, window length, and overlap are such that cohere operates on only a single record, the function returns all ones.

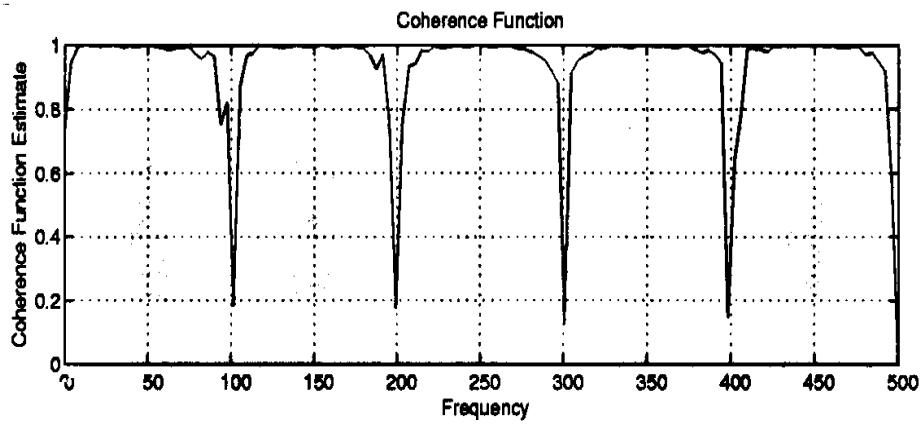

Figure B.6: Coherence Function

C. Uncertainty Analysis

If j is a function of n independent variables xi, the uncertainty in the measurement of J is given by:

$$\Delta J = \left[\sum_{i=1}^{n} \left(\frac{\partial J}{\partial x_i} \Delta x_i \right)^2 \right]^{1/2} \tag{C.1}$$

This equation can be expressed in the non-dimensional form as follows:

$$\frac{\Delta J}{J} = \left[\sum_{i=1}^{n} \left(\frac{x_i}{J} \frac{\partial J}{\partial x_i} \frac{\Delta x_i}{x_i} \right)^2 \right]^{1/2} \tag{C.2}$$

Equations C.1 and C.2 were used to determine the uncertainty in the experimental measurement of all the dimensionless variables used for data reduction.

C.1 Uncertainty in the Reynolds Number

The Reynolds' number can be defined by the following relation:

$$R_e = \frac{N D_i^2}{4\nu} \tag{C.3}$$

Since D_i and ν are constants and the error in reading the speed is about 1% using the microprocessor tachometer, the random error in measuring the Reynolds number is:

$$\frac{\Delta R_e}{R_e} = \frac{\Delta N}{N} = 0.01 \tag{C.4}$$

C.2 Uncertainty in the Mass Flow Rate

The mass flow rate through the compressor was calculated from the following relation:

$$\dot{m} = \rho_{air} A_o \left[\frac{2\Delta h \gamma_{water}}{\rho_{air}} \right]^{1/2} \tag{C.5}$$

The diameter of the inlet flow pipe is machined to very high precision. Therefore, uncertainty in the inlet flow area is neglected. Hence, the uncertainty in the mass flow rate is, using Eq. C.2,

$$\frac{\Delta \dot{m}}{\dot{m}} = \left[\left(\frac{\Delta(\Delta h)}{2\Delta h} \right)^2 \right]^{1/2} \tag{C.6}$$

Estimating the uncertainty in the minimum manometer reading of $\Delta h = 10$ mm. The uncertainty in the manometer reading is 1 mm. Therefore, the relative uncertainty in the mass flow rate is:

$$\frac{\Delta \dot{m}}{\dot{m}} = \left[\left(\frac{1}{2x10} \right)^2 \right]^{1/2} = 0.05 \quad \text{or} \quad 5\% \tag{C.7}$$